Univerzita Karlova v Praze
Matematicko-fyzikální fakulta

DIPLOMOVÁ PRÁCE

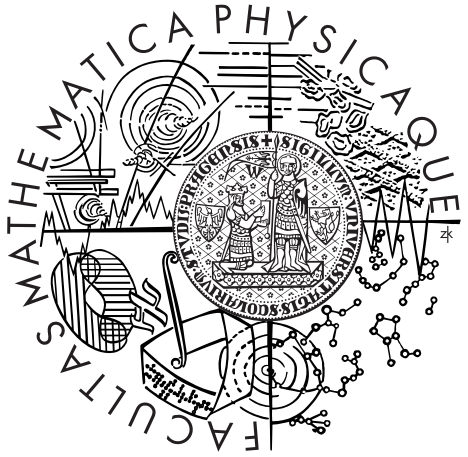

Kateřina Sládková

Viskoelastická deformace v geofyzikálních aplikacích

Katedra geofyziky

Vedoucí diplomové práce: doc. RNDr. Ondřej Čadek, CSc.

Studijní program: Matematika

Studijní obor: Matematické modelování ve fyzice a technice

Prague 2014

V první řadě bych chtěla poděkovat svému vedoucímu Ondřeji Čadkovi a konzultantovi Ondřeji Součkovi za nevídané množství času a energie věnované této práci. Dále bych chtěla poděkovat celé své rodině za neustálou pomoc během celého mého studia, jmenovitě pak Vendule Mokruschové a Michalu Sládkovi, kteří strávili nemalé množství času přímo s tímto textem. Ráda bych též poděkovala Ladislavu Hanykovi z katedry geofyziky za pomoc s numerickými a počítačovými problémy, které byly často vyřešeny dříve než jsem je stačila pojmenovat. V duchu poděkování v mé bakalářské práci přidávám díky kapele Guns N' Roses, která mě provázela strastiplným programováním.

Prohlašuji, že jsem tuto diplomovou práci vypracovala samostatně a výhradně s použitím citovaných pramenů, literatury a dalších odborných zdrojů.

Beru na vědomí, že se na moji práci vztahují práva a povinnosti vyplývající ze zákona č. 121/2000 Sb., autorského zákona v platném znění, zejména skutečnost, že Univerzita Karlova v Praze má právo na uzavření licenční smlouvy o užití této práce jako školního díla podle §60 odst. 1 autorského zákona.

V Praze dne 1.8.2014 Kateřina Sládková

Název práce: Viskoelastická deformace v geofyzikálních aplikacích

Autor: Kateřina Sládková

Katedra: Katedra geofyziky

Vedoucí diplomové práce: doc. RNDr. Ondřej Čadek, CSc., katedra geofyziky

Abstrakt: Práce se zabývá zapojením viskoelastického modelu do modelu pro termální konvekci formou vlastního kódu ve Fortranu 90 a zkoumáním role viskoelasticity v tomto modelu. Původně se viskoelasticita měla vyjádřit formou Maxwellova modelu, z numerických důvodů ovšem přecházíme k Oldroydově-B modelu. U tohoto modelu postupně nahrazujeme objektivní derivaci jejími jednotlivými členy a zkoumáme jejich vliv na chod konvekce - parciální derivace a advekční členy byly zcela zahrnuty, korotační členy vyžadují další numerické testování. Naše práce naznačuje, že vliv viskoelasticity na termální konvekci je znatelný.

Klíčová slova: termální konvekce, viskoelasticita, Oldroydův-B model

Title: Viscoelastic deformation in geophysical applications

Author: Kateřina Sládková

Department: Department of Geophysics

Supervisor: doc. RNDr. Ondřej Čadek, CSc., Department of Geophysics

Abstract: Our aim was to aid the viscoelasticity into the model for thermal convection by developing our own code in Fortran 90 and to study the role of viscoelasticity in this model. We should have included the viscoelasticity by Maxwell model; however, due to numerical instability we changed it for Oldroyd-B model. We were adding the terms of objective derivative into our code step by step and we were observing how they influence the behaviour of thermal convection. Partial time derivative and advective terms were included in whole complexity, the corrotational terms need more numerical testing. Our work suggest that the influence of viscoelasticity on thermal convection is noticeable.

Keywords: thermal convection, viscoelasticity, Oldroyd-B model

Contents

Introduction

0.1 General background

For more than thirty years, numerical simulations of thermal convection have been the major method of studying thermal evolution of the Earth and other planets. During that time, a number of sophisticated numerical codes have been developed. These codes alow the cooling of planetary mantles to be modelled in fully three-dimensional spherical geometry and they often include a complex visco-plastic rhelogy, e.g. Tackley [14], Šrámek and Zhong [15] and Choblet et al. [16]. Thanks to continued progress in numerical methods and computer technologies, the present-day geophysical models can describe the processes in planetary interiors with a high resolution and capture the basic features of the involved physical processes. The only limitation of the current numerical codes is thus the fact that they consider purely viscous (or viscoplastic) materials and usually neglect the elastic part of deformation. The effect of elastic deformation is mostly considered to be of the second order and its neglect is often justified by rather short relaxation times of mantle materials in comparison with the geological time scale. This is, however, valid only for the deep part of the mantle, where the viscosity decreases due to an increse in temperature. In the lithosphere (the cold and highly viscous upper part of the planet), the relaxation time can be very long and the elastic deformation should thus be taken into account. In spite of that, the use of visco-elasto-plastic rheology is not common and one can find only a few studies where the elastic deformation is included, e.g. Regenauer-Lieb and Yuen [17], Zhong [18], Moresi et al.[19], Gerya and Yuen 2007 [3] and Dumoulin et al. [20]. Although the first attempts to model viscoelastic convection date back to early nineties, e.g. Harder [4], there is no systematic study which would properly describe the effect of elasticity in mantle convection. Even in the studies of lithospheric deformation where the viscoelastic rheology is considered, one can hardly find a clear methodological description of its implementation. It is obvious that the current state of our knowledge on viscoelastic convection is insufficient, which motivates us to revisit this problem in the present study.

If we draw our attention to the limited number of works that include elasticity in thermal convection models, we can find that most of them describe the viscoelastic behavior via a Maxwell model. The main reason of this choice is certainly the formal simplicity of this model and the fact that it is described by only two parameters - viscosity and the shear modulus, which both can be obtained from independent observations, e.g. Dziewonski and Anderson [21] and Čížková et al. [22]. The Maxwell model also well describes the behavior of the Earth surface during the last deglaciation, e.g. Wu [23]. This argument may be, however, misleading: It is well-known that various viscoelastic models show a Maxwell-like behavior at times comparable to or larger than the relaxation time (thus in the phase of unloading) but their behavior may significantly differ from the Maxwell model in the initial loading stage. Since the postglacial rebound data sample only the unloading part of the process, it is not surprising that they "confirm" a Maxwellian character of the Earth's mantle.

As mentioned above, the general opinion on the role of elasticity in mantle

convection is that it is a second-order effect. This judgment led to a specific attitude towards viscoelasticity in the convection codes: Instead of developing new modeling tools, which would specifically address the problem of viscoelastic convection, the modellers use their highly sophisticated viscous codes and implement the viscoelastic rheology directly into them by introducing a formal viscosity which depends on the shear modulus and the time step. The non-linear advection and corrotation terms are implemented in the Lagrangian way with the aid of markers or they are enumerated on the grid from the solution in the previous time step and included in the body force. This procedure necessarily requires a reguralization, e.g. Gerya and Yuen 2007 [3], because the "viscosity" goes to zero with the decreasing time step. In the present work, we will deliberately follow this strategy and we will investigate its advantages and possible pitfalls.

0.2 Aim of the work

The main aim of this work is to study the implementation of elastic deformation in a standard thermal convection code and, more generally, to assess the role of viscoelasticity in thermal evolution of an Earth-like system. Our initial plan included the following tasks:

1. to develop a two-dimensional code to simulate thermal convection of higly viscous materials

2. to implement the Maxwellian rheology into this code using a standard strategy indicated above, and

3. to systematically study the influence of elastic deformation on thermal convection for various model parameters.

The first task has been fully accomplished and we have developed and carefully tested our own numerical code to simulate viscous convection with an infinite Prandtl number. However, in the second step, we faced serious troubles when implementing the Maxwell rheology. The numerical reason was that while shortening the time step, the solution diverged because the formal viscosity went to zero. This problem was obvious from the very beginning, but we believed that we would find a suitable way to regularize it. In literature, the need of regularization is usually mentioned but the regularization itself is not properly described or is too rough (for instance in Gerya and Yuen 2007 [3], the time step is chosen rather large and, during the time step, the stress is assumed to exponentially decrease). We performed a number of numerical tests to overcome this problem but these tests only convinced us that the Maxwell rheology is not suitable from numerical point of view and it does not properly describe the behavior of convecting systems. The singular behavior for time steps going to zero is intrinsic if the problem is formulated in velocities and the re-formulation in terms of displacement would be extremely expensive. Instead of the Maxwell model, we finally decided to use the Oldroyd-B model, which seemed to be only slightly more complicated (contains only one additional dashpot) and it reasonably well describes many viscoelastic materials (see also [11]). We believe that this decision was correct, although we later found that the implementation of the Oldroyd model in a standard convection code was rather elaborate and the calculations very time consuming. The

constitutive law for the Oldroyd-B model includes the objective derivatives of stress and strain rate, which consist of partial derivative with respect to time, an advection term and corrotation terms. We have succesfully implemented and tested the partial time derivative and we also achieved the implementation of the advection terms, even though we had to test different numerical schemes to obtain a numerically correct behavior of the code. The corrotation terms, which are considered of minor importance in geophysics, were not succesfully included. The program diverges with the current numerical strategy and we will have to test a different numerical scheme.

Even with the present version of the code we are able to obtain possibly interesting results, indicating potential importance of elastic deformation in mantle convection. The experience we got thanks to our previous failures and searches will help us and our colleagues in further study of viscoelastic convection. At least we have scratched off several possibilites which may not be tested any more. In addition to originally planned aims, we also compared two simplified forms of different viscoelastic models, Maxwell and Oldroyd-B.

0.3 Structure of the thesis

The structure of the thesis is as follows. In the first chapter we present the theoretical background of the whole work, i.e. the balance laws and their form in the Boussinesq approximation, conversion of the equations to dimensionless form, and the boundary and initial conditions. The numerical methods is discussed in chapter 2, where we introduce the spatial discretization and describe the method of time integration. The discretization of the terms arising from the use of the Oldroyd-B model is only outlined, with details being presented in Appendix B. The third chapter is dedicated to the computer implementation of the problem. The numerical code VFD.f90, which we have developed to adress the problem of viscoelastic convection and which is briefly decribed in this chapter, can also be found on the attached DVD. Chapter 4 presents the numerical tests, which we have performed to check the correct function of our code. These tests include the standard benchmark for the viscous code, a comparison of a linearized Maxwellian run with an independent numerical run, and a series of experiments carried out for various implementations of the Oldroyd-B model. The results of our modeling for different Deborah numbers are presented and discussed in chapter 5 and summarized in the final chapter, where also the numerical aspects of the problem are briefly revisited. The Appendices provide more information about the Oldroyd-B model and numerical equations.

1. Theory

In this section we would like to introduce the set of partial differential equations which have been used. We start with the conservation laws, from which we derive the Oberbeck-Boussinesq approximation. Then we include the viscoelastic rheology by substituting Newton model for Oldroyd-B model. From now on we consider to be situated in domain $\Omega \subset \mathbb{R}^2$.

1.1 Balance laws

We begin with the balance laws: balance of mass, balance of linear momentum, balance of angular momentum (in the form of symetry condition for the Cauchy stress) and balance of internal energy.

$$\begin{aligned} \frac{\partial \varrho}{\partial t} + \nabla \cdot (\varrho \mathbf{v}) &= 0, & (1.1)\\ \varrho \frac{d\mathbf{v}}{dt} &= \nabla \cdot \mathcal{T} + \varrho \mathbf{f}, & (1.2)\\ \mathcal{T} &= \mathcal{T}^T, & (1.3)\\ \varrho \frac{de}{dt} &= \mathcal{T} \cdot \mathcal{D} - \nabla \cdot \mathbf{q}, & (1.4) \end{aligned}$$

where $\mathbf{v}$ denotes velocity, ϱ density, $\mathcal{T}$ the Cauchy stress tensor, e internal energy, $\mathcal{D}$ the symmetric part of the velocity gradient $\mathcal{D}(\mathbf{v}) = \frac{1}{2}\big(\nabla \mathbf{v} + (\nabla \mathbf{v})^T\big)$,$\mathbf{q}$ the heat flux and $\mathbf{f}$ denotes the body force (gravity in our setting).

1.2 Boussinesq approximation

Now we will present the reduced system of partial differential equations which have been derived from the conservation laws by several assumptions and approximations by using the fact that we are dealing with the thermal convection in the Earth or other terrestrial planet. We also use the Fourrier law so that we can write the last equation in terms of temperature instead of heat flux. The whole approximation is not explicitly derived here, and it can be found for example in Matyska [9].

$$\begin{aligned} \nabla \cdot \mathbf{v} &= 0, & (1.5)\\ -\nabla p + \nabla \cdot \mathcal{S} &= -\mathbf{f}, & (1.6)\\ \varrho c_p \frac{\partial T}{\partial t} &= k \nabla^2 T - \varrho c_p \mathbf{v} \cdot \nabla T, & (1.7) \end{aligned}$$

where p is the pressure (mean normal stress, i.e. $p = -\frac{1}{3} tr(\mathcal{T})$), $\mathcal{S}$ is the deviatoric part of the Cauchy stress, c_p is the specific heat capacity at constant pressure, k is the thermal conductivity, T is the temperature.

This system must be complemented by the rheology for Cauchy stress tensor or his deviatoric part. As it was said before the most frequently used one in geophysics is constitutive relation for viscous fluid:

$$\mathcal{S} = 2\eta \mathcal{D}, \quad (1.8)$$

where η denotes the viscosity of the fluid. In this case the difficulty of computing process is made by the viscosity which may be dependent on many physical properties such as pressure, temperature, symmetric gradient of velocity or position vector: $\eta_1 = \eta_1(p, T, \mathcal{D}, \mathbf{r})$. However our aim was to employ the viscoelastic rheology; therefore, we present some information about it in geophysics.

Among geophysicists the most popular model extending the viscous rheology for viscoelastic effects is the simple Maxwellian rheology:

$$t_{\text{relax}} \overset{\triangledown}{\mathcal{S}} + \mathcal{S} = 2\eta_1 \mathcal{D}, \tag{1.9}$$

where t_{relax} is the relaxation time and triangle denotes objective time derivative defined as one of the Gordon-Schowalter objective time derivatives dependent on parameter $a \in [-1, 1]$:$\left(\frac{\partial \gamma}{\partial t}\right)_a := \frac{\partial \gamma}{\partial t} + (\mathbf{v} \cdot \nabla)\gamma - (\mathcal{W}\gamma - \gamma\mathcal{W}) + a(\mathcal{D}\gamma - \gamma\mathcal{D})$ where $\mathcal{W} = \frac{1}{2}\left(\nabla \mathbf{v} - (\nabla \mathbf{v})^T\right)$ is the antisymmetric part of the velocity gradient. The mechanical analogue of this model can be seen in in Figure 1.1., the model being composed of a combination of viscous dashpot with viscosity η and elastic spring with shear modulus μ, connected in series. To simplify the Maxwell model

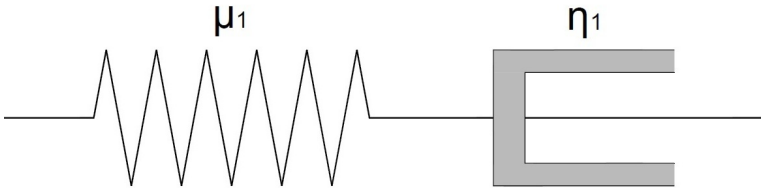

Figure 1.1: Maxwell model

we can replace the objective derivative(denoted by triangle above tensor) by the partial derivative with respect to time. Formally a severe disadvantage of this simplification is the loss of objectivity of the model, but provided the neglected terms can be shown to be negligible or small, such model serves as a good starting point for implementing visco-elastic effects. This, together with the simplicity of the model, is the main reason for popularity of such approach in geophysics. The simplified model looks as follows:

$$t_{\text{relax}} \frac{\partial \mathcal{S}}{\partial t} + \mathcal{S} = 2\eta_1 \mathcal{D}. \tag{1.10}$$

Our aim was to improve this attitude and to slightly overstep the borders of viscoelastic models used in geophysics. We certainly wanted to use viscoelastic model with objective derivative but we also wished to use a model which would describe the geophysical reality properly and would be numerically stable. During the construction of the program with the Maxwell model we realised that even in the unsimplified version this model does not suit well due to numerical instability - the Maxwell model formulated in velocities diverges when we are shortening the time step to zero. This is a consequence of the fact that Maxwell model allows immediate (elastic) response to applied forces leading to a jump in displacement, and, in turn to delta-function response in velocities. Since our model will be formulated primarily in velocities (being an extension of a classical

viscous convection model), such behavior is undesirable and will lead immediatelly to numerical instabilities. Therefore; we decided to use a possibly more appropriate model which should suit the geophysical problems better. It's called Oldroyd-B model. The mechanical analogue is depicted in Figure 1.2.

In the following lines we will describe the Oldroyd-B model in detail. A simple

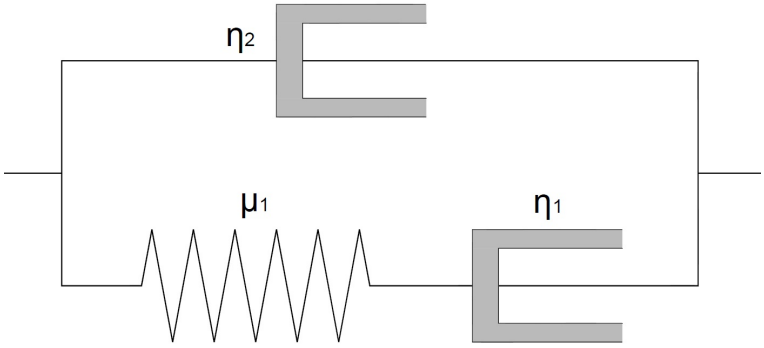

Figure 1.2: Oldroyd model

derivation based on the mechanical analogue in Figure 1.2 is presented in the Appendix A. The rheological relation for Oldroyd-B model follows:

$$\mathcal{S} - 2(\eta_1 + \eta_2)\mathcal{D} = 2\mathrm{De}\,\eta_2 \overset{\triangledown}{\mathcal{D}} - \mathrm{De}\overset{\triangledown}{\mathcal{S}}, \tag{1.11}$$

where, in the mechanical analogue, η_1, η_2 are the viscosities of the two dashpots, and a dimensionless parameter De - Deborah number has been introduced as $\mathrm{De} = \frac{\eta_1}{\mu_1 \tau_{\mathrm{dif}}}$, where μ_1 is the shear modulus and τ_{dif} is the relaxation time.

The Oldroyd-B element is composed of a Maxwellian element in parallel with additional viscous dashpot. This dashpot prevents immediate response of the model in terms of jump of displacement (possible in Maxwell model) and, for small values of η_2 can be viewed as a stabilization of the Maxwellian model.

The objective time derivative (represented by the triangle) in the Oldroyd-B model corresponds to the choice a=-1 in 1.13. It is desribed by triangle over a tensor $\overset{\triangledown}{\gamma}$. This derivative is derived from the family of Gordon-Schowalter objective time derivatives dependent on parameter $a \in [-1, 1]$ which has following form:

$$\left(\frac{\partial \gamma}{\partial t}\right)_a := \frac{\partial \gamma}{\partial t} + (\mathbf{v} \cdot \nabla)\gamma - (\mathcal{W}\gamma - \gamma\mathcal{W}) + a(\mathcal{D}\gamma - \gamma\mathcal{D}), \tag{1.12}$$

where $\mathcal{D}$ is the symmetric part of the velocity gradient and $\mathcal{W}$ is the antisymmetric part of the velocity gradient. For the parameter $a = -1$ we obtain upper convected Oldroyd derivative, which we use in our model:

$$\overset{\triangledown}{\gamma} := \frac{\partial \gamma}{\partial t} + \mathbf{v} \cdot \nabla\gamma - \nabla\mathbf{v}\gamma - \gamma(\nabla\mathbf{v})^T. \tag{1.13}$$

1.3 Dimensionless form of the equations

In order to assess the importance of various terms in the studied system of equations and, possibly also improve conditioning of the resultant system of algebraic equations arising from its discretization, we introduced representative scales in the problem and derived a dimensionless formulation of the system.

1.3.1 Dimensionless variables

Firstly, we present several important parameters:

$$d \quad \text{size of domain in the direction of axis z} \tag{1.14}$$

$$\kappa = \frac{k}{\rho c_p} \quad \text{thermal diffusivity} \tag{1.15}$$

$$k \quad \text{thermal conductivity} \tag{1.16}$$

$$c_p \quad \text{isobaric specific heat capacity} \tag{1.17}$$

$$\tau_{dif} = \frac{d^2}{\kappa} \quad \text{diffusivity time} \tag{1.18}$$

$$\mathrm{Ra} = \frac{\alpha \Delta T g d^3}{\eta_1 \kappa} \quad \text{Rayleigh number} \tag{1.19}$$

$$\mathrm{De} = \frac{\eta_1}{\mu_1 \tau_{dif}} \quad \text{Deborah number} \tag{1.20}$$

$$\mathrm{Vr} = \frac{\eta_2}{\eta_1} \quad \text{stiffness ratio} \tag{1.21}$$

where α it the thermal expansion coefficient and g is the magnitude of gravitational acceleration.

Furthermore, we introduce the dimensionless variables and denote them as dashed. We also prepare the derivatives with respect to them so that we can use it afterwards without more modification:

- Time:

$$t = \tau_{dif} t' \tag{1.22}$$

$$\frac{\partial}{\partial t} = \frac{\kappa}{d^2} \frac{\partial}{\partial t'} \tag{1.23}$$

- Space:

$$x = dx', z' = dz' \tag{1.24}$$

$$\frac{\partial}{\partial x} = \frac{1}{d} \frac{\partial}{\partial x'}, \frac{\partial}{\partial z} = \frac{1}{d} \frac{\partial}{\partial z'}, \tag{1.25}$$

$$\frac{\partial}{\partial^2 x} = \frac{1}{d^2} \frac{\partial}{\partial (x')^2}, \frac{\partial}{\partial^2 z} = \frac{1}{d^2} \frac{\partial}{\partial (z')^2}. \tag{1.26}$$

- Temperature:

$$T = T_{top} + (T_{bot} - T_{top}) T', \tag{1.27}$$

$$= T_{top} + \Delta T T', \tag{1.28}$$

$$\frac{\partial T}{\partial t} = \frac{\Delta T}{t_{dif}} \frac{\partial T'}{\partial t'} = \frac{\kappa \Delta T}{d^2} \frac{\partial T'}{\partial t'}, \tag{1.29}$$

$$\frac{\partial T}{\partial x} = \frac{\Delta T}{d} \frac{\partial T'}{\partial x'}, \frac{\partial T}{\partial z} = \frac{\Delta T}{d} \frac{\partial T'}{\partial z'}, \tag{1.30}$$

where T_{bot} denotes the temperature on the bottom of domain Ω and T_{top} on the top of the domain. Both these values are fixed by boundary conditions and $\Delta T = T_{bot} - T_{top}$.

- Derived quantitites:

$$\mathbf{v} = \frac{\kappa}{d}\mathbf{v}', \tag{1.31}$$

$$p = \frac{\eta_1\kappa}{d^2}p', \tag{1.32}$$

$$\mathcal{S} = \frac{\eta_1\kappa}{d^2}\mathcal{S}'. \tag{1.33}$$

1.3.2 Equations in dimensionless form

The dimensionless form of the governing equations reads as follows:

1) The equation of state

$$\varrho = \varrho_0\big(1-\alpha(T-T_0)\big), \tag{1.34}$$

$$\Delta\varrho = \varrho - \varrho_0 = -\alpha\Delta T T', \tag{1.35}$$

where ϱ_0, T_0 are reference density and temperature, often taken from the solution of the conduction. From these formulas for density we can derive dimensionless gravitational force in incremental formulation, which is actually the only force we consider being involved.[1]

$$\mathbf{f} = \Delta\varrho\mathbf{g} = \Delta\varrho g\mathbf{e}_z \tag{1.36}$$

$$= -\alpha\Delta T g\mathbf{e}_z T', \tag{1.37}$$

where $\mathbf{e}_z$ is the unit vector in the direction of the vertical (z) axis.

2) The equation of continuity

$$\nabla\cdot\mathbf{v} = 0 /. \frac{\kappa}{d} \tag{1.38}$$

$$\nabla\cdot\mathbf{v}' = 0 \tag{1.39}$$

3) The equation of motion

$$-\nabla p + \nabla\cdot\mathcal{S} + \mathbf{f} = 0 \tag{1.40}$$

$$-\frac{\eta_1\kappa}{d^3}\nabla p' + \frac{\eta_1\kappa}{d^3}\nabla\cdot\mathcal{S}' - \alpha\Delta T g\mathbf{e}_z T' = 0 \,/. \frac{d^3}{\eta_1\kappa} \tag{1.41}$$

$$-\nabla p' + \nabla\cdot\mathcal{S}' - \frac{\alpha\Delta T g d^3}{\eta_1\kappa}T'\mathbf{e}_z = 0 \tag{1.42}$$

$$-\nabla p' + \nabla\cdot\mathcal{S}' - \mathrm{RaT}'\mathbf{e}_z = 0 \tag{1.43}$$

4) The rheological relation

We have the rheological relation for Oldroyd-B model:

$$\mathcal{S} + \frac{\eta_1}{\mu_1}\overset{\triangledown}{\mathcal{S}} = 2(\eta_1+\eta_2)\mathcal{D} + 2\frac{\eta_1\eta_2}{\mu_1}\overset{\triangledown}{\mathcal{D}}, \tag{1.44}$$

[1] $\mathbf{g} = g\mathbf{e}_z$ because we have the axis z oriented downwards

i.e. with the upper convected Oldroyd derivative explicitly written:

$$\mathcal{S}+\frac{\eta_1}{\mu_1}\Big(\frac{\partial\mathcal{S}}{\partial t}+\mathbf{v}\cdot\nabla\mathcal{S}-\nabla\mathbf{v}\mathcal{S}-\mathcal{S}(\nabla\mathbf{v})^T\Big)=$$
$$=2(\eta_1+\eta_2)\mathcal{D}+2\frac{\eta_1\eta_2}{\mu_1}\Big(\frac{\partial\mathcal{D}}{\partial t}+\mathbf{v}\cdot\nabla\mathcal{D}-\nabla\mathbf{v}\mathcal{D}-\mathcal{D}(\nabla\mathbf{v})^T\Big). \quad (1.45)$$

Now we switch to dimensionless variables dentoted by dash:

$$\begin{aligned}\frac{\kappa\eta_1}{d^2}\mathcal{S}'+\frac{\eta_1}{\mu_1}\Bigg(\frac{\kappa\eta_1}{d^2\tau_{dif}}\frac{\partial\mathcal{S}'}{\partial t'} &+ \frac{\kappa^2\eta_1}{d^4}\mathbf{v}'\cdot\nabla'\mathcal{S}'-\frac{\kappa^2\eta_1}{d^4}\nabla'\mathbf{v}'\mathcal{S}'-\\ \frac{\kappa^2\eta_1}{d^4}\mathcal{S}'(\nabla'\mathbf{v}')^T\Bigg) &= 2(\eta_1+\eta_2)\frac{\kappa}{d^2}\mathcal{D}'+\\ 2\frac{\eta_1\eta_2}{\mu_1}\Bigg(\frac{\kappa}{d^2\tau_{dif}}\frac{\partial\mathcal{D}'}{\partial t'}+\frac{\kappa^2}{d^4}\mathbf{v}'\cdot\nabla'\mathcal{D}' &- \frac{\kappa^2}{d^4}\nabla'\mathbf{v}'\mathcal{D}'-\frac{\kappa^2}{d^4}\mathcal{D}'(\nabla'\mathbf{v}')^T\Bigg) \quad (1.46)\end{aligned}$$

We divide whole relation by $\frac{\kappa\eta_1}{d^2}$:

$$\mathcal{S}'+\mathrm{De}\big(\frac{\partial\mathcal{S}'}{\partial t'}+\mathbf{v}'\cdot\nabla'\mathcal{S}'-\nabla'\mathbf{v}'\mathcal{S}'-\mathcal{S}'(\nabla'\mathbf{v}')^{\mathrm{T}}\big)=$$
$$\begin{aligned}= \;& 2(1+\frac{\eta_2}{\eta_1})\mathcal{D}'+2\frac{\eta_2}{\mu_1\tau_{dif}}\Bigg(\frac{\partial\mathcal{D}'}{\partial t'}+\mathbf{v}'\cdot\nabla'\mathcal{D}'-\nabla'\mathbf{v}'\mathcal{D}'\\ & -\mathcal{D}'(\nabla'\mathbf{v}')^T\Bigg) \quad (1.47)\end{aligned}$$

And by defining a dimensionless parameter $\mathrm{Vr}=\frac{\eta_2}{\eta_1}$we obtain:

$$\mathcal{S}'+\mathrm{De}\overset{\triangledown}{\mathcal{S}'}=2(1+\mathrm{Vr})\mathcal{D}'+2\mathrm{Vr}\ \mathrm{De}\overset{\triangledown}{\mathcal{D}'} \quad (1.48)$$

5) Internal energy equation in terms of temperature

We start with

$$\varrho c_p\frac{\partial T}{\partial t}=k\nabla^2T-\varrho c_p\mathbf{v}\cdot\nabla T \quad (1.49)$$

We employ the dimensionless variables:

$$\frac{\varrho c_p\Delta T}{\tau_{dif}}\frac{\partial T'}{\partial t'}=\frac{k\Delta T}{d^2}\nabla'^2T'-\varrho c_p\frac{\kappa}{d}\mathbf{v}'\cdot\Big(\frac{\Delta T}{d}\nabla'T'\Big) \quad (1.50)$$

and we use: $\tau_{dif}=\frac{d^2}{\kappa}$; $\kappa=\frac{k}{\varrho c_p}$:

$$\frac{\partial T'}{\partial t'}=\nabla'^2T'-\mathbf{v}'\cdot\nabla T' \quad (1.51)$$

We summarize all the equations with omitting the dashes:

$$\begin{aligned}\nabla\cdot\mathbf{v} &= 0, & (1.52)\\ -\nabla p+\nabla\cdot\mathcal{S} &= \mathrm{Ra}T\mathbf{e_z}, & (1.53)\\ \mathcal{S}+\mathrm{De}\overset{\triangledown}{\mathcal{S}} &= 2(1+\mathrm{Vr})\mathcal{D}+2\mathrm{Vr}\ \mathrm{De}\overset{\triangledown}{\mathcal{D}}, & (1.54)\\ \frac{\partial T}{\partial t} &= \nabla^2T-\mathbf{v}\cdot\nabla T. & (1.55)\end{aligned}$$

1.4 Boundary and initial conditions

It remains to specify the boundary and initial conditions. We present our domain Ω which is rectangular and the boundaries are denoted by Γ_i, $i = 1, \ldots, 4$. See the scetch of our domain in Figure 1.3.

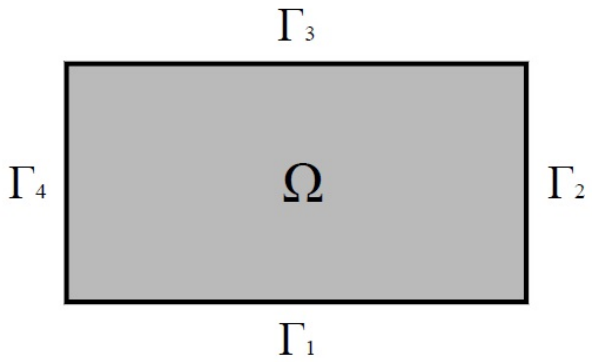

Figure 1.3: The domain and notation of its boundaries

We use free-slip boundary condition on the whole boundary, i.e.:

$$\mathbf{v} \cdot \mathbf{n} = 0 \quad \text{on } \partial\Omega, \tag{1.56}$$

$$\mathcal{S} \cdot \mathbf{n} = \big[(\mathcal{S} \cdot \mathbf{n}) \cdot \mathbf{n}\big]\mathbf{n} \quad \text{on } \partial\Omega. \tag{1.57}$$

Furthermore, we consider the temperature to be constant at the bottom and top boundaries and to follow the mirror boundary conditions on the sides, i.e.

$$T|_{\Gamma_1} = T_{bot}, \tag{1.58}$$

$$T|_{\Gamma_3} = T_{top}, \tag{1.59}$$

$$\mathbf{q} \cdot \mathbf{n}|_{\Gamma_2} = 0, \tag{1.60}$$

$$\mathbf{q} \cdot \mathbf{n}|_{\Gamma_4} = 0. \tag{1.61}$$

where $\mathbf{q}$ is the heat flux defined by Fourrier law as $\mathbf{q} = -k\nabla T$. The initial condition si defined only for temperature. There is no need of the initital conditions for the velocities and pressure because in the Boussinesq approximation, the evolution equation for velocity has been reduced to the Stokes problem. Therefore we only prescribe:

$$T = T_0 \quad \text{in } \Omega. \tag{1.62}$$

2. Numerical methods

In this chapter we would like to present the numerical tools, which we applied to solve our problem 1.52-1.55.

Firstly, we introduce the computational scheme - see Fig. 2.1. We start with

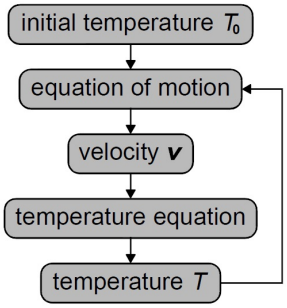

Figure 2.1: The scheme of the order of counting

the inital temperature T_0 and we apply it in the body force expression in the Stokes problem (equation of motion and continuity equation). As we solve the equation of motion, we obtain the velocity $\mathbf{v}$ and pressure p, which we employ in the temperature equation. By computing this equation we obtain temperature T in a new time step, which we utilize in the Stokes equations. The whole process is repeated until some steady state is established or until we decide that there does not exist any steady state for the current setting.

We now proceed to the description of the particular numerical tools involved in the solution scheme in Fig. 2.1. The problems we need to solve are following: space discretization of all the equations, time integration in temperature equation and time derivative in the Oldroyd-B model. Firstly, we will present our space discretization. Secondly, we will introduce Adams-Bashfort method applied for the time integration and finally, we will present the backward Euler method and the its application in the discretization of time derivative in Oldroyd-B model.

2.1 Space discretization

For the space discretization of the whole problem we use the finite differences, more precisely we employ equidistant staggered grid, see Fig. 2.2. The approximation with finite differences on such a grid provides second order of accuracy, see [8]. Even though we decided to use equidistant grid for implementational reasons, the numerical equations and also part of the program are prepared for non-uniform space division the numerical equations. For easier understanding we will in the numerical equations consider the grid being equidistant.

2.1.1 Notation

Our grid actually consists of two grids - the main (marked by a thick line) and the minor (marked by a thin line). The intersections of these grids create nodes,

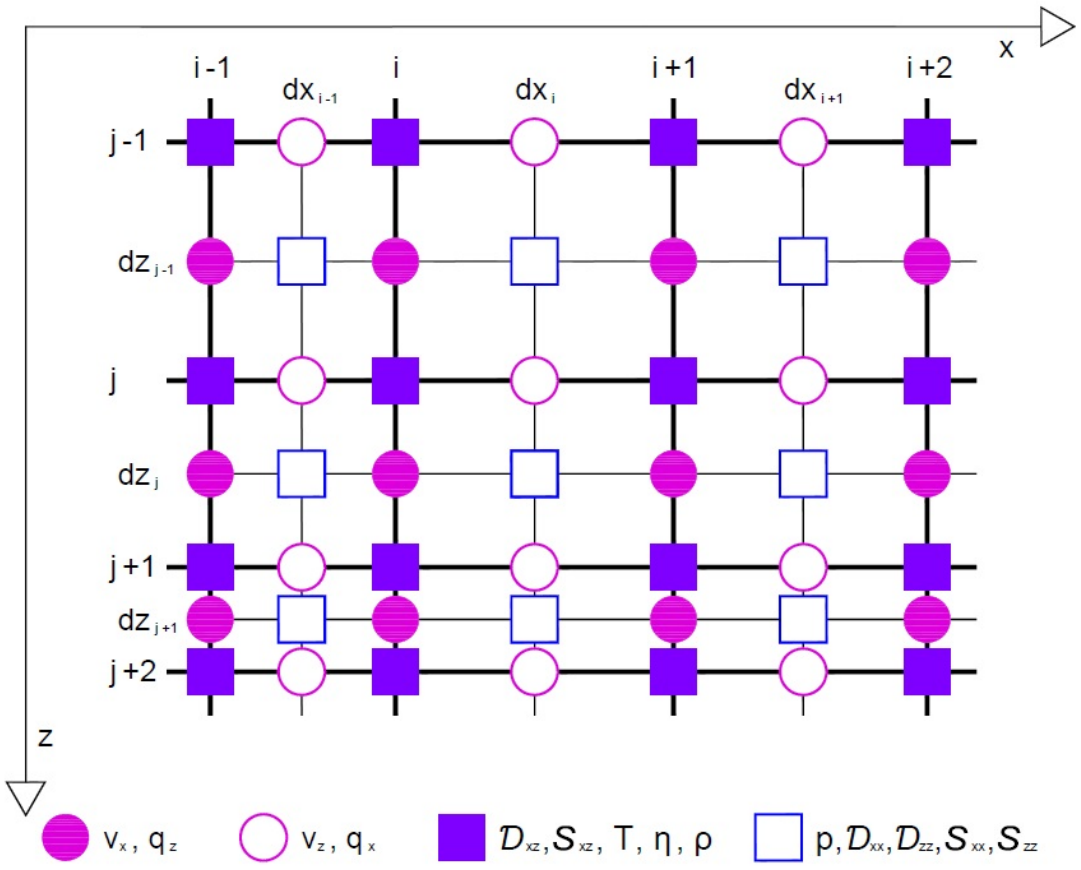

Figure 2.2: Staggered grid

which are also divided into two categories. It is important to understand the notation of the nodes to fully comprehend the numerical equations presented further.

We have one major node, which is denoted by full square 2.3b). To this major node belong three nodes 2.3c),d),e), which are called minor. We call these four nodes a cell, see Figure 2.3a). All physical properties in the nodes of this particular cell are denoted by subscript $_{i,j}$.

2.1.2 Discretized equations

As in all finite difference techniques, it is important to decide in which nodes to discretize which equation. The used numerical method perfectly suits our problem when considering the viscous rheology, therefore; the equations are placed in nodes where we can easily obtain deserved derivatives of the physical properties.

1) **Equation of continuity**
The equation of continuity is written in the minor node which is depicted as the blank rectangle 2.3c). This equation is one of the few which we will present in their whole complexity in the main text, the majority of the numerical equations is presented in the Appendices. The equation reads:

$$\frac{\partial v_x}{\partial x} + \frac{\partial v_z}{\partial z} = 0, \tag{2.1}$$

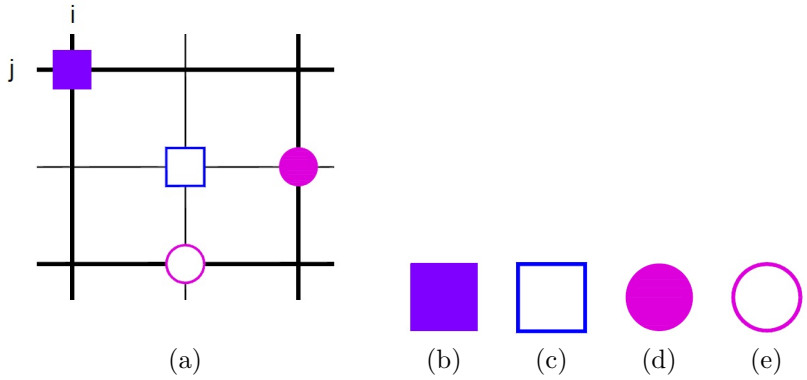

Figure 2.3: a) Package of nodes; b) Main node; c),d),e) Minor nodes

where $\mathbf{v} = (v_x, v_z)$. If we rewrite the equation using a two-point central difference approximation of the spatial derivative, we obtain:

$$\frac{v_{x_{i,j}} - v_{x_{i-1,j}}}{dx} + \frac{v_{z_{i,j}} - v_{z_{i,j-1}}}{dz} = 0 \tag{2.2}$$

2) The equation of motion

We start from the equation of motion which is rewritten in coordinate form. Hence, we have two equations of motion, each to be computed in different node. The first one matching to x-coordinate is placed in the node represented by full circle 2.3d) and the second one matching to z-coordinate is placed in the node pictured as a blank circle 2.3e).

$$-\frac{\partial p}{\partial x} + \frac{\partial S_{xx}}{\partial x} + \frac{\partial S_{xz}}{\partial z} = 0 \tag{2.3}$$

$$-\frac{\partial p}{\partial z} + \frac{\partial S_{zz}}{\partial z} + \frac{\partial S_{xz}}{\partial x} = RaT, \tag{2.4}$$

where

$$\mathcal{S} = \begin{pmatrix} S_{xx} & S_{xz} \\ S_{xz} & S_{zz} \end{pmatrix}$$

Now we express these equation by means of finite differences in its nodes:

$$-\frac{p_{i+1,j} - p_{i,j}}{dx} + \frac{S_{xx_{i+1,j}} - S_{xx_{i,j}}}{dx} + \frac{S_{xz_{i+1,j+1}} - S_{xz_{i+1,j}}}{dz} = 0 \tag{2.5}$$

$$-\frac{p_{i,j+1} - p_{i,j}}{dz} + \frac{S_{zz_{i,j+1}} - S_{zz_{i,j}}}{dz} + \frac{S_{xz_{i+1,j+1}} - S_{xz_{i,j+1}}}{dx} = Ra\frac{1}{2}(T_{i+1,j+1} + T_{i,j+1}). \tag{2.6}$$

We express all the equations in terms of velocity and pressure; therefore, we have to express the deviatoric terms of Cauchy stress tensors via velocity. We will show you how we have done this just for the basic node, i.e. i, j.

The whole discretized equations of motion can be found in Appendix B.

$$S_{xx} = 2\frac{\partial v_x}{\partial x} \quad \rightarrow \quad S_{xx_{i,j}} = 2\frac{v_{x_{i,j}} - v_{x_{i-1,j}}}{dx} \tag{2.7}$$

$$S_{xz} = \frac{1}{2}\Big(\frac{\partial v_x}{\partial z} + \frac{\partial v_z}{\partial x}\Big) \quad \rightarrow \quad S_{xz_{i,j}} = \frac{1}{2}\Big(\frac{v_{x_{i-1,j}} - v_{x_{i-1,j-1}}}{dz} + \tag{2.8}$$

$$\frac{v_{z_{i,j-1}} - v_{z_{i-1,j-1}}}{dx}\Big) \tag{2.9}$$

$$S_{zz} = 2\frac{\partial v_z}{\partial z} \quad \rightarrow \quad S_{zz_{i,j}} = 2\frac{v_{z_{i,j}} - v_{z_{i,j-1}}}{dz} \tag{2.10}$$

$$\tag{2.11}$$

3) Temperature equation

Considering the equation for temperature, we will focus on the right hand side of the equation, because the left hand side consists only of the partial time derivative of temperature, which is handled by Adams-Bashfort scheme described further. We write this equation in the main node, i.e. in the full square 2.3b). So that, we have these terms to discretize:

$$\frac{\partial^2 T}{\partial x^2} + \frac{\partial^2 T}{\partial z^2} - v_x\frac{\partial T}{\partial x} - v_z\frac{\partial T}{\partial z} \tag{2.12}$$

Our scheme does not really suit this kind of a problem because it was designed for solving the Stokes equations. Now we need to compute first and second derivatives in the node, where the physical variable, which we want to differentiate, is defined. So we decided to use a different scheme - Fornberg's pseudospectral method [8]. In the table 2.1 you can see the coefficents for equidistant grid. We have employed the Fornberg's scheme with the second order accuracy because the finite difference scheme, we are using, has also accuracy of the second order. We also use this scheme for discretazing several terms which appear by employing the Oldroyd-B model.

By using the Fornberg scheme we obtain the following numerical expression for the right hand side of the temperature equations:

$$\frac{T_{i+1,j} - 2T_{i,j} + T_{i-1,j}}{dx^2} + \frac{T_{i,j+1} - 2T_{i,j} + T_{i,j-1}}{dz^2} \tag{2.13}$$

$$-\frac{v_{x_{i-1,j}} + v_{x_{i-1,j-1}}}{2}\frac{T_{i+1,j} - T_{i-1,j}}{2dx} \tag{2.14}$$

$$-\frac{v_{z_{i,j-1}} + v_{z_{i-1,j-1}}}{2}\frac{T_{i,j+1} - T_{i,j-1}}{2dz} \tag{2.15}$$

2.2 Time discretization

As we have previously mentioned, we have to deal with time discretization twice. First, during the time integration in the temperature equation and second, when dealing with the partial time derivative in the Oldroyd-B model. We will start with time integration in the temperature equation.

Order of derivative	Position x=-1	of nodes x=0	x=1
1^{st}	0.5	0	0.5
2^{nd}	1	-2	1

Table 2.1: Coefficient for aproximation of first and second derivative at $x = 0$ using Fornberg's pseudospectral method

2.2.1 Adams-Bashforth method

In previous lines we have dealt with space discretization of the right hand side of the temperature equation. That means that now we supposed to deal with the time integration in the equation, which reads as follows:

$$T' = g(\mathbf{v}, T), \tag{2.16}$$

where T' denotes the time derivative and g is the known function of velocity and temperature. We have employed the explicit multistep method called Adams-Bashforth.

We have chosen the explicit method because it is a usual way how to treat the temperature equation in thermal convection. We have chosen specifically the Adams-Bashforth scheme for several reasons, but the main one is that there is only one evaluation of the function per time step. This is quite a big advantage in comparison with, for example, Runge-Kutta method, where for the $k-$step method there is the necessity of k evaluations per time step.

The formula for $k-$step Adams-Bashforth method with uniform time step employed to our problem reads as follows:

$$T^n = T^{n-1} + dt \sum_{i=0}^{k-1} \gamma_i \delta^i g^{n-i}, \tag{2.17}$$

$$\text{where} \quad \gamma_{\mathrm{m}} = (-1)^m \int_0^1 \binom{-\tau}{m} d\tau, \tag{2.18}$$

$$\tau = \frac{t - t_{n-1}}{h}, \tag{2.19}$$

where $\binom{-\tau}{m}$ denotes binomial coefficient. The time step is denoted by dt and δ represents the difference operators, the precise formula follows:

$$\delta^0 g^{n-1} = g^{n-1}, \tag{2.20}$$

$$\delta^1 g^{n-1} = g^{n-1} - g^{n-2}, \tag{2.21}$$

$$\delta^i g^{n-1} = \delta^{i-1} g^{n-1} - \delta^{i-1} g^{n-2} \tag{2.22}$$

This method has the local error $O(dt^{k+1})$. Thus the order of $k-$step Adams-Bashforth is k, for more information [10].

2.2.2 Euler method

For $k = 1$ in Adams-Bashforth method we obtain explicit Euler method. Owing to this fact, we can say that we are consistent concerning the approach to

discretization of the time derivatives. In this section we present, the way we use backward Euler method for approximation of the partial time derivative in Oldroyd-B model.

We can easily approach the viscous model by using the backward Euler method and that is the main reason for employing such a simple scheme. After the approximation, we will have the viscous model on the left hand side accompanied by all the terms in current time step. This formulation of viscous model will have formal viscosity, which would be dependent on elastic modulus, time step and in the case of Oldroyd-B model even on the second viscosity η_2. On the right hand side we will have the rest of the terms - all in previous time step. They will act as formal volume forces.

We simply start with the formula for the deviatoric part of Cauchy stress tensor in the dimensionless form:

$$\mathcal{S} = 2(1+\mathrm{Sr})\mathcal{D} + 2\mathrm{SrDe}\overset{\triangledown}{\mathcal{D}} - \mathrm{De}\overset{\triangledown}{\mathcal{S}} \tag{2.23}$$

We substitute for the triangle derivative by the upper convected Oldroyd derivative, i.e. $\overset{\triangledown}{\mathcal{S}} = \frac{\partial \mathcal{S}}{\partial t} + \mathbf{v}\cdot\nabla\mathcal{S} - \nabla\mathbf{v}\mathcal{S} - \mathcal{S}(\nabla\mathbf{v})^T$, $\overset{\triangledown}{\mathcal{D}} = \frac{\partial \mathcal{D}}{\partial t} + \mathbf{v}\cdot\nabla\mathcal{D} - \nabla\mathbf{v}\mathcal{D} - \mathcal{D}(\nabla\mathbf{v})^T$.

We will use the backward Euler scheme for the partial time derivative and we utilize the explicit computation of the advective and corrotational terms, i.e. we replace $\mathbf{v}\cdot\nabla\mathcal{D}$ by $\mathbf{v^{n-1}}\cdot\nabla\mathcal{D}^{n-1}$, $\mathbf{v}\cdot\nabla\mathcal{S}$ by $\mathbf{v^{n-1}}\cdot\nabla\mathcal{S}^{n-1}$ and $-\nabla\mathbf{v}\mathcal{S} - \mathcal{S}(\nabla\mathbf{v})^T$ by $\nabla\mathbf{v^{n-1}}\mathcal{S}^{n-1} - \mathcal{S}^{n-1}(\nabla\mathbf{v^{n-1}})^T$; $-\nabla\mathbf{v}\mathcal{D} - \mathcal{D}(\nabla\mathbf{v})^T$ by $-\nabla\mathbf{v^{n-1}}\mathcal{D}^{n-1} - \mathcal{D}^{n-1}(\nabla\mathbf{v}^{n-1})^T$, where index $^{n-1}$ denotes that physical quantities are evaluated in the previous time step. Furthermore we denote the current time step by $dt_n = t_n - t_{n-1}$ and the previous time step by $dt_{n-1} = t_{n-1} - t_{n-2}$.

As a result, we obtain:

$$\begin{aligned}
\mathcal{S}^n &= (1+\mathrm{Sr})\mathcal{D}^{\mathrm{n}} \\
&+ \mathrm{SrDe}\left[\frac{\mathcal{D}^{\mathrm{n}} - \mathcal{D}^{\mathrm{n-1}}}{\mathrm{dt_n}} + \mathbf{v}^{\mathrm{n-1}}\cdot\nabla\mathcal{D}^{\mathrm{n-1}} - \nabla\mathbf{v}^{\mathrm{n-1}}\mathcal{D}^{\mathrm{n-1}} - \mathcal{D}^{\mathrm{n-1}}(\nabla\mathbf{v}^{\mathrm{n-1}})^{\mathrm{T}}\right] \\
&- \mathrm{De}\left[\frac{\mathcal{S}^{\mathrm{n}} - \mathcal{S}^{\mathrm{n-1}}}{\mathrm{dt_n}} + \mathbf{v}^{\mathrm{n-1}}\cdot\nabla\mathcal{S}^{\mathrm{n-1}} - \nabla\mathbf{v}^{\mathrm{n-1}}\mathcal{S}^{\mathrm{n-1}} - \mathcal{S}^{\mathrm{n-1}}(\nabla\mathbf{v}^{\mathrm{n-1}})^{\mathrm{T}}\right]
\end{aligned}$$

$$\begin{aligned}
\mathcal{S}^n\big(1+\frac{\mathrm{De}}{dt_n}\big) &= (1+\mathrm{Sr})\mathcal{D}^{\mathrm{n}} + \mathrm{SrDe}\left[\frac{\mathcal{D}^{\mathrm{n}} - \mathcal{D}^{\mathrm{n-1}}}{\mathrm{dt_n}} + \mathbf{v}^{\mathrm{n-1}}\cdot\nabla\mathcal{D}^{\mathrm{n-1}}\right. \\
&- \left.\nabla\mathbf{v}^{n-1}\mathcal{D}^{n-1} - \mathcal{D}^{n-1}(\nabla\mathbf{v}^{n-1})^T\right] \\
&- \mathrm{De}\left[-\frac{\mathcal{S}^{\mathrm{n-1}}}{\mathrm{dt_n}} + \mathbf{v}^{\mathrm{n-1}}\cdot\nabla\mathcal{S}^{\mathrm{n-1}} - \nabla\mathbf{v}^{\mathrm{n-1}}\mathcal{S}^{\mathrm{n-1}} - \mathcal{S}^{\mathrm{n-1}}(\nabla\mathbf{v}^{\mathrm{n-1}})^{\mathrm{T}}\right]
\end{aligned}$$

Now we divide the whole relation by $\frac{dt_n}{dt_n+\mathrm{De}}$ to obtain the unit coefficient at $\mathcal{S}$ and we substitute the symmetric part of gradient of velocity $\mathcal{D}$ by its expression

in velocites:

$$\begin{aligned}
\mathcal{S}^n &- \frac{dt_n(1+\mathrm{Sr})+\mathrm{SrDe}}{dt_n+\mathrm{De}}\big(\nabla\mathbf{v}^n+(\nabla\mathbf{v}^n)^T\big) = \\
&- \frac{\mathrm{SrDe}}{dt_n+\mathrm{De}}\big(\nabla\mathbf{v}^{n-1}+(\nabla\mathbf{v}^{n-1})^T\big)+\frac{dt_n\mathrm{SrDe}}{dt_n+\mathrm{De}}\mathbf{v}^{n-1}\cdot\nabla(\nabla\mathbf{v}^{n-1}+(\nabla\mathbf{v}^{n-1})^T\big) \\
&- \frac{\mathrm{SrDedt_n}}{dt_n+\mathrm{De}}\Big[\nabla\mathbf{v}^{n-1}\big(\nabla\mathbf{v}^{n-1}+(\nabla\mathbf{v}^{n-1})^T\big)+\big(\nabla\mathbf{v}^{n-1}+(\nabla\mathbf{v}^{n-1})^T\big)(\nabla\mathbf{v}^{n-1})^T\Big] \\
&+ \frac{\mathrm{De}}{dt_n+\mathrm{De}}\mathcal{S}^{n-1}-\frac{dt_n\mathrm{De}}{dt_n+\mathrm{De}}\mathbf{v}^{n-1}\cdot\nabla\mathcal{S}^{n-1} \\
&+ \frac{dt_n\mathrm{De}}{dt_n+\mathrm{De}}\big(\nabla\mathbf{v}^{n-1}\mathcal{S}^{n-1}+\mathcal{S}^{n-1}(\nabla\mathbf{v}^{n-1})^T\big)
\end{aligned}$$

Now we have obtained nearly the viscous model on the left hand side of our relation; hence, the last thing we have to do is to introduce the new velocity $\mathbf{w}$, like this:

$$\begin{aligned}
\mathbf{w}^n &= \frac{dt_n(1+\mathrm{Sr})+\mathrm{SrDe}}{dt_n+\mathrm{De}}\mathbf{v}^n \\
\mathbf{v}^n &= \frac{dt_n+\mathrm{De}}{dt_n(1+\mathrm{Sr})+\mathrm{SrDe}}\mathbf{w}^n
\end{aligned} \tag{2.24}$$

Now we will finally obtain the dimensionless viscous model on the left hand side and on the right hand side there remain terms only from previous time step $^{n-1}$:

$$\begin{aligned}
\mathcal{S}^n &- \big(\nabla\mathbf{w}^n+(\nabla\mathbf{w}^n)^T\big) = \\
&-\frac{\mathrm{SrDe}}{dt_n+\mathrm{De}}\frac{dt_{n-1}+\mathrm{De}}{dt_{n-1}(1+\mathrm{Sr})+\mathrm{SrDe}}\big(\nabla\mathbf{w}^{n-1}+(\nabla\mathbf{w}^{n-1})^T\big)+ \\
&\frac{dt_n\mathrm{SrDe}}{dt_n+\mathrm{De}}\left(\frac{dt_{n-1}+\mathrm{De}}{dt_{n-1}(1+\mathrm{Sr})+\mathrm{SrDe}}\right)^2\mathbf{w}^{n-1}\cdot\nabla(\nabla\mathbf{w}^{n-1}+(\nabla\mathbf{w}^{n-1})^T\big) \\
&-\frac{dt_n\mathrm{SrDe}}{dt_n+\mathrm{De}}\left(\frac{dt_{n-1}+\mathrm{De}}{dt_{n-1}(1+\mathrm{Sr})+\mathrm{SrDe}}\right)^2 \\
&\Big[\nabla\mathbf{w}^{n-1}\big(\nabla\mathbf{w}^{n-1}+(\nabla\mathbf{w}^{n-1})^T\big)+\big(\nabla\mathbf{w}^{n-1}+(\nabla\mathbf{w}^{n-1})^T\big)(\nabla\mathbf{w}^{n-1})^T\Big] \\
&+\frac{\mathrm{De}}{dt_n+\mathrm{De}}\mathcal{S}^{n-1}-\frac{dt_n\mathrm{De}}{dt_n+\mathrm{De}}\frac{dt_{n-1}+\mathrm{De}}{dt_{n-1}(1+\mathrm{Sr})+\mathrm{SrDe}}\mathbf{w}^{n-1}\cdot\nabla\mathcal{S}^{n-1} \\
&\frac{dt_n\mathrm{De}}{dt_n+\mathrm{De}}\frac{dt_{n-1}+\mathrm{De}}{dt_{n-1}(1+\mathrm{Sr})+\mathrm{SrDe}}\big[\nabla\mathbf{w}^{n-1}\mathcal{S}^{n-1}+\mathcal{S}^{n-1}(\nabla\mathbf{w}^{n-1})^T\big]
\end{aligned}$$

Simplify the expression, we introduce two new constants dependent on the time step:

$$\varphi_n = \frac{\mathrm{De}}{dt_n+\mathrm{De}} \tag{2.25}$$

$$\psi_{n-1} = \frac{dt_{n-1}+\mathrm{De}}{dt_{n-1}(1+\mathrm{Sr})+\mathrm{SrDe}} \tag{2.26}$$

and we obtain the following expression:

$$\begin{aligned}\mathcal{S}^n - \big(\nabla\mathbf{w}^n + (\nabla\mathbf{w}^n)^T\big) &= -\mathrm{Sr}\varphi_{\mathrm{n}}\psi_{\mathrm{n-1}}\big(\nabla\mathbf{w}^{\mathrm{n-1}} + (\nabla\mathbf{w}^{\mathrm{n-1}})^{\mathrm{T}}\big)\\ &+ \mathrm{Srdt_n}\varphi_{\mathrm{n}}\psi^2_{\mathrm{n-1}}\mathbf{w}^{\mathrm{n-1}}\cdot\nabla(\nabla\mathbf{w}^{\mathrm{n-1}} + (\nabla\mathbf{w}^{\mathrm{n-1}})^{\mathrm{T}})\\ &- \mathrm{Srdt_n}\varphi_{\mathrm{n}}\psi^2_{\mathrm{n-1}}\Big[\nabla\mathbf{w}^{\mathrm{n-1}}\big(\nabla\mathbf{w}^{\mathrm{n-1}} + (\nabla\mathbf{w}^{\mathrm{n-1}})^{\mathrm{T}}\big)\\ &\qquad +\big(\nabla\mathbf{w}^{n-1} + (\nabla\mathbf{w}^{n-1})^T\big)(\nabla\mathbf{w}^{n-1})^T\Big]\\ &+ \varphi_n\mathcal{S}^{n-1} - dt_n\varphi_n\psi_{n-1}\mathbf{w}^{n-1}\cdot\nabla\mathcal{S}^{n-1}\\ &+ dt_n\varphi_n\psi_{n-1}\big[\nabla\mathbf{w}^{n-1}\mathcal{S}^{n-1} + \mathcal{S}^{n-1}(\nabla\mathbf{w}^{n-1})^T\big],\end{aligned}$$

which is the final version of the time-discretized rheology relation.

If we want to use this expression in our equations, we will need $\nabla\cdot\mathcal{S}^n$ for the equation of motion. We have already involved the left hand side in the equation of motion, therefore; we will turn our attention to the divergence of right hand side. In the following procedure we will also use the equation of motion to substitute for $\mathcal{S}^{n-1}$. It holds $\nabla\cdot\mathcal{S}^{n-1} = \nabla p^{n-1} + \mathrm{RaT^{n-1}}\mathbf{e_z}$.

$$\begin{aligned}\nabla\cdot\mathcal{S}^n - \nabla\cdot\big(\nabla\mathbf{w}^n &+ (\nabla\mathbf{w}^n)^T\big) = -\mathrm{Sr}\varphi_{\mathrm{n}}\psi_{\mathrm{n-1}}\nabla\cdot\big\{\nabla\mathbf{w}^{\mathrm{n-1}} + (\nabla\mathbf{w}^{\mathrm{n-1}})^{\mathrm{T}}\big\}\\ &+ \mathrm{Srdt_n}\varphi_{\mathrm{n}}\psi^2_{\mathrm{n-1}}\nabla\cdot\Big\{\mathbf{w}^{\mathrm{n-1}}\cdot\nabla(\nabla\mathbf{w}^{\mathrm{n-1}} + (\nabla\mathbf{w}^{\mathrm{n-1}})^{\mathrm{T}})\Big\}\\ &- \mathrm{Srdt_n}\varphi_{\mathrm{n}}\psi^2_{\mathrm{n-1}}\nabla\cdot\Big\{\nabla\mathbf{w}^{\mathrm{n-1}}\big(\nabla\mathbf{w}^{\mathrm{n-1}} + (\nabla\mathbf{w}^{\mathrm{n-1}})^{\mathrm{T}}\big)\\ &\qquad +\big(\nabla\mathbf{w}^{n-1} + (\nabla\mathbf{w}^{n-1})^T\big)(\nabla\mathbf{w}^{n-1})^T\Big\}\\ &+ \varphi_n(\nabla p^{n-1} + \mathrm{RaT^{n-1}}\mathbf{e_z})\\ &- dt_n\varphi_n\psi_{n-1}\nabla\cdot\big\{\mathbf{w}^{n-1}\cdot\nabla\mathcal{S}^{n-1}\big\}\\ &+ dt_n\varphi_n\psi_{n-1}\nabla\cdot\big\{\nabla\mathbf{w}^{n-1}\mathcal{S}^{n-1} + \mathcal{S}^{n-1}(\nabla\mathbf{w}^{n-1})^T\big\}\end{aligned} \quad (2.27)$$

The resulting formula is quite complex and it is not even discretized. In order to save space, we do not present discrete counterparts to these formula in the main text, they are all listed in the Appendix B.

2.3 Advection and corrotational terms of the Oldroyd-B model

In this section we present the way we dealt with the space discretization of the rest of the Oldroyd-B model, because in the previous section we only discussed the partial time derivative.

2.3.1 Advection terms - Fornberg's pseudospectral method

When the model used to far (involving only partial time derivative in the rheology equation) is extended for the advection terms, two novel terms appear in fact in the formulation. The first one is obvious, it is in the equation of motion as a part of body force as presented above 2.27, where the advection terms are present in the divergence of stress $\nabla\cdot\mathcal{S}$. The second one is in the computation of the

stress $\mathcal{S}$ in the previous time step. Because we use the explicit computation of the advection terms, we actually compute $\mathbf{w}^{n-1} \cdot \nabla \mathcal{S}^{n-1}$ or $\mathbf{w}^{n-1} \cdot \nabla \mathcal{D}^{n-1}$ for the body force. Therefore; we have to also evaluate the $\mathcal{S}^{n-1}$ and $\mathcal{D}^{n-1}$. Hence by employing the advection terms in the Oldroyd-B model, we have to add them also into this computation. Hence, we evaluate four formulas by adding the advection terms: $\mathbf{w}^{n-1} \cdot \nabla \mathcal{S}^{n-1}$, $\mathbf{w}^{n-1} \cdot \nabla \mathcal{D}^{n-1}$, $\mathcal{S}^{n-1}$ and $\mathcal{D}^{n-1}$.

Our attitude to the computation of advection members was straight. We decided to use the central difference scheme via the Fonberg's pseudospectral method as in temperature equation. We can no longer use the "classical" difference scheme of our grid anymore, because as in the temperature equation it did not suit our new problem well. Thus, we needed something new and we chose the closest one, another central scheme, which had already being used. As before we used the version with the second order of accuracy. You can observe the Table 2.1 for the coefficients on the equidistant grid.

The discretization of advection terms was really turned out to be demanding due to number of derivatives also of mixed type, whose discretization required special care. The final version of our approximation scheme is summarized in the Appendix B. Note that the discretized formulas of both advection members (the advection of stress and advection of the symmetric part of the gradient of velocity) took nearly four pages. These formulae moreover, do not involve the boundary conditions, which complicate them even further. In our code we had to consider also the boundary conditions, which lead to many special cases depending on how far from the boundary we are situated. Hence, this was one of the parts of our thesis which took more time than expected. The discretization of the advection terms by the Fornberg method without additional stabilization has shown to be unstable and has led to divergence of the program. Discretization by upwind method, described in the next section has proved to be more suitable.

2.3.2 Advection terms - Upwind scheme

Due to the divergence of the model with the advection terms discretized by the means of Fornberg's scheme, we employed another scheme - second-order upwind scheme, where for the one-sided derivatives we use the one-sided Fornberg's scheme. We present this upwind scheme for velocity components v_x and v_z and for some general S, which is representing arbitrary component of $\mathcal{S}$, e.g. S_{xx} or S_{xz}. Therefore, we discretized the following derivative $v_x \frac{\partial S}{\partial x}$ in some unspecified node i, j.

$$\left(v_x \frac{\partial S}{\partial x}\right)_{i,j} = (v_x^+ S_x^- + v_x^- S_x^+)_{i,j}, \tag{2.28}$$

where

$$v_x^+ = max(v_x, 0), \tag{2.29}$$

$$v_x^- = min(v_x, 0), \tag{2.30}$$

$$S_x^+ = \frac{-0.5S_{i+2,j}^n + 2S_{i+1,j}^n - 1.5S_{i,j}^n}{dx} = \frac{-S_{i+2}^n + 4S_{i+1,j}^n - 3S_{i,j}^n}{2dx}, \tag{2.31}$$

$$S_x^- = \frac{3S_{i,j}^n - 4S_{i-1,j}^n + S_{i-2,j}^n}{2dx} \tag{2.32}$$

We also introduce the upwind scheme for z-component of velocity v_z and derivative of aribitrary component of stress $\mathcal{S}$ according to z,i.e. $v_z \frac{\partial S}{\partial z}$

$$\left(v_z \frac{\partial S}{\partial z}\right)_{i,j} = (v_z^+ S_z^- + v_z^- S_z^+)_{i,j}, \tag{2.33}$$

where

$$\begin{aligned} v_z^+ &= max(v_z, 0), & (2.34)\\ v_z^- &= min(v_z, 0), & (2.35)\\ S_z^+ &= \frac{-S_{i,j+2}^n + 4S_{i,j+1}^n - 3S_{i,j}^n}{2dz}, & (2.36)\\ S_z^- &= \frac{3S_{i,j}^n - 4S_{i,j-1}^n + S_{i,j-2}^n}{2dz} & (2.37) \end{aligned}$$

With this discretization of advection terms, the program is working much better than with the previous one.

2.3.3 Corrotational terms

Owing to two implemented types of discretization of the advection terms, we decided to simplify the model a bit to make it possibly work with corrotational terms. Despite our effort to do so the code with corrotational terms even in the simplified version diverges.

The simplification was that we include only the antisymmetric part of the corrotational terms. That means that instead of adding $-\nabla\mathbf{v}\mathcal{S} - \mathcal{S}(\nabla\mathbf{v})^T$ we include only $-\mathcal{W}\mathcal{S} + \mathcal{S}\mathcal{W}$, where $\mathcal{W} = \frac{1}{2}\big(\nabla\mathbf{v} - (\nabla\mathbf{v})^T\big)$ is the antisymmetric part of gradient of velocity. It is quite a usual attitude in geophysics to use only the rotational term. As mentioned previously, the program diverges with the corrotational terms implemented and we neither had enough time to explore the simplified term with another numerical scheme nor to add the second part of corrotational terms.

We also used the Fornberg's pseudospectral method for discretization of these terms, therefore; will not include any example of the usage of the Fornberg scheme here, because it is similar to the advection terms and you can find the whole discretization in the Appendix B.

3. Numerical implementation - Fortran 90 code VFD.f90

In this chapter we would like to introduce the way we solved the algebraic equations, which we obtained by the space and time discretization of the partial time equations presented in the first chapter. Whole problem was solved by our own numerical code written in Fortran 90.

3.1 Stokes equations

In the previous chapter we discused the space discretization of the Stokes equations - the equation of continuity and the equation of motion. By the space discretization we obtained set of algebraic equations, i.e. equations written in terms of the physical properties in nodes of our grid. More specifically, we got equations written in the velocity (or more precisely in the components of velocity v_x, v_z) and in the pressure p. By this adjustment we obtained the system of linear equations $\mathbb{A}\mathbf{x} = \mathbf{b}$.

Each row of the matrix $\mathbb{A}$ represents one particular algebraic equation of discrete problem. There are three kinds of the numerical equations[1], first is the continuity equation, second and third are the equations of motion. Hence, there is a stack of three rows for each grid cell 2.3a in which these three equations are written. The columns are denoted by the physical properties in which we compute our equations. Thus; there is also a stack of three columns corresponding to three physical properties - v_x, v_z, p - for every grid cell. The sequence of the grid cells is gone through from moves from top to the bottom and then from left to right.

For better understanding please observe the order of the matrix in the Figure 3.1[2]. In the Figure 3.1 you can find the coefficient which stands at the x-component of velocity in the equation of continuity (both placed in the node noted by $i, j+1$) in the red cross $\times$.

With this notation and ordering of the variables and equations, the matrix is

$$\begin{pmatrix} \ldots & \ldots & v_{x_{i,j}} & v_{z_{i,j}} & p_{i,j} & v_{x_{i,j+1}} & v_{z_{i,j+1}} & p_{i,j+1} \\ \text{Eq.of c.(i, j)} & & . & & & & & \\ \text{Eq.of m.1(i, j)} & & & . & & & & \\ \text{Eq.of m.2(i, j)} & & & & . & & & \\ \text{Eq.of c.(i, j + 1)} & & & & & \times & & \\ \text{Eq.of m.1(i, j + 1)} & & & & & & . & \\ \text{Eq.of m.2(i, j + 1)} & & & & & & & . \end{pmatrix}$$

Figure 3.1: The order of the matrix $\mathbb{A}$

band-diagonal and it needs only ten places around the diagonal. This allows compressed representation in so called band storage. The second interesting fact

[1] The boundary conditions are implemented in the form of adjusted equations

[2] Eq. of c stands for equation of continuity; Eq. of m.1 stands for x-component of the equation of motion and Eq. of m.2 for the z.component

concerning the matrix is, that it does not change during the computation, even with the Oldroyd-B model implemented. Hence, the only thing changing in the equation $\mathbb{A}\mathbf{x} = \mathbf{b}$ is the right hand side $\mathbf{b}$. This advantage is used while solving the system of linear equations on the computer, which leads us to the numerical libraries.

We tried couple of solvers for the system of linear equations and the best performance was achieved with the LAPACK library. More precisely we are using two subroutines - DGBTRF, DGBTRS. The first one provides us with the LU decomposition of the matrix $\mathbb{A}$ and the second one solves the system by finding the unknown variable $\mathbf{x}$ with the aid of the LU decomposition. When we focus our attention on the time consumption of these two subroutines, the first one is much more time consuming and it also has much higher demands in terms of available computer memory. Therefore, it is a great advantage of our attitude that this subroutine needs to be executed only once per the program run.

3.2 The temperature equation

In this section we will introduce the library which we use for solving of the temperature equation, more precisely for the time integration in this equation. We utilize the IMSL library, more specifically the *divpag* subroutine, which is version of *ivpag* subroutine working in double precision. You can find more information about both in the User's guide[12].
The *divpag* subroutine computes the time integration of the equation in form $T' = g(\mathbf{v}, T)$, where the velocity $\mathbf{v}$ is considered to be constant during the computation of one time step. We can control this soubroutine via several parameters like time step, tolerance for error control or maximum order of the method.

The time step is directed via Courrant criterion, which controls the stability of the computation. It is composed of two criteria, the first one checks the diffusion and the second one the convection. After applying of these two criteria we get two coefficents, from which we take the minimum of them and multiply it by coefficient c which can reach values from zero to one. Mathematically speaking:

$$dt_{dif} = \frac{dx^2}{\kappa} \tag{3.1}$$

$$dt_{conv} = \min_{i,j}\left(\frac{dx}{v_{x_{i,j}}}, \frac{dz}{v_{z_{i,j}}}\right) \tag{3.2}$$

$$dt_{cour} = c\min(dt_{dif}, dt_{conv}),\ c \in (0, 1] \tag{3.3}$$

The maximum order of the method provided by the subroutine is twelve and the subroutine itself chose the order to obtain the tolerance for error control which we have settled. We can only say what the maximum order of the method will be. In our case we have stayed at twelve.

4. Numerical tests

In this chapter we will present the numerical tests which were taken for the verification of our codes's funcionality. Firstly we will concetrate on viscous model, then we introduce the benchmark with Maxwell model and finally we will show the test for Oldroyd-B model.

4.1 Viscous model

4.1.1 Blankenbach benchmark

Main test for the viscous model was Blankenbach benchmark [7], which bear on several numerical computation of the mantle convection. The precise task of this benchmark is defined as two-dimensional thermal convection of a non-rotating Boussinesq fluid in rectangular closed cells. For the benchmark all material properties are considered constant. The main tool for the comparison is the Nusselt number, which represents mean surface temperature gradient over mean bottom temperature. We denote the Nusselt number by Nu and present the defining formula:

$$\mathrm{Nu} = \frac{\int_{\Gamma_3} q_z \mathrm{dS}}{\int_\Omega \kappa \frac{\Delta T}{d} \mathrm{dV}} \tag{4.1}$$

We concentrated on the Case 1 in Blankenbach et al. [7] which is defined as steady convection with constant viscosity in a square box. The temperature is fixed to zero on top and to ΔT at the bottom, no internal heat sources are considered. As the boundary condition in the Case 1 the reflection symmetry at the sidewall and zero shear stress on all boundaries are taken. All this setting perfectly suits our problem. Three Rayleigh number are followed in this case: $\mathrm{Ra} = 10^4, \mathrm{Ra} = 10^5$ and $\mathrm{Ra} = 10^6$. This benchmark provides several results from different authors. There does not exist one right value of the Nusselt number. For the comparison with this benchmark we were supposed to find the author who used the most similar numerical methods as we do and compare our final Nusselt number with it. Therefore, we chose D. Moore, who used finite differences with direct solver of the matrix, explicit DuFort-Frankel method of second order for the temperature equation and equispaced staggered grid. We computed all three possibilities of Rayleigh number and chose to compare the middle range of resolution provided by D. Moore, i.e. 48×48 and 96×96. The benchmark was suprisingly accurate, see Table 4.1. The temperature fields in stationary state for every Rayleigh number are depicted in Figures 4.1 - 4.3.

4.1.2 Energetic test

The second test was to control the validity of conservation law of energy in the following form:

$$\int_\Omega \varrho c_p \frac{\partial T}{\partial t} \,\mathrm{dV} = -\int_{\partial\Omega} \mathbf{q} \cdot \mathbf{n} \,\mathrm{dS}. \tag{4.2}$$

Rayleigh number	resolution	D. Moore	our computing
10^4	48x48	4.870	4.870
10^4	96x96	4.881	4.881
10^5	48x48	10.423	10.409
10^5	96x96	10.507	10.504
10^6	48x48	21.078	20.950
10^6	96x96	21.759	21.729

Table 4.1: Results of the Blankenbach benchmark via the Nusselt number

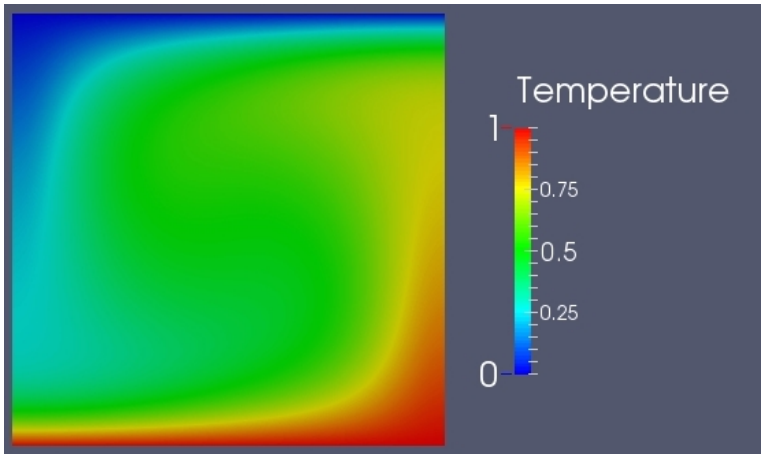

Figure 4.1: Temperature field in the stationary state of the viscous model with Rayleigh number 10^4

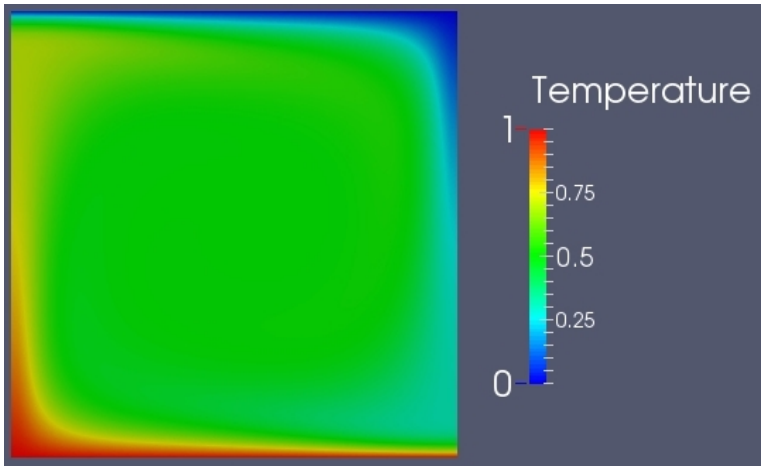

Figure 4.2: Temperature field in the stationary state of the viscous model with Rayleigh number10^5

This test was apllied for every Rayleigh number (10^4, 10^5, 10^6) and for various resolutions and our code achieved the equality with precision at least 0.1%.

4.1.3 Mesh refinement test

Last thing we tested for the viscous model was mesh refinement test. We can find some limitting process of Nusselt number even in the Blankenbach benchmark [7];

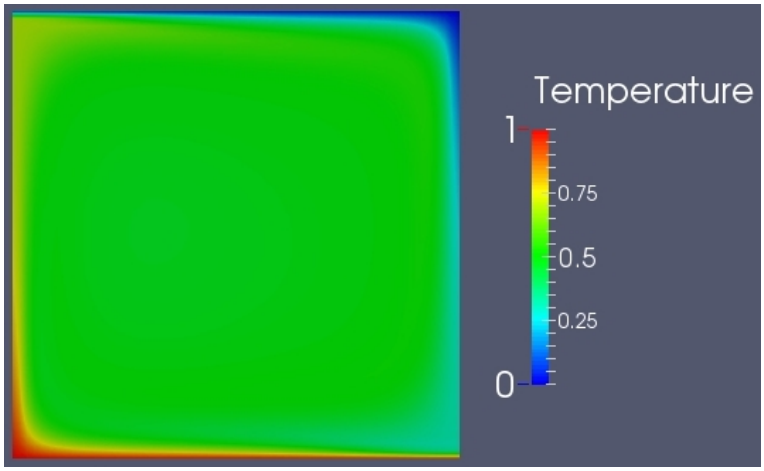

Figure 4.3: Temperature field in the stationary state of the viscous model with Rayleigh number 10^6

therefore, we expected the same development in our code. In addition, the $\mathcal{L}^2$ norms of the velocity are depicted also and the same process can be observed there. See Figures 4.4 - 4.6 and 4.7 - 4.9.

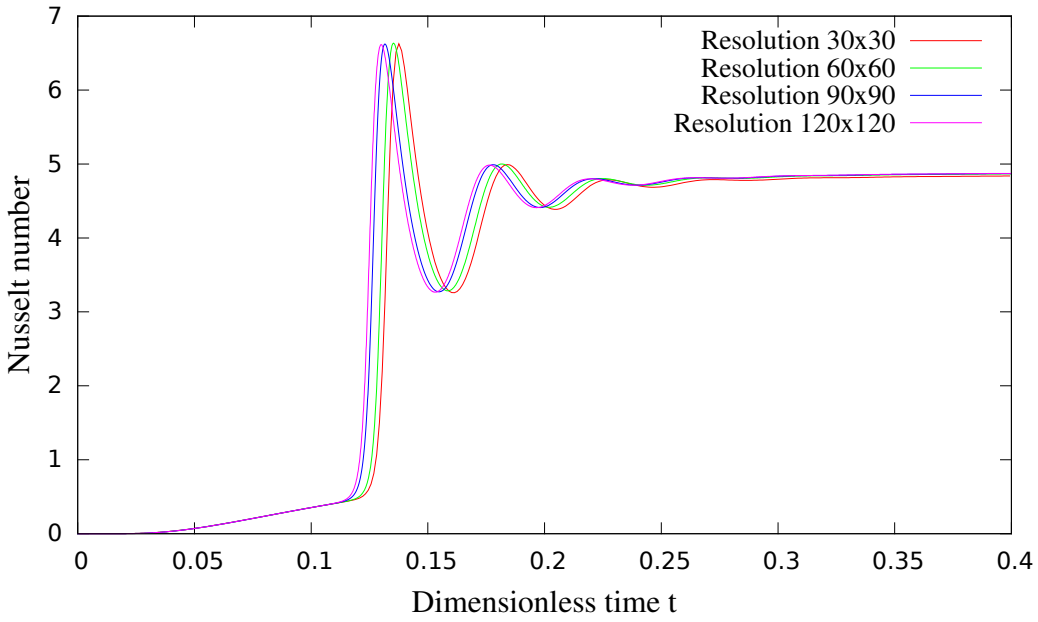

Figure 4.4: Evolution of Nusselt number of viscous model with Rayleigh number 10^4

4.2 Maxwell model

We had the chance to compare our results of Maxwell model with another code, more precisely with the code of Paul Tackley [13] modified by Vojtěch Patočka (personal communication). This code is constructed for the computation of viscous thermal convection in the square with the same boundary conditions as we

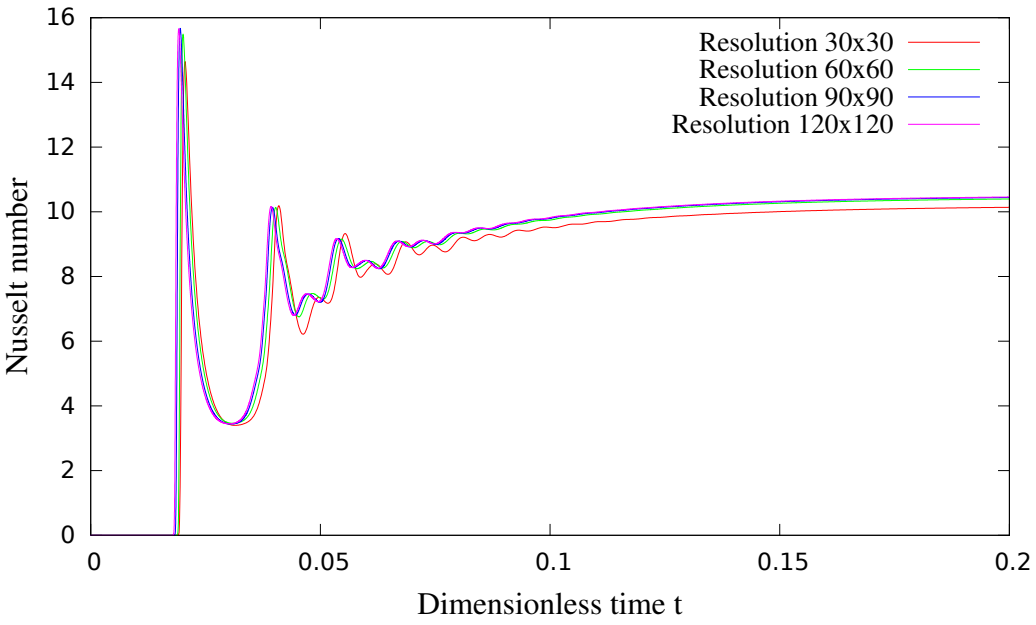

Figure 4.5: Evolution of Nusselt number of viscous model with Rayleigh number 10^5

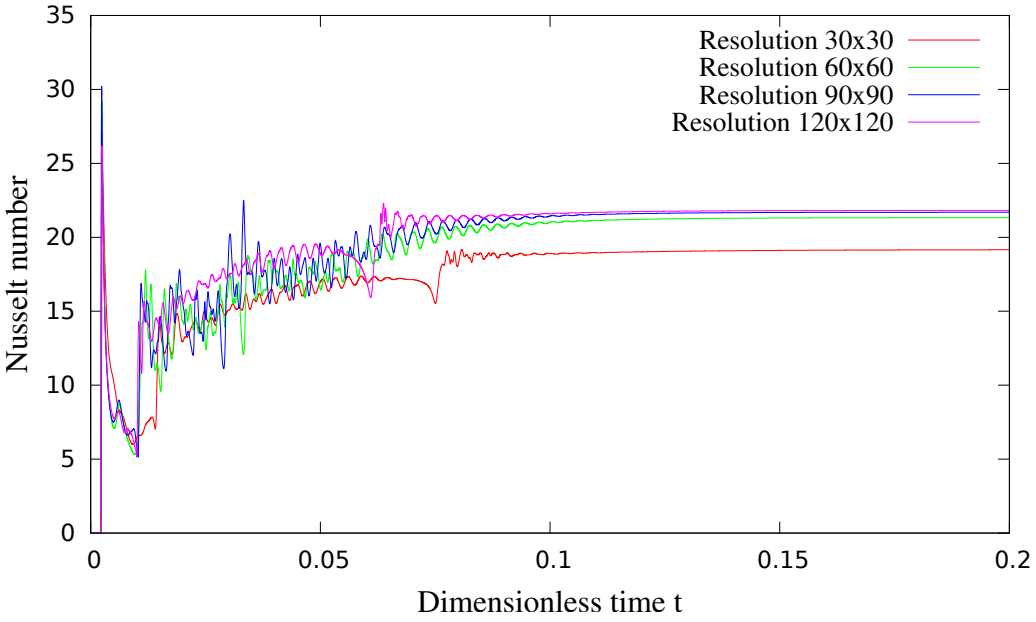

Figure 4.6: Evolution of Nusselt number of viscous model with Rayleigh number 10^6

have. Moreover, V. Patočka had improved the code, so that it provides computation also with the Maxwell model implemented in the version where the objective derivative is reduced to partial time derivative. Therefore, we compared our codes with this type of Maxwell model and we obtain several interesting results. Both ours and the code of V. Patočka diverge for Deborah number higher than 10^{-3}. However, we both have our steady Nusselt numbers compared to the Blankenbach benchmark [7]. Hence we wanted to compare something more, e.g. the evolution of Nusselt number during the time.

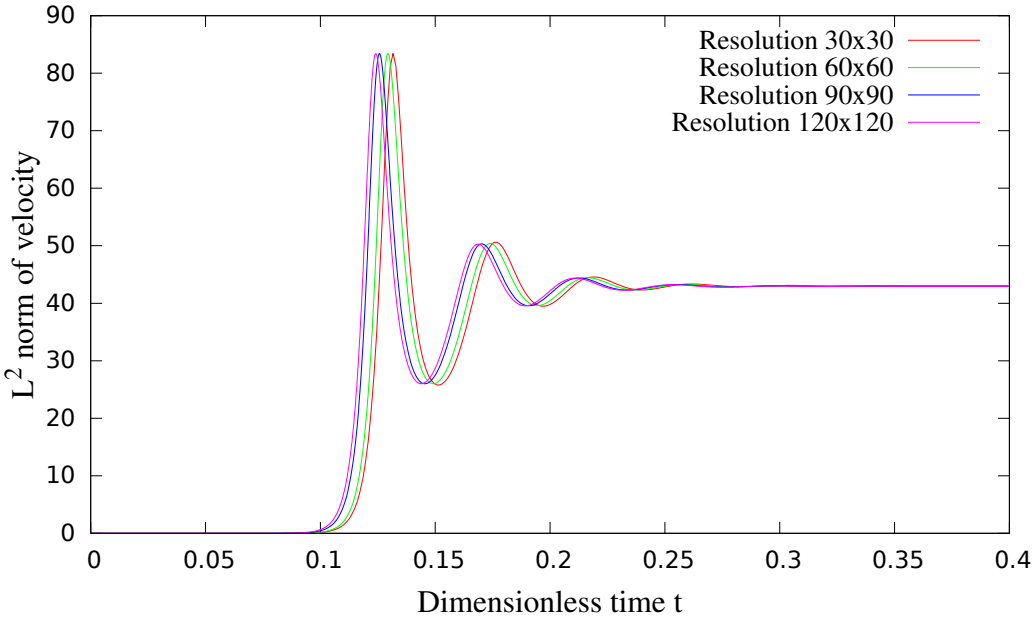

Figure 4.7: Evolution of the $\mathcal{L}^2$ norms of the velocity of viscous model with Rayleigh number 10^4

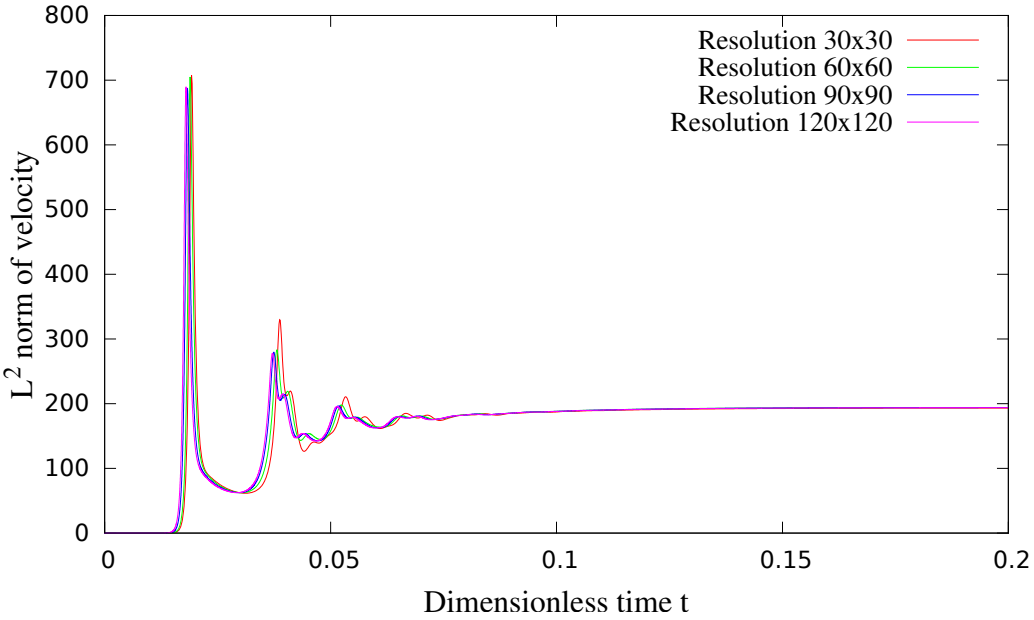

Figure 4.8: Evolution of the $\mathcal{L}^2$ norms of the velocity of viscous model with Rayleigh number 10^5

We started our computation from the initial value of temperature given by analytical function: $T(x,z) = z + 0.1\sin(2\pi x)\sin(\pi z)$. We chose the Rayleigh number in the middle of our range, i.e. Ra $= 10^5$, because too high Rayleigh number could lead to a chaotic behavior of the system and too low Rayleigh number may be controled by diffusion, resulting in only negligible or no deformation. Furthemore, we have chosen the Deborah number equal to 10^{-4} to obtain stable version of the Maxwell model. We employed high resolution (400×400) and we received very nice correspondance, see Figure 4.10.

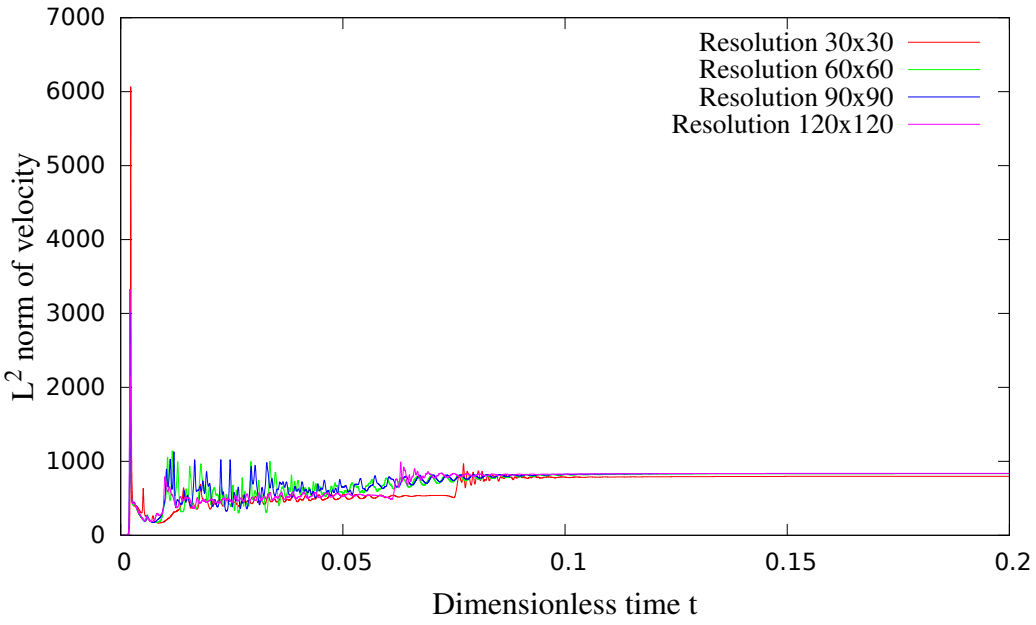

Figure 4.9: Evolution of the $\mathcal{L}^2$ norms of the velocity of viscous model with Rayleigh number 10^6

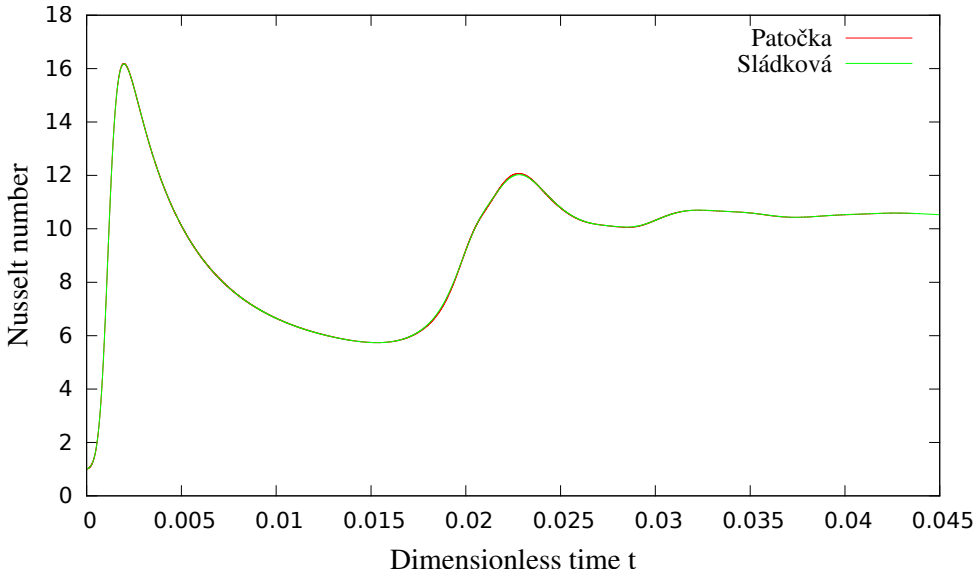

Figure 4.10: Benchmark of two codes via the evolution of Nusselt number

4.3 Oldroyd-B model

4.3.1 Oldroyd-B model with objective derivative substituted by partial time derivative

As far as we know there exist no benchmark for the Oldroyd-B model, therefore; we had to rely on expected behaviour of both Maxwell and Oldroyd-B model which mainly originates from the mechanical analogue of these two models.

Viscous limits

Firstly, we tested the limits of mentioned model, which should lead to viscous model. Afterwards the viscous limit was controled by the value of steady Nusselt number. First limit we tried to employ was that with very small Deborah number and very small stifness ratio, i.e. De $<<$ 1 and Vr $<<$ 1. By dropping the stiffness ratio to zero the limit of the model approaches Maxwell model and by limiting Deborah number to zero in the Maxwell model we approximate the viscous model. This test worked well.

Second limit was more sophisticated, we let the code work for some time with the Deborah number and stiffness ratio settled on finite numbers and when the program started to behave steadily we dropped the stiffness ratio to zero slowly. By doing that we should obtain Maxwell model, which has viscous limit. Thus, we obtained the viscous steady Nusselt number.

Time step and mesh refinement testing

Main thought of this testing is that model (or code) should behave nicer with time step shortening or mesh refinement, in ideal case it should find a limit. Therefore we present this test with setting chosen in advance as to assure the stability of the model. We stayed with the elementary setting the same as in following chapter, which provides the result of this work, i.e. $\mathrm{Ra} = 10^5, \mathrm{Vr} = 10^{-2}$. For explanation of this setting see next chapter. To assure the stability we have chosen the Deborah number equal to 10^{-3}. Figure 4.12 shows the test with following resolution: $60\times60, 120\times120$. The time step shortening was directed by decreasing the coefficient c in the Courrant criterion: $dt_{cour} = c\min(dt_{dif}, dt_{conv})$, $c \in (0, 1]$. Figure 4.11 shows the test for $c = 10^{-2}$, $c = 10^{-3}$ and $c = 10^{-4}$. As you can see both tests does not display much differences. Therefore, we can count this test beeing succesful.

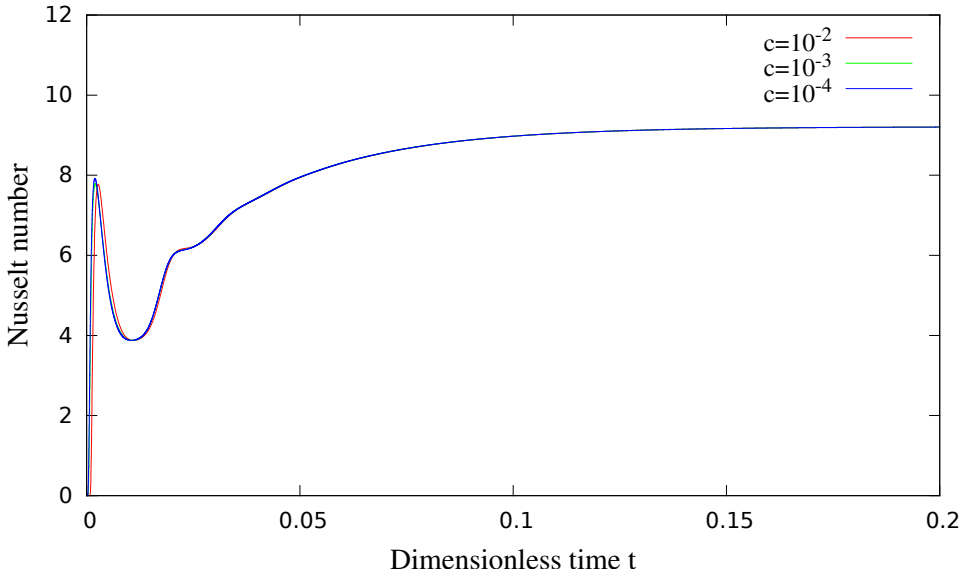

Figure 4.11: Time step shortening test presented via comparison of Nusselt numbers for Oldroyd-B model with the objective derivative substituted with partial time derivative

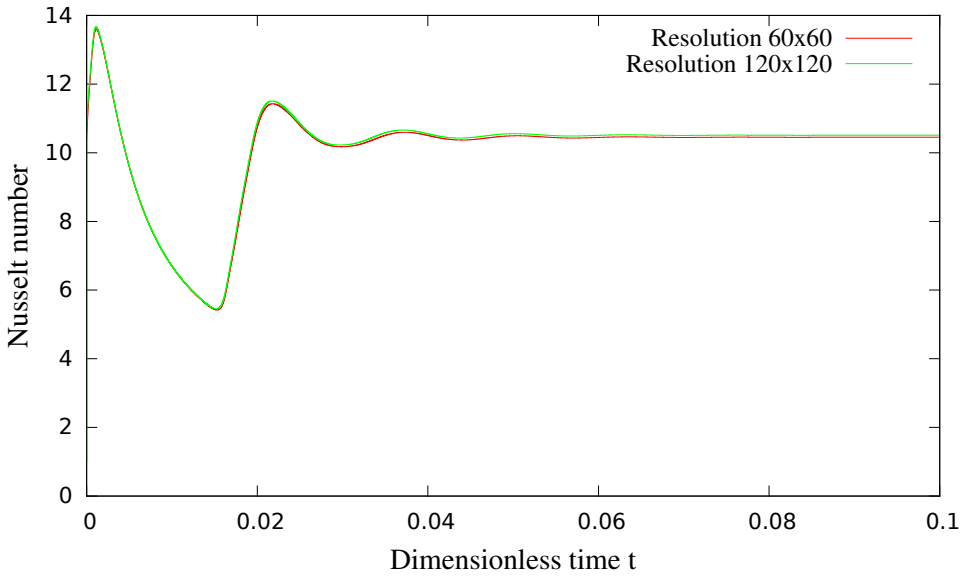

Figure 4.12: Mesh refinement test presented via comparison of Nusselt numbers for Oldroyd-B model with the objective derivative substituted with partial time derivative

4.3.2 Oldroyd-B model with the objective derivative replaced by partial time derivative and advection terms

Time step refinement test

We made similar test as for the setting above also for this type of model. Owing to the fact that the Oldroyd-B model with the objective derivative replaced by partial time derivative and advection terms provides more instability than the one with objective derivative substituted with partial time derivative we have employed smaller Deborah number for our test, i.e. $\mathrm{De} = 10^{-4}$, the other setting remains the same. That means we have $\mathrm{Ra} = 10^5, \mathrm{Vr} = 10^2$ and resolution is 60×60, the range of time coefficient from the Courrant criterion is also the same, i.e. $c = 10^{-2}$, $c = 10^{-3}$ and $c = 10^{-4}$. The results of this testing are depicted in Figure 4.13.

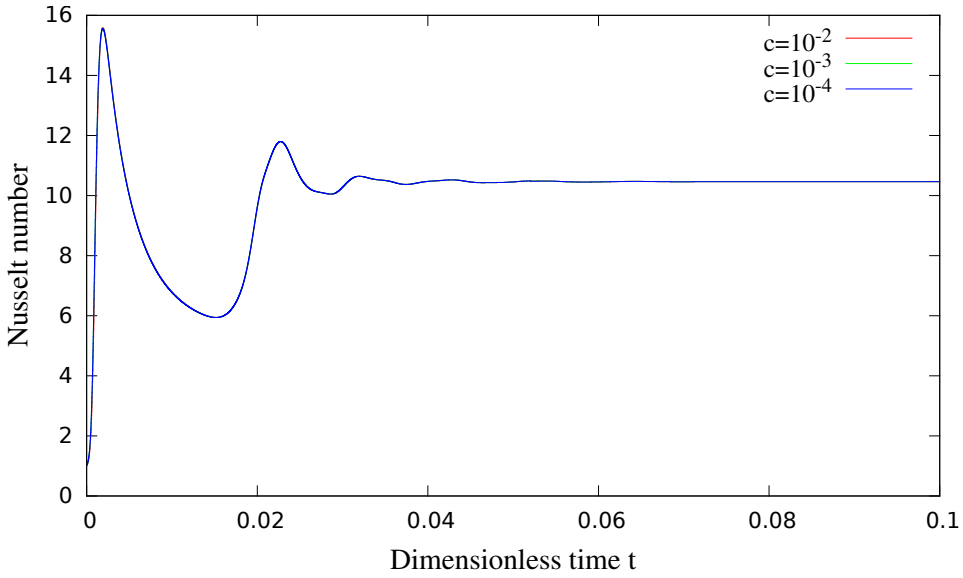

Figure 4.13: Mesh refinement test presented via comparison of Nusselt numbers for Oldroyd-B model, where the objective derivative is replaced by partial time derivative and advection terms

5. Results and discussion

In this chapter we present the preliminary results of our numerical simulations. Despite the incompleteness of the code, which still does not include the corrotation terms, we can show the results obtained for several values of De and use them to illustrate the possible role of the first two terms in the objective material derivative of stress, namely the partial derivative and the advection term. We will compare three basic settings. The first one is the thermal convection with a Newtonian rheology, the second one is the Oldroyd-B model where the objective material derivatives are reduced to partial derivatives, and the last one is the Oldroyd-B rheology with both partial time derivatives and advection terms implemented.

In all our tests, we will consider the Rayleigh number equal to 10^5. This value is significantly smaller that in the Earth's mantle but it is rather close to estimates obtained for other planets (Mercury, Mars) and icy satellites (Titan, Enceladus). The style of viscous convection for this value is in between the steady-state and chaotic regime (depending on the aspect ratio) and therefore it is suitable for the initial set of runs investigating the role of the elastic component: A too high Rayleigh number would lead to a chaotic behavior of the system and the calculations would be very time consuming and possibly also resolution-dependent. In contrast, if the Rayleigh number is too low, the diffusion may take control over the heat transport, resulting in only negligible or no deformation.

For the Deborah number, we consider three values: 10^{-4}, 10^{-3} and 10^{-2}. These values more or less correspond to what we can expect in the most viscous parts of planetary bodies. In the Earth's lithosphere, De does not excceed a value of 10^{-1}, but the most probable value is by one to two orders of magnitude lower. In the Earth's mantle, where temperature is rather high and viscosity drops to a value of about 10^{20} Pa s, value of the Deborah numbers is around 10^{-8} or lower. The last dimensionless parameter characterizing the system is the stiffness ratio Vr. Its value is chosen to assure the stability of the computer runs for the whole range of the Deborah numbers considered, and it is set to 10^{-2}. The initial temperature field is the same for all tested models and is given analytically as $T = z + 0.1 \sin(2\pi x) \sin(\pi z)$. The distribution of the intial temperature is depicted in Figure 5.1. The temperature scale in this figure is valid also for other temperature plots presented in this section.

To summarize, we will show the results for seven models. All the models are characterized by Ra=10^5. The first model is purely viscous (De=0), while the other six models correspond to different combinations of three Deborah number (De=10^{-4}, 10^{-3} and 10^{-2}) and two different settings (material derivative including only partial derivative vs. material derivative including both partial derivative and advection term). The presented models are computed for different resolutions, depending on the rate of chaotic behavior of the model - the more chaotic behavior, the higher resolution is needed for the correct run of code. Since the models with a larger Deborah number show more chaotic behavior than the purely viscous model (which finally reaches a steady state), they are computed with a higher resolution. The whole list of models is provided in Table 5.1 while the basic characteristics of the resultant computer runs (Nusselt number, style of

convection, resolution) are summarized in Table 5.2. The time evolution of the models will also be illustrated by a series of temperature snapshots and the time variations of the Nusselt number.

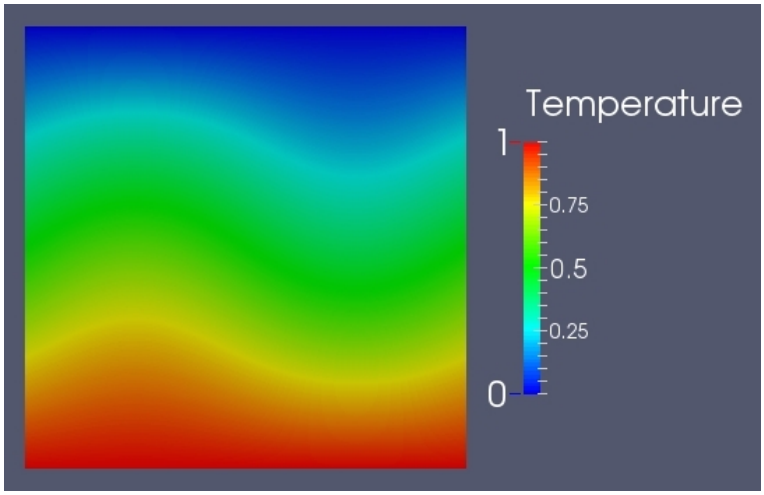

Figure 5.1: Initial temperature

	De	partial time derivative	advection term
Model no. 1	0	×	×
Model no. 2	10^{-4}	✓	×
Model no. 3	10^{-4}	✓	✓
Model no. 4	10^{-3}	✓	×
Model no. 5	10^{-3}	✓	✓
Model no. 6	10^{-2}	✓	×
Model no. 7	10^{-2}	✓	✓

Table 5.1: List of models

	Nusselt number	style of convection	resolution
Model no. 1	10.4548	steady state	60x60
Model no. 2	10.4217	steady state	60x60
Model no. 3	10.4639	steady state	60x60
Model no. 1		steady state	120x120
Model no. 4	10.4809	steady state	120x120
Model no. 5	around 10.4	different steady state	120x120
Model no. 1	10.5293	steady state	240x240
Model no. 6	15-55	chaotic	240x240
Model no. 7	around 30	strongly chaotic	240x240

Table 5.2: List of Nusselt numbers and description of behavior corresponding to models

The computer runs for models showing chaotic or unstable behaviour require a very high resolution and a very short time step. They take a lot of computer time and some of them have not yet reached a statistical steady state at the time when

this thesis is submitted. Nevertheless, we can still estimate (with reservation, of course) the probable behaviour of these models already on the basis of a limited time series. In Table 5.2, the cases where the statistical steady state has not yet been reached are marked in blue.

1. De = 10^{-4}
   We start our discussion with the viscoelastic models which have the lowest value of the Deborah number (De=10^{-4}, models 2 and 3 in Table 5.1). Both models reach a steady state characterized by a Nusselt number which only slightly differs from the viscous case (model 1, see Table 5.2). All three models easily "found" their stationary states even with rather a low spatial resolution, without showing any signature of chaotic behaviour (see Figs. 5.2 and 5.3). Inspecting the values of the Nusselt number in the stationary state, we can conclude that viscoelastic models with De=10^{-4} behave almost like a viscous model, independently of the considered form of material derivative.

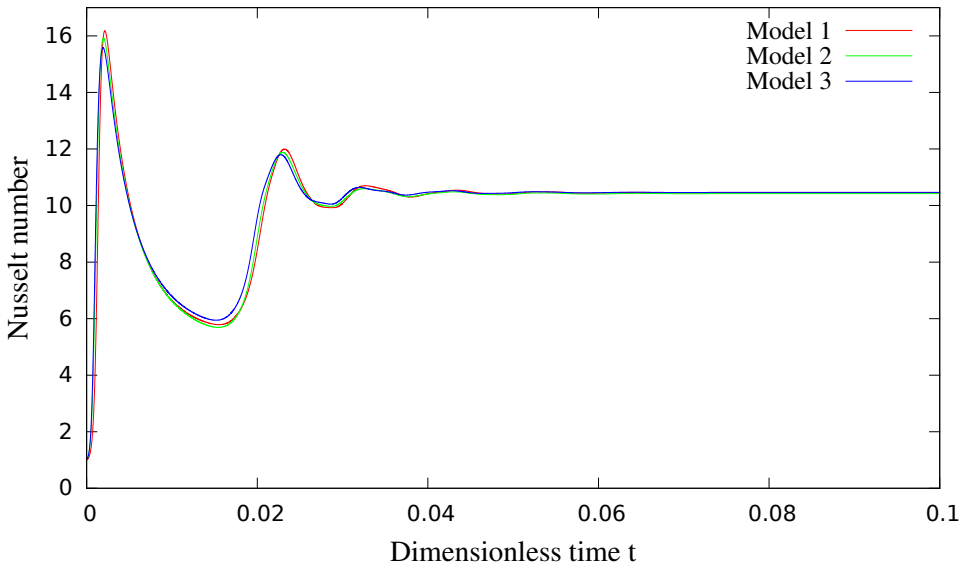

Figure 5.2: Evolution of the Nusselt number for models 1-3.

2. De = 10^{-3}
   With the increasing value of the Deborah number, the effect of viscoelastic deformation is getting more pronounced. For De=10^{-3} (models 4 and 5), the intial evolution of the Nusselt number (Fig. 5.4) significantly differs not only when compared with that obtained for the viscous model but also between models 4 and 5. While model 4 (including partial derivative only) quickly reaches a steady state with the Nusselt number close to the viscous value, model 5 (including both partial time derivative and advection) needs more time to find a stationary solution and shows oscillations about the stationary value even for the time where the other two models are steady (Fig.5.4). The time series is, however, still rather short for final conclusions to be drawn. However from the temperature field (see Fig. 5.5) we can conclude that model 5 probably finds different steady state than the other

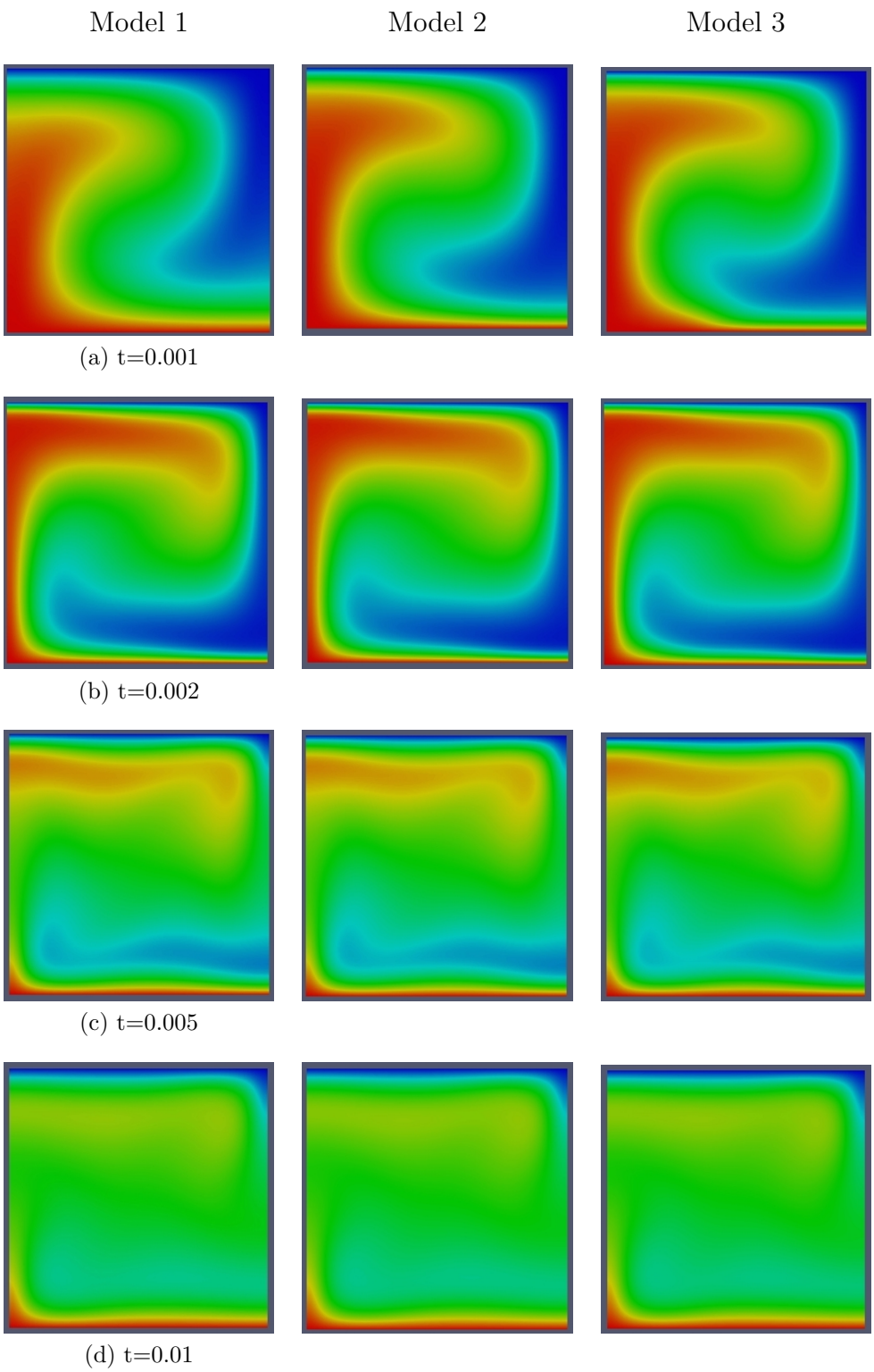

Figure 5.3: Evolution of temperature field for models 1-3 (columns) shown at four different time instants (rows).

models, even though it may be quasi-steady state and the final steady state would be the same. Our preliminary conclusion for models with De=10^{-3} is that with the advection terms implemented the model shows unstable behavior. To assess whether this behavior is physical or only results from numerical instabilities will require more numerical tests with different spatial and temporal resolution.

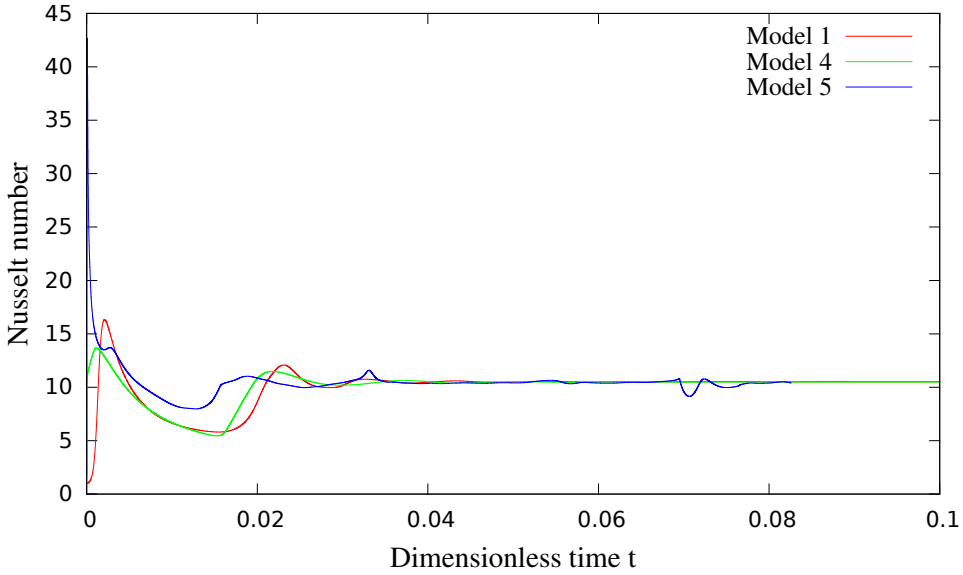

Figure 5.4: Evolution of the Nusselt number for models 1, 4 and 5.

3. De = 10^{-2}
   For De = 10^{-2}, we obtain a chaotic behavior even for the Oldroyd-B model without advection term (model 6, see Figs. 5.6 and 5.7). Therefore, we can also expect a chaotic behavior for model 7 where the non-linear advection term is included. Our preliminary results indicate that this is indeed the case (Fig. 5.8). Unfortunately, the computed time series is still rather short to allow a more specific discussion. To obtain a stable numerical behavior when running this model, we must use a very high (240x240) resolution and also a very short time step, which makes the calculation extremely longish, with one run taking three weeks by now on the computer cluster of the Department of Geophysics.

   Figures 5.6 and 5.7 show that for model 6 the Nusselt number oscillates between 15 and 60, with the latter number being nearly six times larger than the value obtained for a purely viscous model. The shape of the Nusselt curve clearly confirms a chaotic behavior of the model, which is also obvious from the time evolution of the temperature field (Fig. 5.9). As already mentioned, model 7 has not yet reached a statistically stable state and the results for it will be available later.

   To summarize, the models with De = 10^{-2} are likely to show a chaotic behavior with a very high value of the Nusselt number. The role of elastic deformation is crucial in this case because it completely changes the style of thermal convection (from steady state to chaotic) in comparison with

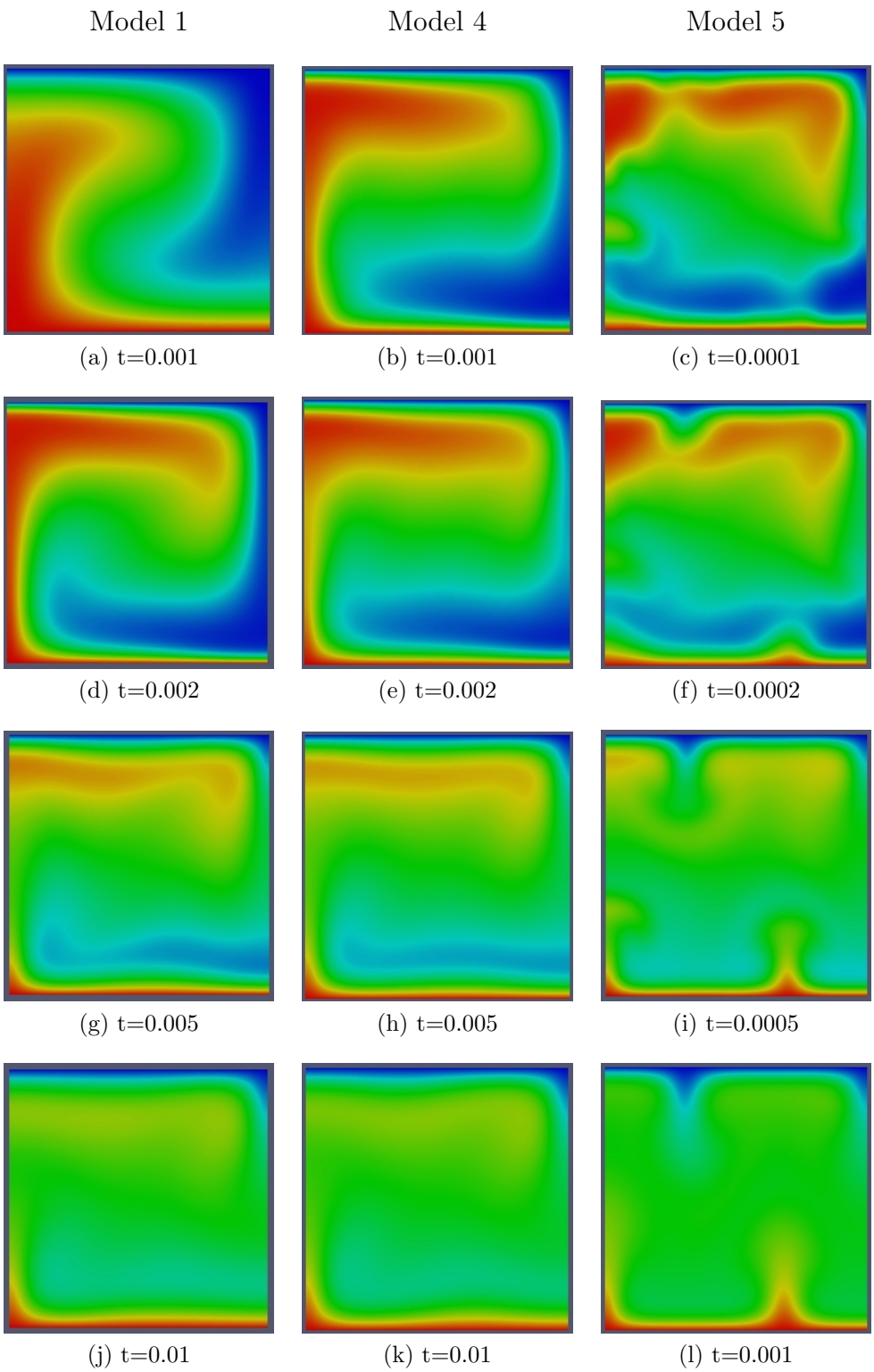

Figure 5.5: Evolution of temperature field for models 1,4-5 (columns) shown at eight different time instants (rows).

the viscous model and dramatically (up to six times) increases the amount of heat transported between the lower and upper boundary. Our results suggest that for Ra=10^5 and Vr=10^{-2}, the critical value of the Deborah number, marking the transition between the steady state and chaotic convection, lies somewhere in between the values of 10^{-3} and 10^{-2}. This value is still acceptable for some of planetary bodies and this finding thus may have potentially important consequences for our view of planetary convection systems. More modeling work is however needed to clarify the role of parameter Vr and to carefully test the numerical implementation. [1]

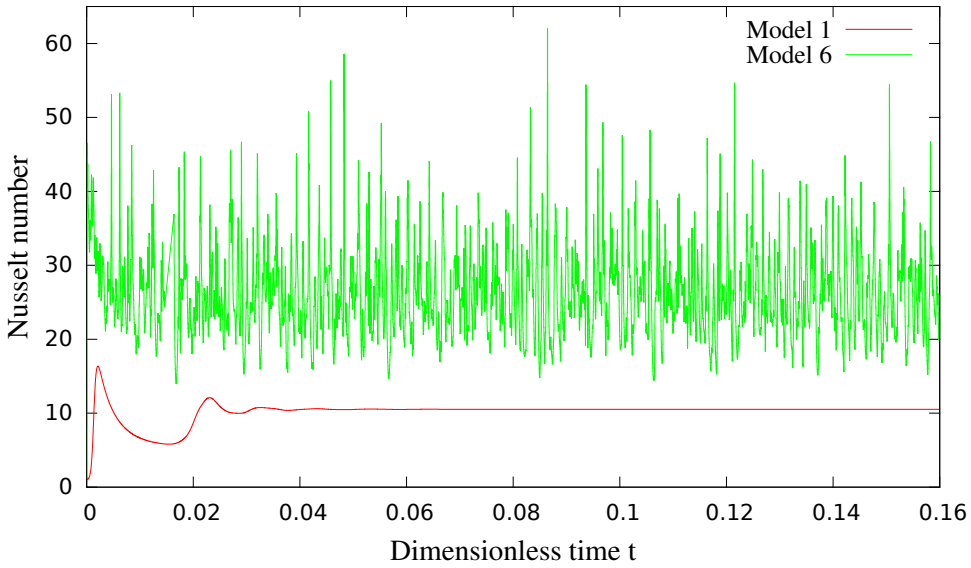

Figure 5.6: Evolution of the Nusselt number for models 1 and 6

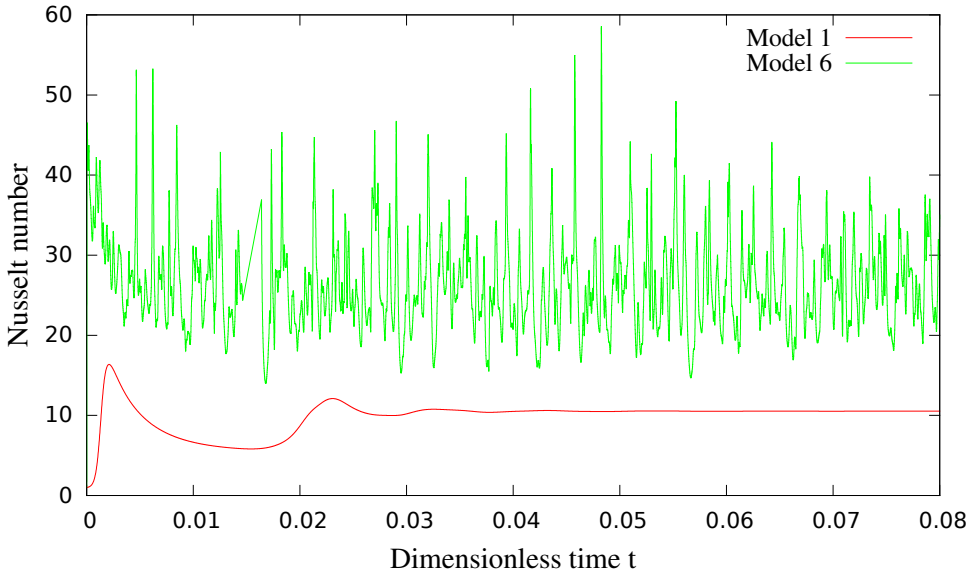

Figure 5.7: Evolution of the Nusselt number for models 1 and 6 (a detail).

[1] The videos of the evolution of the temperature field can be found on attached DVD.

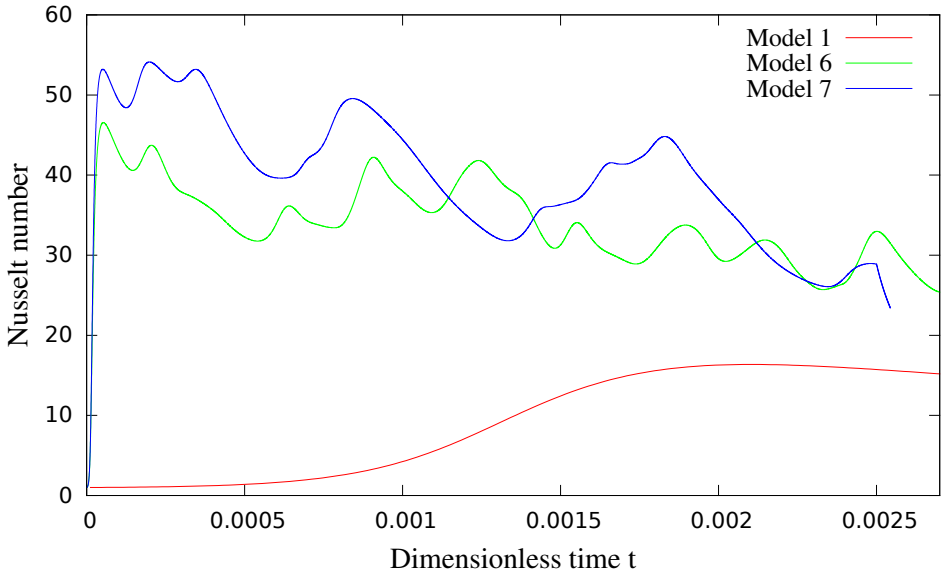

Figure 5.8: Evolution of the Nusselt number for models 1, 6 and 7

Model 6

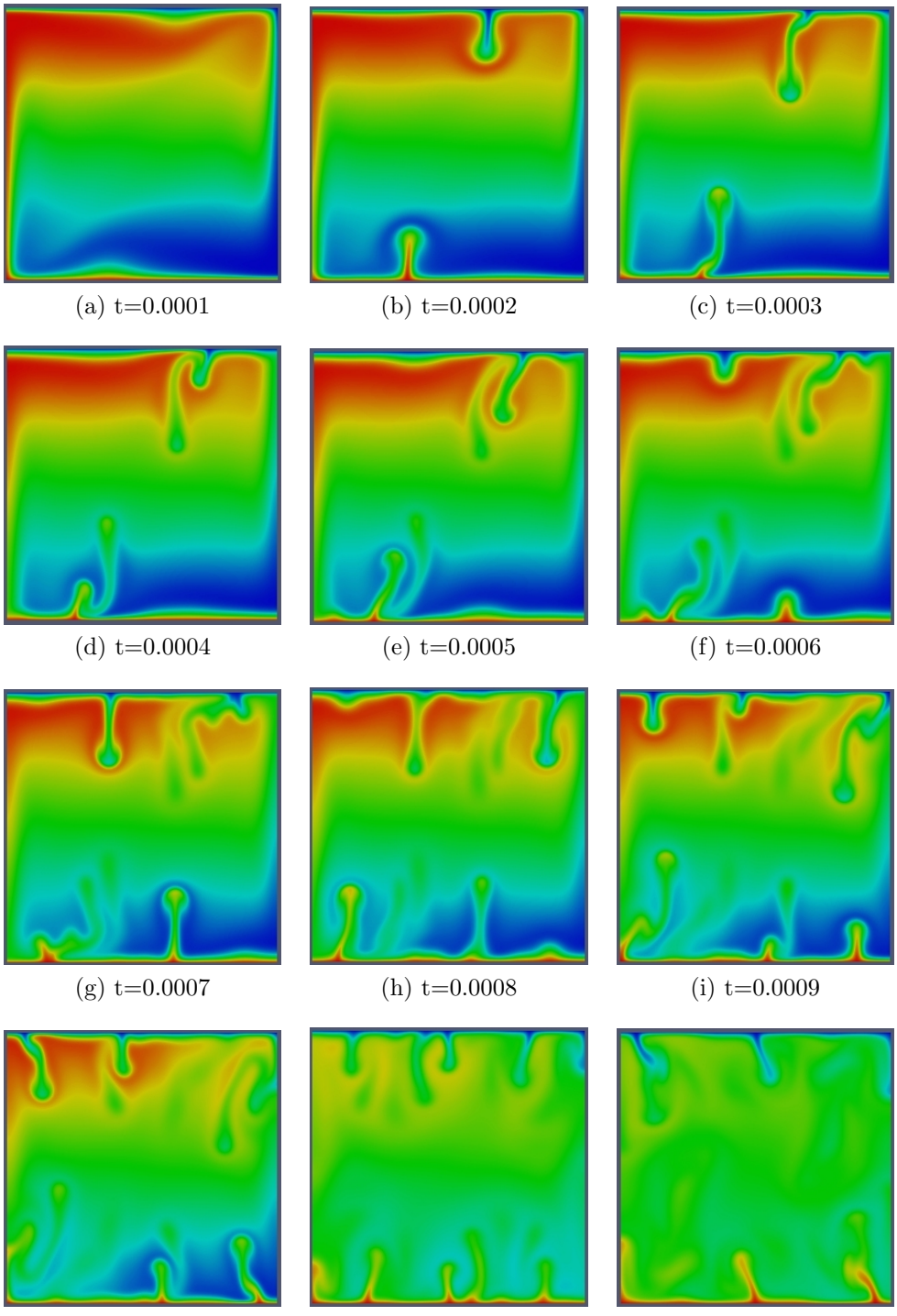

(a) t=0.0001 (b) t=0.0002 (c) t=0.0003

(d) t=0.0004 (e) t=0.0005 (f) t=0.0006

(g) t=0.0007 (h) t=0.0008 (i) t=0.0009

(j) t=0.001 (k) t=0.002 (l) t=0.003

Figure 5.9: Evolution of temperature field for models 6 different time instants

6. Conclusion

6.1 Summary of the work

In the present thesis we have attempted to answer two questions related to geophysical modeling of thermally induced viscoelastic flow. The first question concerns the possibility of implementing the viscoelastic rheology in a traditional numerical code, originaly developed to simulate viscous flow. Is this strategy, which looks very attractive at first sight and is reported as successful by some authors, really feasible and numerically stable? The other question is physical: Is the effect of elastic deformation on thermal convection in a planetary mantle important, or it can be neglected and the flow can be well approximated by a viscous model? The general opinion in the geophysical community is that elasticity plays only a minor role in mantle convection. That is why the numerical codes used to study the thermal evolution of planetary bodies are mostly viscous and the elastic deformation is either completely omitted or implemented in terms of a formal viscosity, resulting from the application of a backward Euler scheme to the time derivative of stress and depending on the time step and the shear modulus.

To answer the former question, we have first developed and tested a new Fortran 90 code to model thermal convection in a 2-dimensional cartesian domain with a Newtonian rheology. The code employs a finite-difference staggered-grid method in spatial domain and an Adams-Bashforth integration scheme in time (both methods are common in contemporary geophysical fluid modeling). The code was carefully tested and benchmarked against the Blankenbach test [7]. In this code, we implemented a linear Maxwell rheology (hence without advection and rotation of stress) using the numerical strategy indicated above. The code was tested for small Deborah numbers against the code of Paul Tackley, adapted to the case of the Maxwell rheology by V. Patočka (personal communication). The agreement of the solutions was excellent but both codes diverged for the Deborah number larger than 10^{-3}. The reason of this behaviour is likely the fact that the formal viscosity goes to zero with the decreasing time step. Although, at a first sight, this problem can be attributed to the numerical method used, it is a pitfall inherent to the Maxwell rheology if the equations are formulated in velocities: When a Maxwell body is loaded, its instantaneous response is purely elastic and the velocity goes to infinity, which corresponds to the case of zero viscosity. Motivated by this finding, we decided to replace the Maxwell model by the Oldroyd-B model, which is numerically more stable and acceptable from the physical point of view. The numerical implementation of all terms arising from the use of this model was rather elaborate since the constitutive law contains objective material derivatives of both stress and strain rate. Each of these derivatives can be split into a partial derivative with respect to time, advection term and corrotational terms. We successfully implemented only the first two terms - partial derivative and advection; in spite of enormous effort we have not yet succeeded in including the corrotational terms.

The question of physical importance of viscoelasticity could thus be answered only by using a preliminary version of the code without the corrotational terms. Since the computations with the viscoelastic rheology were rather time-consuming,

we could run only a limited number of thermal convection models. That is why we fixed the Rayleigh number (Ra=10^5) and the ratio between the two viscosities of the Oldroyd-B model (Vr=10^{-2}) and we only tested the effect of the Deborah number. While for small values of the Deborah number (De=10^{-4} and 10^{-3}) the differences between the viscous and viscoelastic solutions were negligible (De=10^{-4}) or only small (De=10^{-3}), strikingly large effects were found for De=10^{-2}. For this value, the convective system does not reach a steady state solution as in the viscous case, but moves towards a strongly chaotic regime with a Nusselt number that is several times larger than in the viscous model. The role of elastic deformation is crucial in this case because it completely changes the style of thermal convection in comparison with the viscous model and dramatically increases the amount of heat transported between the lower and upper boundary. The transition between the steady state and chaotic convection lies somewhere in between the values of 10^{-3} and 10^{-2}. This value is still acceptable from the geophysical point of view and this finding may thus indicate that the neglect of elasticity can affect our physical interpretation of the studied convection system.

A number of questions, however, remains open. First, it is not yet clear how much the solution depends on the choice of parameter Vr. This parameter is mainly used to stabilize the numerical behavior of the code and its real value is not known from geophysical observations. It is clear that the code will crash if the value of Vr is chosen too small since the Oldroyd-B model transform to a Maxwell model for Vr=0. We should also test the behavior of the viscoelastic system for larger values of Ra and for different spatial and temporal resolutions. To make the model realistic, one should also include a temperature-dependent viscosity varying over severals order of magnitude. We believe that we will be able to answer at least some of these questions in a next study.

6.2 Achieved results

The results of our work can be summarized in the following points:
(i) We have developed a new Fortran 90 code to simulate thermal convection in a 2d cartesian domain with a constant viscosity. The code was carefully tested and found valid even for large Rayleigh numbers.
(ii) The code was used to test the standard implementation of the Maxwell rheology used in geophysics. We found that this implementation is numerically unstable for large values of the Deborah number and requires a regularization which can, however, affect the physical interpretation of the results.
(iii) We used the same numerical strategy as in (ii) but we replaced the Maxwell model by the Oldroyd-B model. This model was found numerically more stable than the Maxwell model.
(iv) We have successfully implemented the linearized version of the Oldroyd-B model and we tested two numerical schemes to implement the non-linear advection term. The problem of stress and strain rate advection was finally successfuly solved using the upwind scheme.
(v) For an intermediate value of the Rayleigh number (Ra=10^5) we performed a series of thermal convection runs which suggested the important role of elastic deformation for Deborah numbers De $\sim 10^{-2}$ and larger.

6.3 Résumé

The growing interest in viscoelastic models in geophysics motivated us to test the numerical implementation of Maxwellian viscoelasticity used in some studies of thermal convection. This implementation consists in modification of an originally viscous model by introducing a new parameter that formally replaces viscosity and depends also on the time step and the shear modulus. To test this implementation, we developed a new Fortran 90 code to simulate thermal convection of viscous materials, we carefully tested it and modified it using the formal viscosity parameter. We found that in the case of a Maxwell rheology this kind of implementation is numerically unstable and must be regularized which, however, may obscure the physical interpretation of the results. In the next step, to avoid the numericabl difficulties, we replaced the Maxwell model by an Oldroyd-B model, which is numerically more stable and it probably better approximates the mechanical behavior of geomaterials. We successfuly implemented in our code the linearized form of this rheological model as well as its non-linear (but not yet fully general) form including advection of stress and strain rate. Our attempt to include the corrotation terms has not yet been successful and will require more effort. Using this code, we explored the role of elastic deformation for the Rayleigh number 10^5 and the stiffness ratio (ratio between the two viscosities considered in Oldroyd-B model) 10^{-2}. We found that the effect of elastic deformation can be significant already for Deborah numbers between 10^{-3} and 10^2 which has potentially important consequences for geophysical interpretations of thermal convection systems.

Bibliography

[1] Gerya T. V.,
Introduction to Numerical Geodynamic modelling,
Cambridge University Press, 2010, ISBN 978-0-521-88754-0.

[2] Gerya T. V., Yuen D. A.,
Characteristics-based marker-in-cell method with conservative finite-differences schemes for modeling geological flows with strongly variable transport properties,
Physics of the Earth and Planetary Interiors, 140, 293-318, 2003.

[3] Gerya Taras V., Yuen David A.,
Robust characteristics method for modelling multiphase visco-elasto-plastic thermo-mechanical problems,
Physics of the Earth and Planetary Interiors, 63, 83-105, 2007.

[4] Harder H.,
Numerical simulation of thermal convection with Maxwellian viscoelasticity,
Journal of Non-Newtonian Fluid Mechanics, 39, 67-88, 1991.

[5] Průša V., Rajagopal K. R.,
On models for viscoelastic materials that are mechanically incompressible and thermally compressible or expansible and their Oberbeck-Boussinesq type approximations,
Mathematical Models and Methods in Applied Sciences, 23, 1761-1794, 2013.

[6] Schubert G., Turcotte D. L., Olson P.,
Mantle Convection in the Earth and Planets,
Cambridge University Press, 2011, ISBN 0-521-70000-0.

[7] Blankenbach B., Busse F., Christensen U., Gunkel D., Hansen U., Harder H., Jarvis G., Koch M., Marquart G., Moore D., Olson P., Schmeling H., Schnaubelt T.
A benchmark comparison for mantle convection codes,
Geophysical Journal International, 98, 23-38, 1988.

[8] Fornberg B.,
A Practical Guide to Pseudospectral Methods,
Cambridge University Press, 1998, ISBN 0-521-64564-6.

[9] Matyska C.,
Mathematical introduction to geothermics and geodynamics(lecture notes),
Department of Geophysics, Faculty of Mathematics and Physics, Charles University in Prague, 2005.

[10] Feistauer M.,
Základy numerické matematiky,
Faculty of Mathematics and Physics, Charles University in Prague.

[11] Tůma K.,
Identification of rate type fluids suitable for modeling geomaterials, Ph.D. thesis
pp. 198, Charles University, Prague, 2013.

[12] IMSL library, *User's Guide* (online),
`http://www.roguewave.com/DesktopModules/Bring2mind/DMX/Download.aspx?entryid=519&command=core_download&PortalId=0&TabId=607`

[13] Tackley P.J.,
Convection2D.m, MATLAB code for mantle convection (online)
`http://jupiter.ethz.ch/~pjt/Convection2D.m`

[14] Tackley P.J.,
Mantle convection and plate tectonics: Toward an integrated physical and chemical theory,
Science, 288, 2002-2007, 2010.

[15] Šrámek O., Zhong S.J.,
Long-wavelength stagnant lid convection with hemispheric variation in lithospheric thickness: Link between Martian crustal dichotomy and Tharsis?,
Journal of Geophysical Research-Planets, 115, E09010, 2010.

[16] Choblet G., Čadek O., Couturier F., Dumoulin C.,
OEDIPUS: a new tool to study the dynamics of planetary interiors,
Geophysical Journal International, 170, 9-30, 2007.

[17] Regenauer-Lieb K., Yuen D.A.,
Rapid conversion of elastic energy into plastic shear heating during incipient necking of the lithosphere,
Geophysical Research Letters, 25, 2737-2740, 1998.

[18] Zhong, S.J.,
Effects of lithosphere on the long-wavelength gravity anomalies and their implications for the formation of the Tharsis rise on Mars,
Journal of Geophysical Research-Planets, 107, 5054, 2002.

[19] Moresi L., Dufour F., Muhlhaus H.B.,
A Lagrangian integration point finite element method for large deformation modeling of viscoelastic geomaterials,
Journal of Computational Physics, 184, 2003.

[20] Dumoulin C., Čadek O., Choblet G.,
Predicting surface dynamic topographies of stagnant lid planetary bodies,
Geophysical Journal International, 195, 1494-1508, 2013.

[21] Dziewonski A.M., Anderson D.L.,
Preliminary reference Earth model,
Physics of the Earth and Planetary Interiors, 25, 297-356, 1981.

[22] Čížková, H., van den Berg A.P., Spakman W., Matyska C.,
The viscosity of Earth's lower mantle inferred from sinking speed of subducted lithosphere,
Physics of the earth and Planetary Interiors, 200, 56-62, 2012.

[23] Wu P., Peltier W.R.,
Glacial isostatic-adjustment and the free air gravity-anomaly as a constraint on deep mantle viscosity,
Geophysical Journal of the Royal Astronomical Society, 74, 377-449, 1983.

Appendix A
Oldroyd-B model

We would like to present the Oldroyd-B model more thoroughly in this section. The Oldroyd-B model is developed from Maxwell model by adding one dashpot parallely or in terms of models by adding viscous Newton term to the Maxwell model. YThe mechanical analogue is depicted in Fig. 6.1. From the fact that

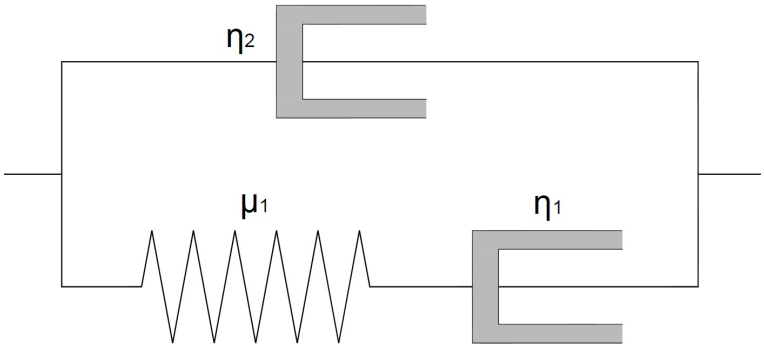

Figure 6.1: Oldroyd model

the model is built from Maxwell model by adding another dashpot we know that this model behaves more like fluid than Maxwell model.

The derivation of the model with help of mechanical analogue

We will derive the constitutive relation in one dimensional version of the models with the help of mechanical analogue. Firstly we remind what holds for linear spring and linear dashpot. Let us denote the forces in whole element, spring and dashpot by F, F_S, F_D, respectively and the prolongation in whole element, spring and dashpot by $\delta, \delta_S, \delta_F$, also respectively. Following relations holds for these two elements:

$$F_S = \mu\delta_2,\ \sigma_S = \mu\varepsilon_S, \qquad \text{where} \quad \varepsilon_S = \frac{\delta_S}{l_0}, \sigma_S = \frac{F_S}{l_0} \tag{6.1}$$

$$F_D = \eta\dot{\delta_D},\ \sigma_D = \eta\dot{\varepsilon_D}, \qquad \text{where} \quad \varepsilon_D = \frac{\delta_D}{l_0}, \sigma_D = \frac{F_D}{l_0} \tag{6.2}$$

$$\tag{6.3}$$

and l_0 is the length of whole element. Now we derive the relation between the stres σ and the strain ε in the Maxwell model and afterwards we add the second dashpot and derive the constitutive relation for Oldroyd-B model. In the series connection the whole prolongation is sum of the prolongation in the dashpot and the spring. On the other hand the stress is the same in both parts of the Maxwell element. Therefore, we have:

$$\delta = \delta_S + \delta_D,\ \sigma = \sigma_D = \sigma_S \tag{6.4}$$

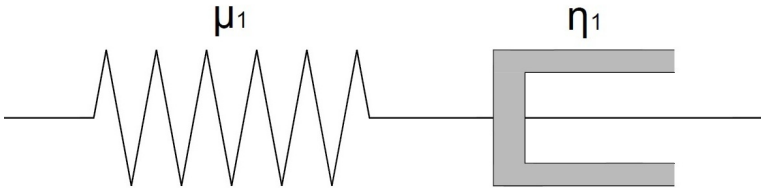

Figure 6.2: Maxwell model

Thus, we have

$$\dot{\delta} = \dot{\delta_S} + \dot{\delta_D} \tag{6.5}$$

$$\dot{\varepsilon} = \frac{\dot{\delta_S}}{l_0} + \frac{\dot{\delta_D}}{l_0} = \frac{\dot{F_S}}{\mu_1 l_0} + \frac{F_D}{\eta_1 l_0} \tag{6.6}$$

$$\dot{\varepsilon} = \frac{\dot{\sigma_S}}{\mu_1} + \frac{\sigma_D}{\eta_1} \tag{6.7}$$

We have the constitutive relation for Maxwell model and we will derive the relation for Oldroyd-B model. The Oldroyd-B model is, as we know, the Maxwell model contected to second dahspot parallelly. For the parallel connection it holds that the prolongations are the same in both parts and the stress for whole element is counted as sum of stress in both parts. We denote the physical properties of Maxwell model by subscript $_M$ and for the second dashpot by subscriot $_{D_2}$. Therefore, we have:

$$\delta = \delta_{D_2} = \delta_M \tag{6.8}$$

$$\varepsilon l_0 = \varepsilon_{D_2} l_0 = \varepsilon_S l_0 \tag{6.9}$$

$$\sigma = \sigma_M + \sigma_{D_2} \tag{6.10}$$

$$\frac{1}{\mu_1}\dot{\sigma} + \frac{1}{\eta_1}\sigma = \frac{1}{\mu_1}(\dot{\sigma}_M + \dot{\sigma}_{D_2}) + \frac{1}{\eta_1}(\sigma_M + \sigma_{D_2}) \tag{6.11}$$

$$= \frac{1}{\mu_1}\dot{\sigma}_{D_2} + \frac{1}{\eta_1}\sigma_{D_2} + \dot{\varepsilon}_M \tag{6.12}$$

Now we use the relation for stress in dashpot $\sigma_{D_2} = \eta_2 \dot{\varepsilon}_{D_2}$ and also the equality of strains in both parts of the model $\varepsilon = \varepsilon_{D_2} = \varepsilon_S$ to obtain:

$$\frac{1}{\mu_1}\dot{\sigma} + \frac{1}{\eta_1}\sigma = \frac{\eta_2}{\mu_1}\ddot{\varepsilon}_{D_2} + \frac{\eta_2}{\eta_1}\dot{\sigma}_{D_2} + \dot{\varepsilon}_M \tag{6.13}$$

$$= \frac{\eta_2}{\mu_1}\ddot{\varepsilon} + \left(1 + \frac{\eta_2}{\eta_1}\right)\dot{\varepsilon} \tag{6.14}$$

By multiplaying last relation with η_1 we get the Oldroyd model in most used version:

$$\sigma + \frac{\eta_1}{\mu_1}\dot{\sigma} = \frac{\eta_1\eta_2}{\mu_1}\ddot{\varepsilon} + (\eta_1 + \eta_2)\dot{\varepsilon} \tag{6.15}$$

However, we need the model in two dimensional real space; thus we need to convert the model. We replace the stress σ with deviatoric part of Cauchy stress tensor $\mathcal{S}$ and the $\dot{\epsilon}$ with the symmetric part of velocity gradient $\mathcal{D}$. One of the problems of model obtained by that substitution is that neither the time derivative nor material derivative are objective derivatives; thus, we have to replace them

by some kind of objective derivative. But there exist plenty of types of objective derivatives so that process is not unique. If we use the upper convected Oldroyd derivative $\overset{\triangledown}{\gamma} := \frac{\partial \gamma}{\partial t} + \mathbf{v} \cdot \nabla \gamma - \nabla \mathbf{v} \gamma - \gamma (\nabla \mathbf{v})^T$ we obtain model which is called Oldroyd-B.

$$\mathcal{S} + \frac{\eta_1}{\mu_1} \overset{\triangledown}{\mathcal{S}} = (\eta_1 + \eta_2)\mathcal{D} + \frac{\eta_1 \eta_2}{\mu_1} \overset{\triangledown}{\mathcal{D}} \tag{6.16}$$

Appendix B
Numerical equations

Equations of motion

We start from the equation discretized in second chapter 2.5 and we will discretize them properly.

$$
\begin{aligned}
- \quad & \frac{p_{i+1,j}-p_{i,j}}{dx} + 2\frac{v_{x_{i+1,j}} - 2v_{x_{i,j}} + v_{x_{i-1,j}}}{dx^2} + \frac{1}{2dz}\Big(\frac{v_{x_{i,j+1}} - v_{x_{i,j}}}{dz} \\
& + \frac{v_{z_{i+1,j}} - v_{z_{i,j}}}{dx} - \frac{v_{x_{i,j}} - v_{x_{i,j-1}}}{dz} - \frac{v_{z_{i+1,j-1}} - v_{z_{i,j-1}}}{dx}\Big) = 0, \\
- \quad & \frac{p_{i,j+1}-p_{i,j}}{dz} + 2\frac{v_{z_{i,j+1}} - 2v_{z_{i,j}} + v_{z_{i,j-1}}}{dz^2} + \frac{1}{2dz}\Big(\frac{v_{x_{i,j+1}} - v_{x_{i,j}}}{dz} \\
& + \frac{v_{z_{i+1,j}} - v_{z_{i,j}}}{dx} - \frac{v_{x_{i-1,j+1}} - v_{x_{i-1,j}}}{dz} - \frac{v_{z_{i,j}} - v_{z_{i-1,j}}}{dx}\Big) = 0.
\end{aligned}
$$

Oldroyd-B model with objective derivative reduced to partial time derivative

By employing only the partial time derivative and using Euler backward scheme we obtain following formula for the computation of the stress in current time step, for derivation see Figure 2.27:

$$
\begin{aligned}
\mathcal{S}^n \quad = \quad & \frac{\mathrm{De}}{dt_n + \mathrm{De}}\mathcal{S}^{n-1} + \left(\nabla \mathbf{w}^n + \left(\nabla \mathbf{w}^n\right)^T\right) \\
& - \frac{\mathrm{VrDe}}{dt_n + \mathrm{De}} \frac{dt^{n-1} + \mathrm{De}}{dt^{n-1}(1+\mathrm{Vr}) + \mathrm{DeVr}} \left(\nabla \mathbf{w}^{n-1} + \left(\nabla \mathbf{w}^{n-1}\right)^T\right)
\end{aligned}
$$

For the evaluation of the "new" right hand side we need following expression $-\nabla \cdot \mathcal{S}^n$, with knowing that $\left(\nabla \mathbf{w}^n + \left(\nabla \mathbf{w}^n\right)^T\right)$ is already composed in the left hand side of the equation. We will also utilize the equation of motion as follows $-\nabla p + \nabla \cdot \mathcal{S} = \mathrm{Ra}T\mathbf{e}_z$ for easier computation of $\nabla \cdot \mathcal{S}^{n-1}$.
Right hand side in x-coordinate:

$$
\begin{aligned}
= \quad & -\frac{\mathrm{De}}{dt_n + \mathrm{De}}\left(\frac{\partial p^{n-1}}{\partial x}\right) + \frac{\mathrm{VrDe}}{dt_n + \mathrm{De}} \frac{dt^{n-1} + \mathrm{De}}{dt^{n-1}(1+\mathrm{Vr}) + \mathrm{DeVr}} \cdot \\
& \left(2\frac{\partial^2 w_x^{n-1}}{\partial^2 x^2} + \frac{\partial^2 w_x^{n-1}}{\partial^2 z^2} + \frac{\partial^2 w_z^{n-1}}{\partial x \partial z}\right)
\end{aligned}
$$

Right hand side in z-coordinate:

$$
\begin{aligned}
= \quad & -\mathrm{Ra}T^n - \frac{\mathrm{De}}{dt_n + \mathrm{De}}\left(\frac{\partial p^{n-1}}{\partial z} - \mathrm{Ra}T^{n-1}\right) + \\
& \frac{\mathrm{VrDe}}{dt_n + \mathrm{De}} \frac{dt^{n-1} + \mathrm{De}}{dt^{n-1}(1+\mathrm{Vr}) + \mathrm{DeVr}} \cdot \\
& \left(2\frac{\partial^2 w_z^{n-1}}{\partial^2 z^2} + \frac{\partial^2 w_z^{n-1}}{\partial^2 x^2} + \frac{\partial^2 w_x^{n-1}}{\partial x \partial z}\right)
\end{aligned}
$$

Expressed via finite differences

Right hand side in x-coordinate:

$$
\begin{aligned}
&= -\frac{\mathrm{De}}{Dt^n + \mathrm{De}} \left(\frac{2(p^{n-1}_{i+1,j} - p^{n-1}_{i,j})}{dx_i + dx_{i+1}} \right) \\
&+ \frac{\mathrm{De}\,\eta_2}{dt_n + \mathrm{De}} \frac{dt^{n-1} + \mathrm{De}}{dt^{n-1}(1+\eta_2) + \mathrm{De}\,\eta_2} \\
&\Big\{ \frac{2}{dx^2} \big(w^{n-1}_{x_{i-1,j}} - 2w^{n-1}_{x_{i,j}} + w^{n-1}_{x_{i+1,j}} \big) \\
&+ \frac{1}{dz^2} \big(w^{n-1}_{x_{i,j-1}} - 2w^{n-1}_{x_{i,j}} + w^{n-1}_{x_{i,j+1}} \big) \\
&+ \frac{1}{dz_j} \frac{2}{dx_i + dx_{i+1}} \big(w^{n-1}_{z_{i+1,j}} - w^{n-1}_{z_{i,j}} - w^{n-1}_{z_{i+1,j-1}} + w^{n-1}_{z_{i,j-1}} \big) \Big\}
\end{aligned}
$$

Right hand side in z-coordinate:

$$
\begin{aligned}
&= -\frac{\mathrm{Ra}}{2}(T_{i+1,j+1} - T_{i,j+1}) - \frac{\mathrm{De}}{Dt^n + \mathrm{De}} \\
&\left(\frac{2(p^{n-1}_{i,j+1} - p^{n-1}_{i,j})}{dz_j + dz_{j+1}} - \frac{\mathrm{Ra}}{2}(T^{n-1}_{i+1,j+1} - T^{n-1}_{i,j+1}) \right) \\
&+ \frac{\mathrm{De}\,\eta_2}{dt_n + \mathrm{De}} \frac{dt^{n-1} + \mathrm{De}}{dt^{n-1}(1+\eta_2) + \mathrm{De}\,\eta_2} \\
&\Big\{ \frac{2}{dz^2} \big(w^{n-1}_{z_{i,j-1}} - 2w^{n-1}_{z_{i,j}} + w^{n-1}_{z_{i,j+1}} \big) \\
&+ \frac{1}{dx^2} \big(w^{n-1}_{z_{i-1,j}} - 2w^{n-1}_{z_{i,j}} + w^{n-1}_{z_{i+1,j}} \big) \\
&+ \frac{1}{dx_i} \frac{2}{dz_j + dz_{j+1}} \big(w^{n-1}_{x_{i,j+1}} - w^{n-1}_{x_{i,j}} - w^{n-1}_{x_{i-1,j+1}} + w^{n-1}_{x_{i-1,j}} \big) \Big\}
\end{aligned}
$$

Oldroyd-B model with the objective derivative replaced by partial time derivative and advection terms

We start with the prescription for Oldroyd-B model:

$$\mathcal{S} = 2(1 + \mathrm{Vr})\mathcal{D} + 2\mathrm{VrDe}\overset{\triangledown}{\mathcal{D}} - \mathrm{De}\overset{\triangledown}{\mathcal{S}}$$

Now we substitute the triangle derivative by partial time derivative and advective member, i.e. $\overset{\triangledown}{\mathcal{S}} = \frac{\partial \mathcal{S}}{\partial t} + \mathbf{v} \cdot \nabla \mathcal{S}$, $\overset{\triangledown}{\mathcal{D}} = \frac{\partial \mathcal{D}}{\partial t} + \mathbf{v} \cdot \nabla \mathcal{D}$, where we use the backward Euler scheme for the partial time derivative as in chapter number two and we utilise explicit computation of the advective terms, i.e. we replace $\mathbf{v} \cdot \mathcal{D}$ by $\mathbf{v^{n-1}} \cdot \mathcal{D}^{n-1}$ and $\mathbf{v} \cdot \mathcal{S}$ by $\mathbf{v^{n-1}} \cdot \mathcal{S}^{n-1}$, where index $n-1$ denotes that physical quantities are expressed in previous time step and $dt_n = t^n - t^{n-1}$ denotes time step. We also use the fact that $\mathcal{D}$ is symmetric part of velocity gradient. And by several fitting

showed in chapter 2, we obtain:

$$\begin{aligned}\mathcal{S}^n - \big(\nabla\mathbf{w}^n + (\nabla\mathbf{w}^n)^T\big) &= -\mathrm{Vr}\varphi_n\psi_{n-1}\big(\nabla\mathbf{w}^{n-1} + (\nabla\mathbf{w}^{n-1})^T\big) \\ &+ \mathrm{Vr}dt_n\varphi_n\psi_{n-1}^2\mathbf{w}^{n-1}\cdot\nabla(\nabla\mathbf{w}^{n-1} + (\nabla\mathbf{w}^{n-1})^T\big) \\ &+ \varphi_n\mathcal{S}^{n-1} - dt_n\varphi_n\psi_{n-1}\mathbf{w}^{n-1}\cdot\nabla\mathcal{S}^{n-1} \qquad (6.17)\end{aligned}$$

That means that on the right hand side of our equations appears following terms:

$$\begin{gathered}+\mathrm{Vr}\varphi_n\psi_{n-1}\nabla\cdot\big(\nabla\mathbf{w}^{n-1} - (\nabla\mathbf{w}^{n-1})^T\big) - \\ \mathrm{Vr}dt_n\varphi_n\psi_{n-1}^2\nabla\cdot\Big[\mathbf{w}^{n-1}\cdot\nabla(\nabla\mathbf{w}^{n-1} - (\nabla\mathbf{w}^{n-1})^T\big)\Big] \\ -\varphi_n\nabla\cdot\mathcal{S}^{n-1} + dt_n\varphi_n\psi_{n-1}\nabla\cdot\Big(\mathbf{w}^{n-1}\cdot\nabla\mathcal{S}^{n-1}\Big)\end{gathered}$$

Discretization of the advection terms via central difference scheme

1. $\nabla\cdot(\mathbf{v}\cdot\nabla\mathcal{S})$

$$\nabla\cdot(\mathbf{v}\cdot\nabla\mathcal{S}) = \nabla\cdot(\mathbf{v}\cdot\nabla\mathcal{S}) = \Big(\frac{\partial}{\partial x},\frac{\partial}{\partial z}\Big)\cdot\Big(v_x\frac{\partial\mathcal{S}}{\partial x} + v_z\frac{\partial\mathcal{S}}{\partial z}\Big)$$

$$= \begin{pmatrix} \frac{\partial}{\partial x}(v_x\frac{\partial S_{xx}}{\partial x} + v_z\frac{\partial S_{xx}}{\partial z}) & +\frac{\partial}{\partial z}(v_x\frac{\partial S_{xz}}{\partial x} + v_z\frac{\partial S_{xz}}{\partial z}) \\ \frac{\partial}{\partial x}(v_x\frac{\partial S_{xz}}{\partial x} + v_z\frac{\partial S_{xz}}{\partial z}) & +\frac{\partial}{\partial z}(v_x\frac{\partial S_{zz}}{\partial x} + v_z\frac{\partial S_{zz}}{\partial z}) \end{pmatrix}$$

Now we split the expression above into two coordinates, x-coordinate of the advection of stress follows:

$$\begin{aligned}\frac{\partial}{\partial x}\Big(v_x\frac{\partial S_{xx}}{\partial x} + v_z\frac{\partial S_{xx}}{\partial z}) + \frac{\partial}{\partial z}(v_x\frac{\partial S_{xz}}{\partial x} + v_z\frac{\partial S_{xz}}{\partial z}\Big) = \\ \frac{\partial v_x}{\partial x}\frac{\partial S_{xx}}{\partial x} + v_x\frac{\partial^2 S_{xx}}{\partial x^2} + \frac{\partial v_z}{\partial x}\frac{\partial S_{xx}}{\partial z} + v_z\frac{\partial^2 S_{xx}}{\partial z\partial x} \\ +\frac{\partial v_x}{\partial z}\frac{\partial S_{xz}}{\partial x} + v_x\frac{\partial^2 S_{xz}}{\partial x\partial z} + \frac{\partial v_z}{\partial z}\frac{\partial S_{xz}}{\partial z} + v_z\frac{\partial^2 S_{xz}}{\partial z^2}\end{aligned}$$

Z-coordinate of the advection of stress follows:

$$\begin{aligned}\frac{\partial}{\partial x}(v_x\frac{\partial S_{xz}}{\partial x} + v_z\frac{\partial S_{xz}}{\partial z}) + \frac{\partial}{\partial z}(v_x\frac{\partial S_{zz}}{\partial x} + v_z\frac{\partial S_{zz}}{\partial z}) = \\ \frac{\partial v_x}{\partial x}\frac{\partial S_{xz}}{\partial x} + v_x\frac{\partial^2 S_{xz}}{\partial x^2} + \frac{\partial v_z}{\partial x}\frac{\partial S_{xz}}{\partial z} + v_z\frac{\partial^2 S_{xz}}{\partial z\partial x} \\ +\frac{\partial v_x}{\partial z}\frac{\partial S_{zz}}{\partial x} + v_x\frac{\partial^2 S_{zz}}{\partial x\partial z} + \frac{\partial v_z}{\partial z}\frac{\partial S_{zz}}{\partial z} + v_z\frac{\partial^2 S_{zz}}{\partial z^2}\end{aligned}$$

Expressed via finite differences

Expressed in numerical way, i.e. by physical properties in nodes:
X-coordinate:

$$\frac{1}{2dx_i^2}\big(v_{x_{i+1,j}} - v_{x_{i-1,j}}\big)\big(S_{xx_{i+1,j}} - S_{xx_{i,j}}\big) +$$
$$\frac{1}{2dx_i^2}v_{x_{i,j}}\big(S_{xx_{i+2,j}} - S_{xx_{i+1,j}} - S_{xx_{i,j}} + S_{xx_{i-1,j}}\big) +$$
$$\frac{1}{2dz_j}(v_{z_{i,j}} - v_{z_{i,j-1}} + v_{z_{i+1,j}} - v_{z_{i+1,j-1}})$$
$$\frac{1}{4dx_i}\big(S_{xx_{i+1,j+1}} - S_{xx_{i+1,j-1}} + S_{xx_{i,j+1}} - S_{xx_{i,j-1}}\big) +$$
$$\frac{1}{4}(v_{z_{i,j}} + v_{z_{i+1,j}} + v_{z_{i+1,j-1}} + v_{z_{i,j-1}})$$
$$\frac{1}{2}\frac{1}{dx_i dz_j}(S_{xx_{i+1,j+1}} - S_{xx_{i,j+1}} - S_{xx_{i+1,j-1}} + S_{xx_{i,j-1}}) +$$
$$\frac{1}{2dz_j}(v_{x_{i,j+1}} - v_{x_{i,j-1}})\frac{1}{4dx_i}(S_{xz_{i+2,j+1}} + S_{xz_{i+2,j}} - S_{xz_{i,j+1}} - S_{xz_{i,j}}) +$$
$$+v_{x_{i,j}}\frac{1}{2}\frac{1}{dx_i dz_j}(S_{xz_{i+2,j+1}} - S_{xz_{i+2,j}} - S_{xz_{i,j+1}} + S_{xz_{i,j}})$$
$$\frac{1}{2dz_j}(v_{z_{i,j}} - v_{z_{i,j-1}} + v_{z_{i+1,j}} - v_{z_{i+1,j-1}})\frac{1}{dz_j}\Big(S_{xz_{i+1,j+1}} - S_{xz_{i+1,j}}\Big)$$
$$\frac{1}{4}(v_{z_{i,j}} + v_{z_{i+1,j}} + v_{z_{i+1,j-1}} + v_{z_{i,j-1}})\frac{1}{2dz_j^2}$$
$$(S_{xz_{i+1,j+2}} - S_{xz_{i+1,j+1}} - S_{xz_{i+1,j}} + S_{xz_{i+1,j-1}})$$

Z-coordinate:

$$\frac{1}{2dx_i^2}(v_{x_{i,j+1}} - v_{x_{i,j}} + v_{x_{i-1,j+1}} - v_{x_{i-1,j}})$$
$$(S_{xz_{i+1,j+1}} - S_{xz_{i,j+1}})$$
$$+\frac{1}{8dx_i^2}(v_{x_{i-1,j}} + v_{x_{i,j}} + v_{x_{i-1,j+1}} + v_{x_{i,j+1}})$$
$$(S_{xz_{i+2,j+1}} - S_{xz_{i+1,j+1}} - S_{xz_{i,j+1}} + S_{xz_{i-1,j+1}})$$
$$+\frac{1}{8dx_i dz_j}(v_{z_{i+1,j}} - v_{z_{i-1,j}})$$
$$(S_{xz_{i+1,j+2}} + S_{xz_{i,j+2}} - S_{xz_{i+1,j}} - S_{xz_{i,j}})$$
$$+\frac{1}{2dx_i dz_j}v_{z_{i,j}}(S_{xz_{i+1,j+2}} - S_{xz_{i,j+2}} - S_{xz_{i+1,j}} + S_{xz_{i,j}})$$
$$+\frac{1}{dz_j + dz_{j+1}}(v_{x_{i,j+1}} - v_{x_{i,j}} + v_{x_{i-1,j+1}} - v_{x_{i-1,j}})$$
$$\frac{1}{4dx_i}(S_{zz_{i+1,j}} - S_{zz_{i-1,j}} + S_{zz_{i+1,j+1}} - S_{zz_{i-1,j+1}})$$
$$+\frac{1}{8dx_i dz_j}(v_{x_{i-1,j}} + v_{x_{i,j}} + v_{x_{i-1,j+1}} + v_{x_{i,j+1}})$$

$$
\begin{aligned}
&(S_{zz_{i+1,j+1}} - S_{zz_{i+1,j}} - S_{zz_{i-1,j+1}} + S_{zz_{i-1,j}}) \\
&+\frac{1}{2dz_j}(v_{z_{i,j+1}} - v_{z_{i,j-1}})\frac{2}{dz_j + dz_{j+1}}(S_{zz_{i,j+1}} - S_{zz_{i,j}}) \\
&+\frac{1}{4dz_j^2}v_{z_{i,j}}(S_{zz_{i,j+2}} - S_{zz_{i,j+1}} - S_{zz_{i,j}} + S_{zz_{i,j-1}})
\end{aligned}
$$

2. $2\nabla \cdot (\mathbf{v} \cdot \nabla \mathcal{D})$

$$
\begin{aligned}
&= 2\nabla \cdot (\mathbf{v} \cdot \nabla \mathcal{D}) = 2\Big(\frac{\partial}{\partial x}, \frac{\partial}{\partial z}\Big) \cdot \Big(v_x \frac{\partial \mathcal{D}}{\partial x} + v_z \frac{\partial \mathcal{D}}{\partial z}\Big) \\
&= 2 \begin{pmatrix} \frac{\partial}{\partial x}(v_x \frac{\partial D_{xx}}{\partial x} + v_z \frac{\partial D_{xx}}{\partial z}) & +\frac{\partial}{\partial z}(v_x \frac{\partial D_{xz}}{\partial x} + v_z \frac{\partial D_{xz}}{\partial z}) \\ \frac{\partial}{\partial x}(v_x \frac{\partial D_{xz}}{\partial x} + v_z \frac{\partial D_{xz}}{\partial z}) & +\frac{\partial}{\partial z}(v_x \frac{\partial D_{zz}}{\partial x} + v_z \frac{\partial D_{zz}}{\partial z}), \end{pmatrix}
\end{aligned}
$$

where

$$
2\mathcal{D} = \begin{pmatrix} 2\frac{\partial v_x}{\partial x} & \frac{\partial v_x}{\partial z} + \frac{\partial v_z}{\partial x} \\ \frac{\partial v_x}{\partial z} + \frac{\partial v_z}{\partial x} & 2\frac{\partial v_z}{\partial z} \end{pmatrix}.
$$

Therefore we obtain following expression for the x-coordinate of advection of strain rate:

$$
\begin{aligned}
2\frac{\partial}{\partial x}\Big(v_x \frac{\partial D_{xx}}{\partial x} + v_z \frac{\partial D_{xx}}{\partial z}\Big) + \frac{\partial}{\partial z}\Big(v_x \frac{\partial D_{xz}}{\partial x} + v_z \frac{\partial D_{xz}}{\partial z}\Big) = \\
2\Big(\frac{\partial v_x}{\partial x}\frac{\partial D_{xx}}{\partial x} + v_x \frac{\partial^2 D_{xx}}{\partial x^2} + \frac{\partial v_z}{\partial x}\frac{\partial D_{xx}}{\partial z} + v_z \frac{\partial^2 D_{xx}}{\partial z \partial x} \\
+\frac{\partial v_x}{\partial z}\frac{\partial D_{xz}}{\partial x} + v_x \frac{\partial^2 D_{xz}}{\partial x \partial z} + \frac{\partial v_z}{\partial z}\frac{\partial D_{xz}}{\partial z} + v_z \frac{\partial^2 D_{xz}}{\partial z^2}\Big)
\end{aligned}
$$

$$
\begin{aligned}
&= 2\frac{\partial v_x}{\partial x}\frac{\partial^2 v_x}{\partial^2 x} + 2v_x \frac{\partial^3 v_x}{\partial x^3} + 2\frac{\partial v_z}{\partial x}\frac{\partial^2 v_x}{\partial x \partial z} + 2v_z \frac{\partial^3 v_x}{\partial z \partial x^2} \\
&+\frac{\partial v_x}{\partial z}\Big(\frac{\partial^2 v_x}{\partial z \partial x} + \frac{\partial^2 v_z}{\partial x^2}\Big) + v_x\Big(\frac{\partial^3 v_x}{\partial x \partial z^2} + \frac{\partial^3 v_z}{\partial z \partial x^2}\Big) \\
&+\frac{\partial v_z}{\partial z}\Big(\frac{\partial^2 v_x}{\partial z^2} + \frac{\partial^2 v_z}{\partial x \partial z}\Big) + v_Z\Big(\frac{\partial^3 v_x}{\partial z^3} + \frac{\partial^3 v_z}{\partial x \partial z^2}\Big).
\end{aligned}
$$

and following term for z-coordinate of advection of strain rate:

$$
\begin{aligned}
&\frac{\partial}{\partial x}\Big(v_x \frac{\partial D_{xz}}{\partial x} + v_z \frac{\partial D_{xz}}{\partial z}\Big) + \frac{\partial}{\partial z}\Big(v_x \frac{\partial D_{zz}}{\partial x} + v_z \frac{\partial D_{zz}}{\partial z}\Big) = \\
&\frac{\partial v_x}{\partial x}\frac{\partial D_{xz}}{\partial x} + v_x \frac{\partial^2 D_{xz}}{\partial x^2} + \frac{\partial v_z}{\partial x}\frac{\partial D_{xz}}{\partial z} + v_z \frac{\partial^2 D_{xz}}{\partial z \partial x} + \\
&\frac{\partial v_x}{\partial z}\frac{\partial D_{zz}}{\partial x} + v_x \frac{\partial^2 D_{zz}}{\partial x \partial z} + \frac{\partial v_z}{\partial z}\frac{\partial D_{zz}}{\partial z} + v_z \frac{\partial^2 D_{zz}}{\partial z^2} = \\
&\frac{\partial v_x}{\partial x}\Big(\frac{\partial^2 v_x}{\partial x \partial z} + \frac{\partial^2 v_z}{\partial x^2}\Big) + v_x\Big(\frac{\partial^3 v_x}{\partial z \partial x^2} + \frac{\partial^3 v_z}{\partial x^3}\Big) + \frac{\partial v_z}{\partial x}\Big(\frac{\partial^2 v_x}{\partial z^2} + \frac{\partial^2 v_z}{\partial x \partial z}\Big) + \\
&v_z\Big(\frac{\partial^3 v_x}{\partial z^2 \partial x} + \frac{\partial^3 v_z}{\partial x^2 \partial z}\Big) + 2\frac{\partial v_x}{\partial z}\frac{\partial^2 v_z}{\partial z \partial x} + 2v_x \frac{\partial^3 v_z}{\partial x \partial z^2} + 2\frac{\partial v_z}{\partial z}\frac{\partial^2 v_z}{\partial z^2} + 2v_z \frac{\partial^3 v_z}{\partial z^3}
\end{aligned}
$$

Expressed via finite differences

Expressed in numerical way, i.e. by physical properties in nodes:
X-coordinate=

$$\frac{1}{dx_i^3}(v_{x_{i+1,j}} - v_{x_{i-1,j}})(v_{x_{i+1,j}} - 2v_{x_{i,j}} + v_{x_{i-1,j}}) +$$
$$2v_{x_{i,j}}\frac{1}{dx_i^3}(\frac{1}{2}v_{x_{i+2,j}} - v_{x_{i+1,j}} + v_{x_{i-1,j}} - \frac{1}{2}v_{x_{i-2,j}}) +$$
$$\frac{2}{dx_i + dx_{i+1}}(v_{z_{i+1,j}} - v_{z_{i,j}} + v_{z_{i+1,j-1}} - v_{z_{i,j-1}})$$
$$\frac{1}{4dx_i dz_j}(v_{x_{i+1,j+1}} - v_{x_{i-1,j+1}} - v_{x_{i+1,j-1}} + v_{x_{i-1,j-1}})$$
$$\frac{1}{2}(v_{z_{i+1,j}} + v_{z_{i+1,j-1}} + v_{z_{i,j}} + v_{z_{i,j-1}})\frac{1}{2dx_i^2 dz_j}$$
$$(v_{x_{i+1,j+1}} - v_{x_{i+1,j-1}} - 2v_{x_{i,j+1}} + 2v_{x_{i,j-1}} + v_{x_{i-1,j+1}} - v_{x_{i-1,j-1}})$$
$$\frac{1}{2dz_j}(v_{x_{i,j+1}} - v_{x_{i,j-1}})\Big(\frac{1}{4dx_i dz_j}(v_{x_{i+1,j+1}} - v_{x_{i-1,j+1}} - v_{x_{i+1,j-1}} + v_{x_{i-1,j-1}}) +$$
$$\frac{1}{4dx_i^2}(v_{z_{i+2,j-1}} - v_{z_{i+1,j-1}} - v_{z_{i,j-1}} + v_{z_{i-1,j-1}} + v_{z_{i+2,j}} - v_{z_{i+1,j}} - v_{z_{i,j}} + v_{z_{i-1,j}})\Big) +$$
$$v_{x_{i,j}}\Big(\frac{1}{2dx_i dz_j^2}(v_{x_{i+1,j+1}} - v_{x_{i-1,j+1}} - 2v_{x_{i+1,j}} + 2v_{x_{i-1,j}} + v_{x_{i+1,j-1}} - v_{x_{i-1,j-1}}) +$$
$$\frac{1}{2dx_i^2 dz_j}(v_{z_{i+2,j}} - v_{z_{i+2,j-1}} - v_{z_{i+1,j}} + v_{z_{i+1,j-1}} - v_{z_{i,j}} + v_{z_{i,j-1}} +$$
$$v_{z_{i-1,j}} - v_{z_{i-1,j-1}})\Big) +$$
$$\frac{1}{2dz_j}(v_{z_{i+1,j}} - v_{z_{i+1,j-1}} + v_{z_{i,j}} - v_{z_{i,j-1}})\Big(\frac{1}{dx_i^2}(v_{x_{i,j+1}} - 2v_{x_{i,j}} + v_{x_{i,j-1}}) +$$
$$\frac{2}{dz_j(dx_i + dx_{i+1})}(v_{z_{i+1,j}} - v_{z_{i,j}} - v_{z_{i+1,j-1}} + v_{z_{i,j-1}})\Big) +$$
$$\frac{1}{4}(v_{z_{i+1,j}} + v_{z_{i,j}} + v_{z_{i+1,j-1}} + v_{z_{i,j-1}})\Big(\frac{1}{dz_j^3}(\frac{1}{2}v_{x_{i,j+2}} - v_{x_{i,j+1}} +$$
$$+v_{x_{i,j-1}} - \frac{1}{2}v_{x_{i,j-2}}) + \frac{1}{(dx_i + dx_{i+1})dz_j^2}(v_{z_{i+1,j+1}} - v_{z_{i,j+1}} - v_{z_{i+1,j}} + v_{z_{i,j}} -$$
$$v_{z_{i+1,j-1}} + v_{z_{i,j-1}} + v_{z_{i+1,j-2}} - v_{z_{i,j-2}})\Big)$$

Z-coordinate=

$$\frac{1}{2dx_i}(v_{x_{i,j+1}} - v_{x_{i-1,j+1}} + v_{x_{i,j}} - v_{x_{i-1,j}})\Big(\frac{2}{dx_i(dz_j + dz_{j+1})}$$
$$(v_{x_{i,j+1}} - v_{x_{i-1,j+1}} - v_{x_{i,j}} + v_{x_{i-1,j}}) + \frac{1}{dx_i^2}(v_{z_{i+1,j}} - 2v_{z_{i,j}} + v_{z_{i-1,j}})\Big)$$
$$\frac{1}{4}(v_{x_{i,j+1}} + v_{x_{i-1,j+1}} + v_{x_{i,j}} + v_{x_{i-1,j}})\Big(\frac{1}{(dz_j + dz_{j+1})dx_i^2}$$
$$(v_{x_{i+1,j+1}} - v_{x_{i,j+1}} - v_{x_{i-1,j+1}} + v_{x_{i-2,j+1}} - v_{x_{i+1,j}} + v_{x_{i,j}} + v_{x_{i-1,j}} - v_{x_{i-2,j}}) +$$
$$\frac{1}{dx_i^3}(\frac{1}{2}v_{z_{i+2,j}} - v_{z_{i+1,j}} + v_{z_{i-1,j}} - \frac{1}{2}v_{z_{i-2,j}})\Big) +$$
$$\frac{1}{2dx_i}(v_{z_{i+1,j}} - v_{z_{i-1,j}})\Big(\frac{1}{4dz_j^2}(v_{x_{i,j+2}} - v_{x_{i,j+1}} - v_{x_{i,j}} + v_{x_{i,j-1}} + v_{x_{i-1,j+2}} -$$
$$v_{x_{i-1,j+1}} - v_{x_{i-1,j}} + v_{x_{i-1,j-1}}) +$$
$$\frac{1}{4dx_i dz_j}(v_{z_{i+1,j+1}} - v_{z_{i-1,j+1}} - v_{z_{i+1,j-1}} + v_{z_{i-1,j-1}})\Big)$$
$$v_{z_{i,j}}\Big(\frac{1}{2dx_i dz_j^2}(v_{x_{i,j+2}} - v_{x_{i,j+1}} - v_{x_{i,j}} + v_{x_{i,j-1}} - v_{x_{i-1,j+2}} + v_{x_{i-1,j+1}} +$$
$$v_{x_{i-1,j}} - v_{x_{i-1,j-1}}) + \frac{1}{2dx_i^2 dz_j}(v_{z_{i+1,j+1}} - v_{z_{i+1,j-1}} - 2v_{z_{i,j+1}} + 2v_{z_{i,j-1}} +$$
$$v_{z_{i-1,j+1}} - v_{z_{i-1,j-1}}) + \frac{2}{dz_j + dz_{j+1}}(v_{x_{i,j+1}} - v_{x_{i,j}} + v_{x_{i-1,j+1}} - v_{x_{i-1,j}})$$
$$\frac{1}{4dx_i dz_j}(v_{z_{i+1,j+1}} - v_{z_{i+1,j-1}} - v_{z_{i-1,j+1}} + v_{z_{i-1,j-1}}) +$$
$$\frac{1}{2}(v_{x_{i,j+1}} + v_{x_{i-1,j+1}} + v_{x_{i,j}} + v_{x_{i-1,j}})$$
$$\frac{1}{2dx_i dx z_j^2}(v_{z_{i+1,j+1}} - 2v_{z_{i+1,j}} + v_{z_{i+1,j-1}} - v_{z_{i-1,j+1}} + 2v_{z_{i-1,j}} - v_{z_{i-1,j-1}}) +$$
$$\frac{1}{dz_j}(v_{z_{i,j+1}} - v_{z_{i,j-1}})\frac{1}{dz_j^2}(v_{z_{i,j+1}} - 2v_{z_{i,j}} + v_{z_{i,j-1}}) +$$
$$2v_{z_{i,j}}\frac{1}{dz_j^3}(\frac{1}{2}v_{z_{i,j+2}} - v_{z_{i,j+1}} + v_{z_{i,j-1}} - \frac{1}{2}v_{z_{i,j-2}})$$

Discretization of the advection terms via second-order upwind scheme

Now we present the divergence of the advection of stress to show how we use the upwind scheme. The advection of strain rate would look the same.

So that, for the first coordinate, by which we mean coordinate of the node, where we write the first equation of motion we shall compute following derivatives:

Now we present the divergence of the advection of stress to show how we use the upwind scheme. The advection of strain rate would look the same.

So that, for the first coordinate, by which we mean coordinate of the node, where we write the first equation of motion we shall compute following derivatives: $v_x\frac{\partial S_{xx}}{\partial x}$, $v_z\frac{\partial S_{xx}}{\partial z}$, $v_x\frac{\partial S_{xz}}{\partial x}$, $v_z\frac{\partial S_{xz}}{\partial z}$.

1. $v_x \frac{\partial S_{xx}}{\partial x}$

   - $v_{x_{i,j}} > 0$

$$\begin{aligned}\left(v_x \frac{\partial S_{xx}}{\partial x}\right)_{i,j}^n &= \frac{v_{x_{i,j}}}{2dx} \cdot \big(3 \cdot 0.5 \cdot (S_{xx_{i,j}} + S_{xx_{i+1,j}}) \\ &\quad -4 \cdot 0.5 \cdot (S_{xx_{i-1,j}} + S_{xx_{i,j}}) \\ &\quad +0.5 \cdot (S_{xx_{i-2,j}} + S_{xx_{i-1,j}})\big) \\ &= \frac{v_{x_{i,j}}}{4dx} \cdot \\ &\quad \big(- S_{xx_{i,j}} + 3S_{xx_{i+1,j}} \\ &\quad -3S_{xx_{i-1,j}} + S_{xx_{i-2,j}}\big)\end{aligned}$$

   - $v_{x_{i,j}} < 0$

$$\begin{aligned}\left(v_x \frac{\partial S_{xx}}{\partial x}\right)_{i,j}^n &= \frac{v_{x_{i,j}}}{2dx} \cdot \big(- 0.5(S_{xx_{i+2,j}} + S_{xx_{i+3,j}}) \\ &\quad +4 \cdot 0.5 \cdot (S_{xx_{i+2,j}} + S_{xx_{i+1,j}}) \\ &\quad -3 \cdot 0.5 \cdot (S_{xx_{i+1,j}} + S_{xx_{i,j}})\big) \\ &= \frac{v_{x_{i,j}}}{4dx} \cdot \\ &\quad \big(- S_{xx_{i+3,j}} + 3S_{xx_{i+2,j}} \\ &\quad +S_{xx_{i+1,j}} - 3S_{xx_{i,j}}\big)\end{aligned}$$

2. $v_z \frac{\partial S_{xx}}{\partial z}$

   - $v_{z_{i,j}} > 0$
     Here $v_{z_{i,j}}$ is substituted by the arithmetic mean of v_z from surrounding nodes (from now further denoted by $arv_{z_{i,j}}$), i.e. $arv_{z_{i,j}} = 0.25 * (v_{z_{i+1,j-1}} + v_{z_{i,j-1}} + v_{z_{i+1,j}} + v_{z_{i,j}})$.

$$\begin{aligned}\left(v_z \frac{\partial S_{xx}}{\partial z}\right)_{i,j}^n &= \frac{arv_{z_{i,j}}}{2dz} \cdot \big(3 \cdot 0.5(S_{xx_{i,j}} + S_{xx_{i+1,j}}) \\ &\quad -4 \cdot 0.5(S_{xx_{i+1,j-1}} + S_{xx_{i,j-1}}) \\ &\quad +0.5(S_{xx_{i+1,j-2}} + S_{xx_{i,j-2}})\big)\end{aligned}$$

   - $v_{z_{i,j}} < 0$

$$\begin{aligned}\left(v_z \frac{\partial S_{xx}}{\partial z}\right)_{i,j}^n &= \frac{arv_{z_{i,j}}}{2dz} \cdot \big(- 0.5(S_{xx_{i+1,j+2}} + S_{xx_{i,j+2}}) \\ &\quad +4 \cdot 0.5(S_{xx_{i+1,j+1}} + S_{xx_{i,j+1}}) \\ &\quad -3 \cdot 0.5(S_{xx_{i+1,j}} + S_{xx_{i,j}})\big)\end{aligned}$$

3. $v_x \frac{\partial S_{xz}}{\partial x}$

   - $v_{x_{i,j}} > 0$

$$\begin{aligned}\left(v_x \frac{\partial S_{xz}}{\partial x}\right)_{i,j}^n &= \frac{v_{x_{i,j}}}{2dx} \cdot \Big(3 \cdot 0.5\big(S_{xz_{i+1,j}} + S_{xz_{i+1,j+1}}\big) \\ &\quad -4 \cdot 0.5\big(S_{xz_{i,j}} + S_{xz_{i,j+1}}\big) \\ &\quad +0.5\big(S_{xz_{i-1,j}} + S_{xz_{i-1,j+1}}\big)\end{aligned}$$

- $v_{x_{i,j}} < 0$

$$\begin{aligned}\Big(v_x\frac{\partial S_{xz}}{\partial x}\Big)^n_{i,j} &= \frac{v_{x_{i,j}}}{2dx}\cdot\Big(-0.5\big(S_{xz_{i+3,j}}+S_{xz_{i+3,j+1}}\big)\\ &\quad +4\cdot 0.5\big(S_{xz_{i+2,j}}+S_{xz_{i+2,j+1}}\big)\\ &\quad -3\cdot 0.5\big(S_{xz_{i+1,j}}+S_{xz_{i+1,j+1}}\big)\end{aligned}$$

4. $v_z\frac{\partial S_{xz}}{\partial z}$

- $arv_{z_{i,j}} > 0$

$$\begin{aligned}\Big(v_z\frac{\partial S_{xz}}{\partial z}\Big)^n_{i,j} &= \frac{arv_{z_{i,j}}}{2dz}\cdot\Big(3\cdot 0.5\big(S_{xz_{i+1,j}}+S_{xz_{i+1,j+1}}\big)\\ &\quad -4\cdot 0.5\big(S_{xz_{i+1,j}}+S_{xz_{i+1,j-1}}\big)\\ &\quad +0.5\big(S_{xz_{i+1,j-1}}+S_{xz_{i+1,j-2}}\big)\\ &= \frac{arv_{z_{i,j}}}{4dz}\cdot\\ &\quad \Big(3S_{xz_{i+1,j+1}}-S_{xz_{i+1,j}}-3S_{xz_{i+1,j-1}}\\ &\quad +S_{xz_{i+1,j-2}}\Big)\end{aligned}$$

- $arv_{z_{i,j}} < 0$

$$\begin{aligned}\Big(v_z\frac{\partial S_{xz}}{\partial z}\Big)^n_{i,j} &= \frac{arv_{z_{i,j}}}{2dz}\cdot\Big(-0.5\big(S_{xz_{i+1,j+3}}+S_{xz_{i+1,j+2}}\big)\\ &\quad +4\cdot 0.5\big(S_{xz_{i+1,j+2}}+S_{xz_{i+1,j+1}}\big)\\ &\quad -3\cdot 0.5\big(S_{xz_{i+1,j+1}}+S_{xz_{i+1,j}}\big)\\ &= \frac{arv_{z_{i,j}}}{4dz}\cdot\\ &\quad \Big(-S_{xz_{i+1,j+3}}+3S_{xz_{i+1,j+2}}\\ &\quad +S_{xz_{i+1,j+1}}-3S_{xz_{i+1,j}}\Big)\end{aligned}$$

Second equation of motion - second coordinate, derivatives to count:
$v_x\frac{\partial S_{xz}}{\partial x}$, $v_z\frac{\partial S_{xz}}{\partial z}, v_x\frac{\partial S_{zz}}{\partial x}, v_z\frac{\partial S_{zz}}{\partial z}$.
$arv_{x_{i,j}} := 0.25(v_{x_{i,j-1}} + v_{x_{i+1,j-1}} + v_{x_{i,j}} + v_{x_{i+1,j}})$

1. $v_x\frac{\partial S_{xz}}{\partial x}$

- $arv_{x_{i,j}} > 0$

$$\begin{aligned}\Big(v_x\frac{\partial S_{xz}}{\partial x}\Big)^n_{i,j} &= -\frac{arv_{x_{i,j}}}{2dx}\cdot\Big(3\cdot 0.5\big(S_{xz_{i,j+1}}+S_{xz_{i+1,j+1}}\big)\\ &\quad -4\cdot 0.5\big(S_{xz_{i-1,j+1}}+S_{xz_{i,j+1}}\big)\\ &\quad +0.5\big(S_{xz_{i-1,j+1}}+S_{xz_{i-2,j+1}}\big)\\ &= \frac{arv_{x_{i,j}}}{4dx}\cdot\\ &\quad \Big(3S_{xz_{i+1,j+1}}-S_{xz_{i,j+1}}-3S_{xz_{i-1,j+1}}\\ &\quad +S_{xz_{i-2,j+1}}\Big)\end{aligned}$$

- $arv_{x_{i,j}} < 0$

$$\begin{aligned}\Big(v_x\frac{\partial S_{xz}}{\partial x}\Big)^n_{i,j} &= \frac{arv_{x_{i,j}}}{2dx}\cdot\Big(-0.5\big(S_{xz_{i+2,j+1}}+S_{xz_{i+3,j+1}}\big)\\ &\quad +4\cdot 0.5\big(S_{xz_{i+2,j+1}}+S_{xz_{i+1,j+1}}\big)\\ &\quad -3\cdot 0.5\big(S_{xz_{i+1,j+1}}+S_{xz_{i,j+1}}\big)\\ &= \frac{arv_{x_{i,j}}}{4dx}\cdot\\ &\quad \Big(-S_{xz_{i+3,j+1}}+3S_{xz_{i+2,j+1}}\\ &\quad +S_{xz_{i+1,j+1}}-3S_{xz_{i,j+1}}\Big)\end{aligned}$$

2. $v_z\frac{\partial S_{xz}}{\partial z}$

- $v_{z_{i,j}} > 0$

$$\begin{aligned}\Big(v_z\frac{\partial S_{xz}}{\partial z}\Big)^n_{i,j} &= \frac{v_{z_{i,j}}}{2dz}\cdot\Big(3\cdot 0.5\big(S_{xz_{i,j+1}}+S_{xz_{i+1,j+1}}\big)\\ &\quad -4\cdot 0.5\big(S_{xz_{i+1,j}}+S_{xz_{i,j}}\big)\\ &\quad +0.5\big(S_{xz_{i+1,j-1}}+S_{xz_{i,j-1}}\big)\end{aligned}$$

- $v_{z_{i,j}} < 0$

$$\begin{aligned}\Big(v_z\frac{\partial S_{xz}}{\partial z}\Big)^n_{i,j} &= \frac{v_{z_{i,j}}}{2dz}\cdot\Big(-0.5\big(S_{xz_{i+1,j+3}}+S_{xz_{i,j+3}}\big)\\ &\quad +4\cdot 0.5\big(S_{xz_{i+1,j+2}}+S_{xz_{i,j+2}}\big)\\ &\quad -3\cdot 0.5\big(S_{xz_{i+1,j+1}}+S_{xz_{i,j+1}}\big)\end{aligned}$$

3. $v_x\frac{\partial S_{zz}}{\partial x}$

- $arv_{x_{i,j}} > 0$

$$\begin{aligned}\Big(v_x\frac{\partial S_{zz}}{\partial x}\Big)^n_{i,j} &= \frac{arv_{x_{i,j}}}{2dx}\cdot\Big(3\cdot 0.5\big(S_{zz_{i,j}}+S_{zz_{i,j+1}}\big)\\ &\quad -4\cdot 0.5\big(S_{zz_{i-1,j+1}}+S_{zz_{i-1,j}}\big)\\ &\quad +0.5\big(S_{zz_{i-2,j+1}}+S_{zz_{i-2,j}}\big)\Big)\end{aligned}$$

- $arv_{x_{i,j}} < 0$

$$\begin{aligned}\Big(v_x\frac{\partial S_{zz}}{\partial x}\Big)^n_{i,j} &= \frac{arv_{x_{i,j}}}{2dx}\cdot\Big(-0.5\big(S_{zz_{i+2,j+1}}+S_{zz_{i+2,j}}\big)\\ &\quad +4\cdot 0.5\big(S_{zz_{i+1,j+1}}+S_{zz_{i+1,j}}\big)\\ &\quad -3\cdot 0.5\big(S_{zz_{i,j+1}}+S_{zz_{i,j}}\big)\Big)\end{aligned}$$

4. $v_z\frac{\partial S_{zz}}{\partial z}$

- $v_{z_{i,j}} > 0$

$$\begin{aligned}\left(v_z\frac{\partial S_{zz}}{\partial z}\right)^n_{i,j} &= \frac{v_{z_{i,j}}}{2dz}\Big(3\cdot 0.5\big(S_{zz_{i,j}}+S_{zz_{i,j+1}}\big)\\ &\quad -4\cdot 0.5\big(S_{zz_{i,j-1}}+S_{zz_{i,j}}\big)\\ &\quad +0.5\big(S_{zz_{i,j-2}}+S_{zz_{i,j-1}}\big)\Big)\\ &= \frac{z_{i,j}}{4dz}\cdot\\ &\quad \Big(3S_{zz_{i,j+1}}-S_{zz_{i,j}}-3S_{zz_{i,j-1}}\\ &\quad +S_{zz_{i,j-2}}\Big)\end{aligned}$$

- $v_{z_{i,j}} < 0$

$$\begin{aligned}\left(v_z\frac{\partial S_{zz}}{\partial z}\right)^n_{i,j} &= \frac{v_{z_{i,j}}}{2dz}\cdot\Big(-0.5\big(S_{zz_{i,j+2}}+S_{zz_{i,j+3}}\big)\\ &\quad +4\cdot 0.5\big(S_{zz_{i,j+1}}+S_{zz_{i,j+2}}\big)\\ &\quad -3\cdot 0.5\big(S_{zz_{i,j}}+S_{zz_{i,j+1}}\big)\Big)\\ &= \frac{v_{z_{i,j}}}{4dz}\cdot\\ &\quad \Big(-S_{zz_{i,j+3}}+3S_{zz_{i,j+2}}+S_{zz_{i,j+1}}\\ &\quad -3S_{zz_{i,j}}\Big)\end{aligned}$$

Oldroyd-B model with objective derivative reduced to partial time derivative, advection terms and antisymmetric part of corrotational members

$$\mathcal{S} = 2(1+\mathrm{Vr})\mathcal{D} + 2\mathrm{VrDe}\overset{\triangledown}{\mathcal{D}} - \mathrm{De}\overset{\triangledown}{\mathcal{S}} \tag{6.18}$$

Now we substitute the triangle derivative by following expression, i.e. $\overset{\triangledown}{\mathcal{S}} = \frac{\partial \mathcal{S}}{\partial t} + \mathbf{v}\cdot\nabla\mathcal{S} - \mathcal{W}\mathcal{S} + \mathcal{S}\mathcal{W}$, $\overset{\triangledown}{\mathcal{D}} = \frac{\partial \mathcal{D}}{\partial t} + \mathbf{v}\cdot\nabla\mathcal{D} - \mathcal{D}\mathcal{S} + \mathcal{D}\mathcal{W}$. Further we proceed as in previous sections, i.e. we use backward Euler scheme for the partial time derivative and we utilise explicit computation of the advective and corrotational members. And we obtain:

$$\begin{aligned}\mathcal{S}^n \quad & -\big(\nabla\mathbf{w}^n + (\nabla\mathbf{w}^n)^T\big) = -\mathrm{Vr}\varphi_n\psi_{n-1}\big(\nabla\mathbf{w}^{n-1}\\ + \quad & (\nabla\mathbf{w}^{n-1})^T\big) + \mathrm{Vr}dt_n\varphi_n\psi^2_{n-1}\mathbf{w}^{n-1}\cdot\nabla(\nabla\mathbf{w}^{n-1} + (\nabla\mathbf{w}^{n-1})^T\big)\\ - \quad & \mathrm{Vr}dt_n\varphi_n\psi^2_{n-1}\Big(\mathcal{W}^{n-1}\big(\nabla\mathbf{w}^{n-1} + (\nabla\mathbf{w}^{n-1})^T\big) - \big(\nabla\mathbf{w}^{n-1} + (\nabla\mathbf{w}^{n-1})^T\big)\mathcal{W}^{n-1}\Big)\\ + \quad & \varphi_n\mathcal{S}^{n-1} - dt_n\varphi_n\psi_{n-1}\mathbf{w}^{n-1}\cdot\nabla\mathcal{S}^{n-1} + dt_n\varphi_n\psi_{n-1}\big(\mathcal{W}^{n-1}\mathcal{S}^{n-1} - \mathcal{S}^{n-1}\mathcal{W}^{n-1}\big)\end{aligned}$$

Therefore we have to count following expression: $\nabla\cdot(-\mathcal{W}\mathcal{S}+\mathcal{S}\mathcal{W})$ and $\nabla\cdot(-\mathcal{W}\mathcal{D}+\mathcal{D}\mathcal{W})$. We will provide the numerical equations only for the stress, because for the strain rate it looks similar. The only change is in swapping of letters S and D.

Corrotational terms

$$\nabla \cdot (-\mathcal{W}\mathcal{S} + \mathcal{S}\mathcal{W}) =$$
$$(\frac{\partial}{\partial x}, \frac{\partial}{\partial z}) \cdot \begin{pmatrix} -W_{xz}S_{xz} & \frac{1}{2}W_{xz}(S_{xx} - S_{zz}) \\ \frac{1}{2}W_{xz}(S_{xx} - S_{zz}) & W_{xz}S_{xz} \end{pmatrix} =$$
$$\begin{pmatrix} -\frac{\partial}{\partial x}(W_{xz}S_{xz}) + \frac{\partial}{\partial z}(\frac{1}{2}W_{xz}(S_{xx} - S_{zz})) \\ \frac{\partial}{\partial x}(\frac{1}{2}W_{xz}(S_{xx} - S_{zz})) + \frac{\partial}{\partial z}(W_{xz}S_{xz}) \end{pmatrix}$$

Expressed via finite differences

Expressed in numerical way, i.e. by physical properties in nodes:
X-coordinate:

$$-\Big[\Big(\frac{\partial^2 w_x}{\partial x \partial z} - \frac{\partial^2 w_z}{\partial x^2}\Big)S_{xz} + \Big(\frac{\partial w_x}{\partial z} - \frac{\partial w_z}{\partial x}\Big)\frac{\partial S_{xz}}{\partial x}\Big] +$$
$$\frac{1}{2}\Big(\frac{\partial^2 w_x}{\partial z^2} - \frac{\partial^2 w_z}{\partial x \partial z}\Big)(S_{xx} - S_{zz}) + \frac{1}{2}\Big(\frac{\partial w_x}{\partial z} - \frac{\partial w_z}{\partial x}\Big)\Big(\frac{\partial S_{xx}}{\partial z} - \frac{\partial S_{zz}}{\partial z}\Big) \approx$$
$$-\Big[\frac{1}{4dxdz}(w_{x_{i+1,j+1}} - w_{x_{i+1,j-1}} - w_{x_{i-1,j+1}} + w_{x_{i-1,j-1}})$$
$$-\frac{1}{4dx^2}(w_{z_{i+2,j}} - w_{z_{i+1,j}} - w_{z_{i,j}} + w_{z_{i-1,j}} + w_{z_{i+2,j-1}} - w_{z_{i+1,j-1}}$$
$$-w_{z_{i,j-1}} + w_{z_{i-1,j-1}})\Big] \cdot \Big[\frac{1}{2}(S_{xz_{i+1,j+1}} + S_{xz_{i+1,j}})\Big]$$
$$-\Big[\Big(\frac{1}{2dz}(w_{x_{i,j+1}} - w_{x_{i,j-1}}) - \frac{1}{2dx}(w_{z_{i+1,j}} - w_{z_{i,j}} + w_{z_{i+1,j-1}} - w_{z_{i,j-1}})\Big) \cdot$$
$$\frac{1}{4dx}\Big(S_{xz_{i+2,j+1}} - S_{xz_{i,j+1}} + S_{xz_{i+2,j}} - S_{xz_{i,j}}\Big)\Big]$$
$$+\frac{1}{2}\Big[\Big(\frac{1}{dz^2}(w_{x_{i,j+1}} - 2w_{x_{i,j}} + w_{x_{i,j-1}}) - \frac{1}{dzdx}(w_{z_{i+1,j}} - w_{z_{i,j}} - w_{z_{i+1,j-1}} + w_{z_{i,j-1}})\Big) \cdot$$

$$\frac{1}{2}\Big(S_{xx_{i+1,j}} + S_{xx_{i,j}} - S_{zz_{i+1,j}} - S_{zz_{i,j}}\Big)\Big] +$$
$$\frac{1}{2}\Big[\frac{1}{2dz}(w_{x_{i,j+1}} - w_{x_{i,j-1}}) - \frac{1}{2dx}(w_{z_{i+1,j}} - w_{z_{i,j}} + w_{z_{i+1,j-1}} - w_{z_{i,j-1}})\Big] \cdot$$
$$\Big[\frac{1}{2}\frac{1}{2dz}(S_{xx_{i+1,j+1}} - S_{xx_{i+1,j-1}} + S_{xx_{i,j+1}} - S_{xx_{i,j-1}})$$
$$-\frac{1}{2}\frac{1}{2dz}(S_{zz_{i+1,j+1}} - S_{zz_{i+1,j-1}} + S_{zz_{i,j+1}} - S_{zz_{i,j-1}})\Big]$$

Z-coordinate:

$$\frac{1}{2}\Big(\frac{\partial^2 w_x}{\partial x \partial z} - \frac{\partial^2 w_z}{\partial x^2}\Big)(S_{xx} - S_{zz}) + \frac{1}{2}\Big(\frac{\partial w_x}{\partial z} - \frac{\partial w_z}{\partial x}\Big)(\frac{\partial S_{xx}}{\partial x} - \frac{\partial S_{zz}}{\partial x}) +$$
$$\Big(\frac{\partial^2 w_x}{\partial z^2} - \frac{\partial^2 w_z}{\partial x \partial z}\Big)S_{xz} + \Big(\frac{\partial w_x}{\partial z} - \frac{\partial w_z}{\partial x}\Big)\frac{\partial S_{xz}}{\partial z} \approx$$
$$\frac{1}{2}\Big[\frac{1}{dxdz}(w_{x_{i,j+1}} - w_{x_{i,j}} - w_{x_{i-1,j+1}} + w_{x_{i-1,j}}) - \frac{1}{dx^2}(w_{z_{i+1,j}} - 2w_{z_{i,j}} + w_{z_{i-1,j}})\Big] \cdot$$
$$\Big[\frac{1}{2}(S_{xx_{i,j+1}} + S_{xx_{i,j}} - S_{zz_{i,j+1}} - S_{zz_{i,j}})\Big]$$
$$+\frac{1}{2}\Big[\Big(\frac{1}{2dz}(w_{x_{i,j+1}} - w_{x_{i,j}} + w_{x_{i-1,j+1}} - w_{x_{i-1,j}}) - \frac{1}{2dx}(w_{z_{i+1,j}} - w_{z_{i-1,j}})\Big) \cdot$$
$$\Big[\frac{1}{2}\frac{1}{2dx}\Big(S_{xx_{i+1,j+1}} - S_{xx_{i-1,j+1}} + S_{xx_{i+1,j}} - S_{xx_{i-1,j}}$$
$$-S_{zz_{i+1,j+1}} + S_{zz_{i-1,j+1}} - S_{zz_{i+1,j}} + S_{zz_{i-1,j}}\Big)\Big]$$
$$+\Big[\frac{1}{4dz^2}(w_{x_{i,j+2}} - w_{x_{i,j+1}} - w_{x_{i,j}} + w_{x_{i,j-1}} + w_{x_{i-1,j+2}} - w_{x_{i-1,j+1}}$$
$$-w_{x_{i-1,j}} + w_{x_{i-1,j-1}}) - \frac{1}{4dxdz}(w_{z_{i+1,j+1}} - w_{z_{i+1,j-1}} - w_{z_{i-1,j+1}} + w_{z_{i-1,j-1}})\Big] \cdot$$
$$\frac{1}{2}(S_{xz_{i+1,j+1}} + S_{xz_{i,j+1}})$$
$$+\Big(\frac{1}{2dz}(w_{x_{i,j+1}} - w_{x_{i,j}} + w_{x_{i-1,j+1}} - w_{x_{i-1,j}}) - \frac{1}{2dx}(w_{z_{i+1,j}} - w_{z_{i-1,j}})\Big) \cdot$$
$$\frac{1}{4dz}\Big(S_{xz_{i+1,j+2}} - S_{xz_{i+1,j}} + S_{xz_{i,j+2}} - S_{xz_{i,j}}\Big)$$